ISSN 1000-9620

Marine Science Bulletin

海洋通报

Volume 9 • Number 2 2007

ISSN 1000-9620

NATIONAL MARINE DATA AND
INFORMATION SERVICE OF CHINA

MARINE SCIENCE BULLETIN

Vol.9 No.2 Oct. 2007

CONTENTS

Research on the Testing Methods of Instrumental System
in the Marine Magnetic Survey ····· BIAN Gang et al. (1)

Application of BDRM Theory in the Two-AXIS Underwater Channel ····· ZHANG Lin et al. (12)

Research into Uncertainty in Measurement of Seawater Chemical Oxygen Demand
by Potassium Iodide-Alkaline Potassium Permanganate
Determination Method ····· ZHANG Shiqiang et al. (18)

Changes of Water Temperature and Harmful Algal Bloom
in the Daya Bay in the Northern South China Sea ····· YU Jing et al. (25)

Effect of Fouling on Feeding, Oxygen Consumption and Waste Excretion of
Pearl Oyster *Pinctada martensii* in Daya Bay Cultivation ····· SU Zhenxia et al. (34)

Preliminary Study of Microzooplankton Grazing and Community Composition
in the North of South China Sea in Autumn ····· SU Qiang et al. (43)

New Species of Punctariaceae (Phaeophyta) from China ····· LUAN Shujun et al. (54)

Coral Reef and High Sea Level at Luhuitou,
Hainan Island during the Holocene ····· HUANG Deyin et al. (61)

An Overview of the Concept of Regional Sediment Management ····· LEI Huaiyan et al. (71)

[illegible] Prospect in the South Yellow Sea
emote Sensing ····· GONG Jianming et al. (82)

he Sea Water Quality Status in the 2008
Field and Adjacent Area ····· SHI Xiaoyong et al. (90)

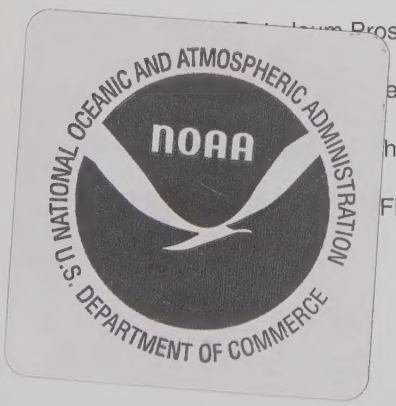

Research on the Testing Methods of Instrumental System in the Marine Magnetic Survey

LIBRARY
JAN 30 2008
National Oceanic & Atmospheric Administration
U.S. Dept. of Commerce

BIAN Gang, LIU Yanchun, YU Bo, XIAO Fumin, BIAN Guanglang

Dept. of Marine and Surveying Science, Dalian Naval Academy, Dalian 116018, *Liaoning, China*

Abstract: Testing methods of instrumental system in the marine magnetic survey have been studied in this paper, and the feasibility of each method has been testified by the observed data. The conclusion shows that the method brought out can effectively eliminate the systematic error caused by the instrumental system, and greatly improve the surveying precision and the reliability of the survey results .

Keywords: Marine magnetic survey; instrumental system; testing method

Introduction

The instrumental system of the marine geomagnetic survey consists of GPS, marine magnetometer and ground-based magnetometer which simultaneously measure the time-varying magnetic field for later subtraction from the survey data [1]. The development of the GPS techniques provides the guarantee for the high-precision marine geomagnetic survey. The technical performances of the marine magnetometer have been effectively improved by the application of the optical pump techniques, the sensitivity of the advanced marine magnetometer has reached 0.001 nT, which can meet the need of any surveying in the world [2, 3]. But influenced by the dynamic effect and magnetic influence of the surveying vessels, the practical performance of each system cannot reach the performances given by the manufacturers. To insure the reliability of the survey, test for each system must be done before the survey. The large-scale and normal marine geomagnetic survey is underway, the specifications of the instrumental system testing methods is incomplete. The practical tests are based on the experience of the surveyor and the procedure is very simple, which greatly lowers the reliability of the survey results. Based on the above problem which exists in the marine magnetic survey, and the testing method for each system studied, the method brought out by the author can provide criteria for the instrumental system tests in the marine geomagnetic survey and greatly improve the reliability of the survey results.

LIBRARY
Pacific Islands Fisheries Science Center
NOAA Fisheries
Honolulu, Hawai'i

1 Testing method

The technical requirements for each instrument system in different surveying classes has been given out by the Specifications for Oceanographic Survey-Marine Geology and Geophysics Investigation[4], as shown in Tab.1.

Received on March 6, 2007

Tab.1 The surveying classes and the technical requirements

Class	Class1	Class2	Class3	Class4
Precision of the positioning	±5 m	±15 m	±30 m	±30 m
Precision of the magnetic field survey	2.0 nT	5.0 nT	10.0 nT	15.0 nT
Precision of magnetometer	0.1 nT	0.25 nT	1 nT	1 nT
The applicability distance of the monitor station	50 km	200 km	500 km	1 000 km

To meet the requirements of the Specifications, the instrumental systems must be tested before the surveying. The tests methods for each system are detailed as below.

1.1 The static test of the GPS

1.1.1 The items of the GPS static test

a) The fittings of the GPS system must be complete and in good shape.

b) The antenna of the GPS must be installed on the surveying vessel with good sight.

c) The collocation of the receiver must be done as required.

d) The parameters of the base station and the mobile station must be set as required.

1.1.2 The static test of the GPS

The GPS system has its theoretical precision, but its practical precision must be measured and evaluated. The measurement of the precision must be done in the existent station before the surveying. The interval of the sampling is less than 3 minutes, and the duration must be more than 8 hours. The measurement is the repetition in equi-accuracy. Given the coordinates of the existent station, we can obtain the precision of the GPS system. The formula is shown as below.

$$\sigma_B = \sqrt{\frac{1}{N-1}\sum_{i=1}^{N}\left(B_i - \bar{B}\right)^2}\ ,\quad \sigma_L = \sqrt{\frac{1}{N-1}\sum_{i=1}^{N}\left(L_i - \bar{L}\right)^2} \tag{1}$$

Where, L_i and B_i are the observed longitude and latitude data, $\bar{L}$ and $\bar{B}$ are the arithmetic means, and also $\bar{B} = \frac{1}{N}\sum_{i=1}^{N} B_i$, $\bar{L} = \frac{1}{N}\sum_{i=1}^{N} L_i$. N is the total number of recorders. The practical precision of the GPS system can be calculated by σ_L and σ_B .

$$\sigma = \pm\sqrt{\sigma_L^2 + \sigma_B^2} \tag{2}$$

After obtaining the practical precision of the GPS system, we can give the objective evaluation, and only when it meets the requirements of the Specifications can the GPS system be used for the surveying. Otherwise the fixed deviation correction must be done [5].

1.2 The test of the marine magnetometer

The marine magnetometer system consists of tow sensor (tow fish), electronic part of the sensor,

main frame and tow cable. The testing methods for the marine magnetometer have been studied with the example of the G881 cesium marine magnetometer developed by the Geometrics. Inc [6].

1.2.1 The items and requirements of the magnetometer test

a) The noise level, sensitivity, accuracy and operating range.

b) The system is in good shape, the sensitivity(technical index is 0.01 Nt) of the measured items must be 1Hz-0.004 nT, 5Hz-0.01 nT, 10Hz-0.02 nT. The maximum dithering intensity is 0.36 nT., less than 0.1 nT.

c) The S/N ratio in static mode is less than 50.

d) The heading error is less than ±1.0 nT.

1.2.2 The static and dynamic tests of the magnetometer

After debugging, the working persistence of the magnetometer must be tested, which includes the static and dynamic tests.

1.2.2.1 The static test of the magnetometer

Only has the marine magnetometer been installed on the surveying vessel, can the static test be done [7]. During the test, the other systems must be powered off. The duration and the static test must be more than 24 hours, the interval of the sampling is less than 10 seconds, the local variation of the observed data must be less than 0.5 nT.

The static precision of the marine magnetometer can be calculated by the observed data. The formula is shown as below.

$$S_n = \sqrt{\frac{1}{n-1}\sum_{i=1}^{n}\left(B_i' - \bar{B}'\right)^2} \qquad (3)$$

Where, $B_i' = (T_{i-2} - 4T_{i-1} + 6T_i - 4T_{i+1} + T_{i+2})/16$ and $\bar{B}' = \frac{1}{n}\sum_{i=1}^{n} B_i'$.

The evaluating index S_n of the static precision are shown in (Tab.2).

Tab.2 The evaluating index of the static precision (Unit : nT)

Class1	Class2	Class3	Class4
0.01	0.011 - 0.03	0.031 - 0.1	more than 0.1（unqualified）

According to Tab.2, we cam evaluate the static precision of the marine magnetometer, if it meets the requirements of the task, the magnetometer can be applied in the survey. Otherwise a re-test must be done.

1.2.2.2 The dynamic test of the magnetometer

To assure that the dynamic precision of the magnetometer can meet the requirements of the task, and the magnetic influence of the surveying vessels be eliminated, the test for the dynamic stability of the magnetometer and the magnetic influence of the surveying vessels must be done.

1) Test for the dynamic stability of the magnetometer

The test area must be chosen in the surveying area, and the gradient of the magnetic anomaly must be less than other areas. The variation of the depth in the test area must be ess than 20 meters and have smaller wind and current. The turning of the surveying vessel, the underwater barriers and the fishing nets must be considered. During the test, the surveying vessel must sail linearly at constant speed. The abrupt turning and large change of the speed must be avoided. The interval of the sampling must be less than 10 seconds and the duration of the test must be more than 30 minutes. After removing the recorders which are more than 100nT/km in the horizontal gradient of the whole surveying line, the dynamic precision of the magnetometer can be obtained by the formula below.

$$S_i = \frac{1}{\sqrt{70}} \sqrt{\frac{1}{n-1} \sum_{i=1}^{n} \left(B_i - \bar{B}\right)^2} \qquad (4)$$

Where, $B_i = T_{i-2} - 4T_{i-1} + 6T_i - 4T_{i+1} + T_{i+2}$ and $\bar{B} = \frac{1}{n} \sum_{i=1}^{n} B_i$, n is the total number of the recorders, B_i is the fourth order difference of the observed magnetic anomaly value in the point i.

The evaluation index S_i of the dynamic precision is shown in Tab.3.

Tab. 3 The evaluation index of the dynamic precision Unit / nT

Class1	Class2	Class3	Class4
8.0 S_n	8.1 - 14.0 S_n	14.1 - 20.0 S_n	more than 20.0 S_n (unqualified)

According to Tab.3 we can evaluate the dynamic precision of the marine magnetometer, if it meets the requirements of the task, the magnetometer can be applied in the survey. Otherwise a re-test must be done. In addition, the data quality and the signal intensity of the magnetometer must be checked at different vessel speeds.

2) Test for the magnetic influence of the surveying vessels

The test for the magnetic influence of the surveying vessels includes the test for the optimum depth of the tow-fish and tow cable length, the magnetic influence of the surveying vessels in eight azimuths. The test area is chosen on the same condition as in the dynamic test of the magnetometer.

a) Test for the optimum depth of the tow-fish and tow cable length

The depth of the tow-fish and tow cable length of the magnetometer must be determined through the test in different surveying areas with different surveying vessels and different magnetometers. Testing methods are described as below:

We can change the tow cable length when the surveying vessel keeps cruising along the magnetic meridian. The noise of the magnetometer will be increased with the cable length. The optimum tow cable length can be determined when the dithering intensity of the magnetometer tends to be invariable. For the stability of the tow-fish (sensor), the nonmagnetic clog must be installed on the sensor according to the vessel speed. The optimum depth of the tow-fish can be determined by the quality of the recorders.

b) Test for the magnetic influence of the surveying vessel in eight azimuths

A base mark in the testing area must be selected and a nonmagnetic buoy set on it. In the test, eight surveying lines are planned to pass through the base mark. During the test, the course of the surveying vessel must be kept in line with the sensor, the bow and the stern of the vessel passing through the base mark. We can obtain the magnetic field data when the sensor passes through the base mark. After subtracting the geomagnetic diurnal variation, the curve of the magnetic influence of the surveying vessels in different azimuths can be obtained. To ensure the precision of the curve, the test must be done about 3 times. The heading error of the vessel must be less than 10 degrees and the standard deviation σ of the observed data must be less than 4nT. The formula is shown as below.

$$\sigma = \sqrt{\frac{1}{7}\sum_{i=1}^{8}(T_i(\alpha) - T_0)^2} \tag{5}$$

Where, $T_O = \frac{1}{8}\sum_{i=1}^{8}[T(\alpha_i) + \Delta T(\alpha_i)]$ is the mean value of the eight azimuths. T_0 is the base value of the magnetic influence of the surveying vessels, $T(\alpha_i)$ is the observed value in different azimuths. $\Delta T(\alpha_i)$ is the correction of the geomagnetic diurnal variation during the test.

1.3 The test of the ground-based magnetometer system

The strict requirements are also required for the selection of the monitor station for the geomagnetic diurnal variation and the ground-based magnetometer in the marine geomagnetic survey. The testing methods have been studied with the example of the HC-90D helium magnetometer[8].

1.3.1 The selection of the monitor station for the geomagnetic diurnal variation

The monitor station should be built as far as possible in the center of the surveying area, and can control the geomagnetic diurnal variation of the whole surveying area. The applicability distance of the monitor station is given out in the Specifications, as shown in Tab.1. If the surveying area is large enough, two or more monitor stations are needed. The horizontal gradient of the magnetic field around the monitor station must be less than 1.0nT/km.

1.3.2 Test for the ground-based magnetometer system

The ground-based magnetometer system consists of helium magnetometer, data collection system

and power source. The precision of the ground-based magnetometer must match the marine magnetometer.

The items and requirements of the ground-based magnetometer test

a) The fittings of the system must be complete and in good shape.

b) The static index of the system must match the marine magnetometer.

c) The heading of the sensor must be set the same as the magnetic inclination

d) The S/N ratio in static mode is less than 50. The dithering intensity is less than 0.1 nT.

e) The clock of the system must synchronize with the marine magnetometer.

In addition, the stability test of the ground-based magnetometer must be done. The test method is also the same as the marine magnetometer.

2 Examples

The validity of the testing methods is testified by the following examples.

In an offshore magnetic survey, there has been no obvious magnetic anomaly in the surveying area. The range of the values is between 46 000 – 47 000 nT, the magnetic inclination is about 56 degrees. The requirements of the task are planned in light of the Specifications, which are shown in Tab.4.

Tab. 4 The requirements of the surveying task

Surveying class	The property of the surveying area	Precision of positioning	Positioning mode	Precision of the magnetic field survey	Precision of magnetometer	Precision of ground-based magnetometer	The applicability distance of the monitor station
Class.1	Key passage (channel)	± 5 m	differential positioning	±2.0 nT	Less than 0.1 nT	±0.01 nT	50 km

Based on the requirements of the surveying task, the NGD-60 differential positioning system and the G881 cesium marine magnetometer system are selected. The HC-90D helium magnetometer system is used as ground-based magnetometer.

The main technical performances have been checked before the surveying according to the requirements, and the static and dynamic tests are also done according to the detailed method above.

2.1 The static stability test of the GPS

The receiver type is H/HCZ-02B, the level of the control point is first-class for the hydrographic survey, the coordinates of the point X=××°57′05.143″, Y=××°41′59.564′. The time interval of the test

was from 11:38 to 21:38 of May 24th in 2004. The sampling interval was 3 minutes. Part of the recorders was shown in Tab.5.

Tab. 5 The recorders of GPS static test

Time	Latitude	Difference of latitude	Longitude	Difference of longitude
11:38:48	57′05.095″	-0.032″	41′59.588″	0.021″
11:41:48	57′05.119″	-0.008″	41′59.576″	0.009″
11:44:49	57′05.089″	-0.038″	41′59.582″	0.015″
…	…	…	…	…
21:32:02	57′05.119″	-0.008″	41′59.558″	-0.009″
21:35:03	57′05.149″	0.022″	41′59.558″	-0.009″
21:38:03	57′05.155″	0.028″	41′59.558″	-0.009″
Mean	57′05.127″		41′59.567″	
Max	57′05.401″	0.274″	41′59.138″	-0.429″

The mean values of the coordinates are $\bar{X} = \times\times°57'05.127''$, $\bar{Y} = \times\times°41'59.567'$. The precession of longitude and latitude data can be determined by the expression (1), and $\sigma_B = \pm 0.0006$, $\sigma_L = \pm 0.0013$. So the static precision can be obtained $\sigma = \pm 0.0014$. Compared to the Specifications, the precision calculated meet the requirements of the surveying task. So the magnetometer can be used in the surveying task.

2.2 The static and dynamic tests of the magnetometer

2.2.1 The static test of the magnetometer

The magnetometer was installed on the existent station, the time interval of the test was from 10:27 of 20th to 21:38 of 21st in May 2004. The sampling interval was 10 seconds. There were 8752 recorders. Part of the recorders were shown in Tab.6 and the curve of the magnetic field strength was shown in Fig.1.

The static precision of the magnetometer was obtained through the recorders using the expression (3) and $S_n = 0.0287nT$, which was less than the required 0.036nT given by the Specifications. The local variation of the value was less than 0.5nT between 10 seconds. The conclusion was that the magnetometer is qualified.

2.2.2 The dynamic test of the magnetometer

The testing area lies in the surveying area without fishing nets and underwater barriers. The mean depth of the testing area is 25 meters. During the test, the speed of the surveying vessel was 8 knots and the surveying track keeps a line. The sampling interval of the magnetometer was 1 second, and the time interval of the test was from 10:30 to 10:58 of 22nd in May 2004. The total number of the recorders was 1628 in the whole track. Part of the recorders were shown in Tab.7 and the curve of the magnetic field strength was shown in Fig.2.

Tab.6 The recorders of magnetometer static test (Unit: nT)

Time	Magnetic field value	Time	Magnetic field value
10:27:48	47623.031	21:32:30	47640.819
10:27:58	47623.160	21:32:40	47641.006
10:28:08	47623.420	21:32:50	47641.093
...		...	
21:32:02	47640.970	13:34:22	47621.777
21:32:11	47640.939	13:34:30	47621.166
21:32:21	47640.888	13:34:39	47621.685

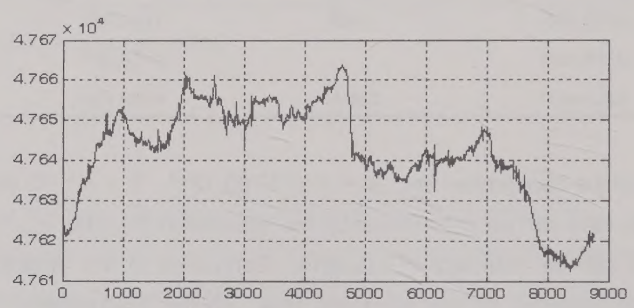

Fig.1 The curve of magnetic field strength

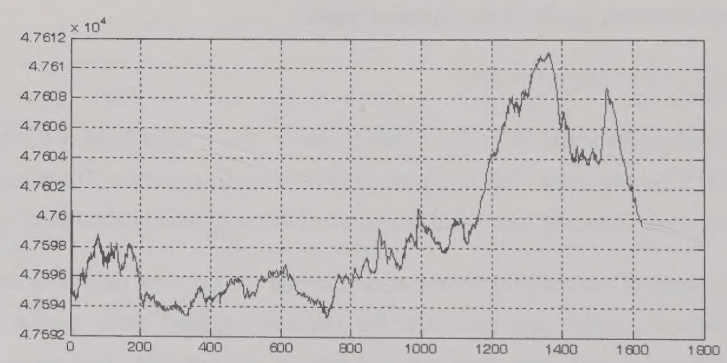

Fig.2 The curve of magnetic field strength

2.2.3 Tests for the magnetic influence of the surveying vessels

Two tests for the influence of the surveying vessel in eight azimuths were done, respectively before and after surveying. The tow cable length chosen was 3 times the surveying vessel's length(about 210 meters), the depth of the tow-fish chosen was about 5 meters under the surface. After subtracting of the normal magnetic field and the diurnal variation during the test, the magnetic influence of the surveying vessels was shown in Tab.8.

Tab.7 The recorders of magnetometer static test (Unit: nT)

Time	Magnetic field value	Time	Magnetic field value
10:30:48	47600.798	10:45:53	47599.663
10:30:49	47600.8250	10:45:54	47599.560
10:30:50	47600.352	10:45:55	47599.520
…		…	
10:45:50	47600.123	10:58:13	47599.651
10:45:51	47599.918	10:58:14	47599.539
10:45:52	47599.826	10:58:15	47599.441

Tab. 8 The result of the test (Unit: nT)

No	Azimuth	Before surveying	After surveying	Mean value
1	0º	-163	-161.8	-162.4
2	45º	-162.5	-162.5	-162.5
3	90º	-162.5	-166.5	-164.5
4	135º	-164.4	-163.2	-163.8
5	180º	-162.7	-163.2	-163.0
6	225º	-164.7	-164.2	-164.5
7	270º	-164.4	-165.3	164.8
8	315º	-163.3	-162.7	-161.9

The standard deviations are respectively $\sigma = 2.17$ nT before surveying and $\sigma = 2.25$ nT after surveying, with a mean value $\sigma = 1.71$ nT. The result meets the requirement that the value be less than 4 nT. So the results can be used in the later data processing for correcting the influence of surveying vessel. The curve of the correction value for the influence of surveying vessel is shown in Fig.3.

In Fig.3, the coordinate X means the azimuth of the surveying vessel in degree, the coordinate Y means the observed magnetic anomaly caused by the surveying vessel.

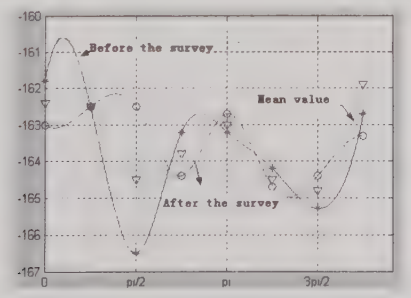

Fig.3 The curve of the correction value for the influence of surveying vessel

2.3 The establishment of the monitor station and test for the ground-based magnetometer

The monitor station was about 50 km away from the surveying area. The coordinates of the station was X=××°35.7′, Y=××°52.0′. No ferromagnetic disturbance was found near the monitor station. The gradient of the magnetic field around the monitor station is less than 1.0 nt/km. The technical performance index of ground-based magnetometer has been checked according to the manual for the HC-90D helium magnetometer. At last, the test for the stability of the magnetometer was done with the sampling interval of 10 seconds and the time interval of 24 hours. Part of the recorders are shown in Tab.9 and the curve of the geomagnetic diurnal variation is shown in Fig.4.

Tab.9 The recorders of static test for the ground-based magnetometer (Unit: nT)

Time	Magnetic field value	Time	Magnetic field value
00:00:48	46997.550	12:00:30	46957.79
00:00:58	46997.520	12:00:40	46957.66
00:01:08	46997.490	12:00:50	46957.48
...		...	
12:00:00	46957.89	12:00:01	46987.89
12:00:10	46957.82	12:00:02	46987.89
12:00:20	46957.86	12:00:03	46987.88

The characteristics of the geomagnetic diurnal variation are reflected in Fig.4 and the local variation of the value is less than 0.5 nT between 10 seconds. The static precision of the magnetometer $\sigma = 0.022$ nT, which is less than 0.036 nT as required by the Specifications. The conclusion shows that this magnetometer is qualified for this surveying task.

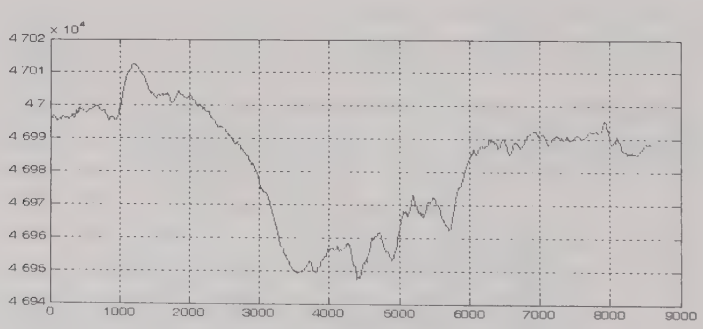

Fig.5 The curve of the geomagnetic diurnal variation

3 Conclusions

To ensure the precision and reliability of the survey, the test of instrumental system must be done before the surveying. The testing items of each system and the static/dynamic testing methods have been

studied. The conclusions show that the methods can effectively eliminate the systematic error caused by the instrumental system, and greatly improve the surveying precision and the reliability of the survey results.

References

[1] Liu Y C, Zhai G J, Huang M T. The Development and Trend of the Military Marine Geomagnetism Surveying [J]. Hydrographic Surveying and Charting.2001, (12): 1-4.

[2] M.N.Nabighian, V.J.S.Grauch. The Historical Development of the Magnetic Method in Exploration [J]. Geophysics. 2005(6): 33-61.

[3] Jin X L. The Technology Development of the Marine Physical Geography [J]. Journal of Institute of Technology . 2004,27 (1): 6-13.

[4] The Criteria of Marine Geological Survey, the Specification for oceanographic survey-Marine geology and geophysics investigation [M]. Beijing: China Criteria Press. Chinese Supervisor Bureau for Quality Technique. 1993.

[5] The criteria of hydrographic survey [M]. Beijing: China Criteria Press. Chinese Supervisor Bureau for Quality Technique .1999.

[6] The Manual for G-880 Cesium Marine Magnetometer Operation. Geometrics, Inc. 1997.

[7] The Criteria of Aeromagnetic Survey. Beijing: The Bureau of Geology and Mineral.1995.

[8] Yao J J, Xu H Z, Sun Y. The Principle and Operation of HC-90D helium magnetometer [J]. Hydrographic Surveying and Charting. 2003, 23(6): 18-20.

海洋磁力测量仪器系统检验方法研究

边刚，刘雁春，于波，肖付民，卞光浪

（海军大连舰艇学院海测工程系，辽宁 大连 116018）

摘 要：高精度的海洋磁力测量对磁测仪器系统的测量精度提出了更高的要求，文中对海洋磁力测量仪器系统检验的内容和动静态检验方法进行了研究，并通过实例验证其可行性。结论表明：所提出的仪器系统检验方法可以消除仪器系统误差的影响，提高海洋磁力测量精度，保证成果的可靠性。

关键词：海洋磁力测量；仪器系统；检验方法

Application of BDRM Theory in the Two-AXIS Underwater Channel

ZHANG Lin, DA Lianglong, LU Xiaoting

Underwater Acoustics Data Center, Navy Submarine Academy, Qingdao 266071, *Shandong, China*

Abstract: Two-axis underwater channel often exists in deep ocean. Because of the coupling between surface channel and SOFAR channel, sound propagation in the two-axis underwater channel is complex and so its calculations of acoustic fields are difficult. The beam-displacement ray-mode (BDRM) theory is a normal mode method for propagation modeling in the common horizontally stratified shallow water. We improve the theory, proposing a new method for computing the upper boundary reflection coefficient, and apply it to calculate the acoustic fields of two-axis underwater channel. Transmission losses in the two-axis underwater channel are calculated by the BDRM theory. The results are in good agreement with the KRAKEN code and the computational speed excels those of the other methods.

Keywords: two-axis underwater channel; BDRM theory; reflection coefficient; phase-shift correction

Introduction

Sound propagation problems in deep ocean have interested us for a long time and we have been looking for not only fast but also accurate methods for computing acoustic fields.

SOFAR channel and two-axis underwater channel are two typical environments in the deep ocean. The sound fields of SOFAR channel have been predicted by the WKBZ mode approach accurately and efficiently. Because of the coupling between surface channel and SOFAR channel, sound propagation in the two-axis underwater channel is complex. YAN Jin extends the WKBZ approach and applies it to deal with the sound propagation in the two-axis underwater channel [1]. In this paper, on the basis of the WKBZ eigenfunction, the expression of upper boundary reflection coefficient is proposed, and in order to solve the speed and precision problems, the beam-displacement ray-mode(BDRM) theory [2] is applied to calculate the sound fields of two-axis underwater channel.

1 Beam-displacement ray-mode (BDRM) theory

The beam-displacement ray-mode theory is an effective method for computing acoustic fields in shallow water. The advantages of this theory are not only fast and accurate, but also that the boundary effects on the acoustic fields can be expressed by the equivalent boundary reflection coefficient.

Received on August 27, 2005

In the common horizontally stratified water, the sound field excited by a harmonic point source can be expressed as a sum of normal modes:

$$p(r,z_s,z;\omega)=\sqrt{\frac{8\pi}{r}}e^{i\pi/4}\sum_l \Phi(z_s,\nu_l)\Phi(z,\nu_l)\sqrt{\nu_l}e^{i\mu_l r-\beta_l r} \tag{1}$$

where $\nu_l=\mu_l+i\beta_l$ is the complex eigenvalue, the real part μ_l is the horizontal wavenumber, and the image part β_l is the mode attenuation. The eigenfunction $\Phi(z,\nu_l)$ satisfies

$$\frac{d^2\Phi(z,\nu_l)}{dz^2}+(k^2(z)-\nu_l^2)\Phi(z,\nu_l)=0 \tag{2}$$

and its boundary conditions. The eigenfunction between the the upper and lower boundaries can be expressed by the generalized phase integral (WKBZ) [3].

The eigen-equation of the normal mode can be expressed as

$$2\int_{\zeta_{l1}}^{\zeta_{l2}}\sqrt{k^2(z)-\mu_l^2}\,dz+{}_1(\mu_l)+{}_2(\mu_l)=2l\pi,l=0,1,\cdots, \tag{3}$$

and

$$\beta_l=\frac{\ln|V_1(\mu_l)V_2(\mu_l)|}{S(\mu_l)+\delta_1(\mu_l)+\delta_2(\mu_l)} \tag{4}$$

where $\varphi_1(\mu_l)$ and $\varphi_2(\mu_l)$ are the phases of the reflection coefficients on the upper and lower boundaries. $S(\mu_l)$ is the cycle distance of eigen-ray, $\delta_1(\mu_l)$ and $\delta_2(\mu_l)$ are the beam displacements of the eigen-ray on the upper and lower boundaries.

By partial differentiation with respect to μ and ω on the equation (3), the mode group velocity can be obtained as

$$v_l=\frac{\partial\mu_l}{\partial\omega}=\frac{S(\mu_l)+\delta_1(\mu_l)+\delta_2(\mu_l)}{T(\mu_l)+\tau_1(\mu_l)+\tau_2(\mu_l)} \tag{5}$$

where $T(\mu_l)$ is the travel time along the eigen-ray, $\tau_1(\mu_l)$ and $\tau_2(\mu_l)$ are the time delays corresponding to the beam displacements $\delta_1(\mu_l)$ and $\delta_2(\mu_l)$ at the the upper and lower boundaries.The method using equations (3), (4) and (5) to calculate the sound field is called the beam-displacement ray-mode theory.

2 Method for computing the upper boundary reflection coefficient

Computation of the upper boundary reflection coefficient is the key to the theory, the accuracy of which will affect the calculating precision of eigenvalues directly, and further the accuracy of calculating the acoustic fields.

The upper boundary reflection coefficient can be expressed as $V_1=e^{i\varphi_1(\mu_l)}$. Because the sound speed in the area above the upper boundary changes rapidly, the upper boundary phase-shift $\varphi_1(\mu_l)$ can not be omitted easily or disposed of approximately. In the two-axis underwater channel in Fig.1, according

to the distribution of the horizontal wavenumber μ_l, the normal modes can be divided into two kinds. One is called reversed normal modes, the eigenrays of which are reversed below the upper boundary, that is $\mu_l \geq k_0$; The other is called reflected normal modes, the eigenrays of which are reflected at the upper boundary, that is $\mu_l < k_0$, where k_0 is the wavenumber at the upper boundary.

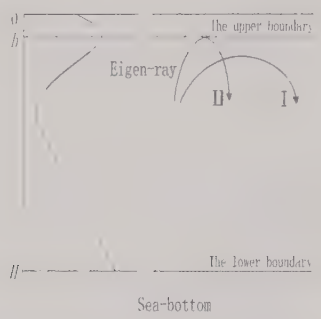

Fig.1 Two-axis underwater channel

For the normal mode Ⅰ, the phase-shift function $\varphi_1(\mu_l)$ of the upper boundary reflection coefficient can be expressed as [4]

$$\varphi_1 = \begin{cases} \dfrac{\pi}{2} + \arctan\left(\dfrac{Ai(t)}{Bi(t)}\right) + \arctan\left(\dfrac{Ai'(t)}{Bi'(t)}\right) & t \geq 0 \\ \dfrac{\pi}{2} + \arctan\left(\dfrac{Ai(t)}{Bi(t)}\right) + \arctan\left(\dfrac{Ai'(t)}{Bi'(t)}\right) - 2\omega_0 & t < 0 \end{cases} \tag{6}$$

where $t = \dfrac{\mu_l^2 - k_0^2}{b_0^{2/3}}$, $b_0 = \left|\dfrac{dk^2(z)}{dz}\right|_h$, $\omega_0 = \dfrac{2}{3}|t|^{3/2}$, $Ai(t)$ and $Bi(t)$ are Airy functions respectively. In fact, because of $\mu_l \geq k_0$ for the normal mode Ⅰ, the phase-shift function $\varphi_1(\mu_l)$ only uses the part of $t \geq 0$. Fig.2 is the curve of phase-shift function φ_1 for $-10 \leq t \leq 10$.

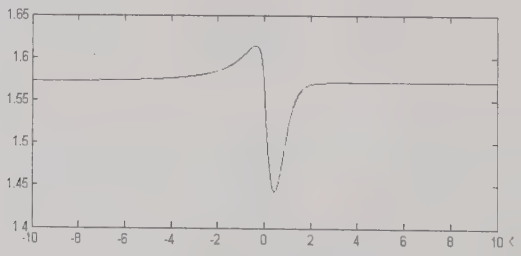

Fig.2 The curve of phase-shift function φ_1 of t

For the normal mode Ⅱ, the phase-shift function $\varphi_1(\mu_l)$ can be acquired by means of eigenfunction continuity at the upper boundary. The area for $0 \leq z \leq h + dh$ is divided into n+1 equidistant grids, and the width of the grid is dh. And the differential form of the wave equation can be expressed as [5]

$$\left\{12+dh^2\left[\frac{\omega^2}{c^2(z_j)}-\mu_l^{\ 2}\right]\right\}\Phi_j=\left\{24-10dh^2\left[\frac{\omega^2}{c^2(z_{j-1})}-\mu_l^{\ 2}\right]\right\}\Phi_{j-1}-\left\{12+dh^2\left[\frac{\omega^2}{c^2(z_{j-2})}-\mu_l^{\ 2}\right]\right\}\Phi_{j-2} \quad (7)$$

where $z_j = jdh$, Φ_j is the value of eigenfunction at the grid j. We assume that the surface is a pressure release boundary and so $\Phi_0 = 0$. We take Φ_1 as a random constant ε' and from the equation (7) we can get Φ_n and Φ_{n+1} at the grid n and the grid n+1. The eigenfunction continuity at the upper boundary can be expressed as [6]

$$\Phi_n = \varepsilon\Phi(h,\mu_l,\varphi_1) \quad (8)$$

$$\Phi_{n+1} = \varepsilon\Phi(h+dh,\mu_l,\varphi_1) \quad (9)$$

where ε is a constant relative to ε', $\Phi(h,\mu_l,\varphi_1)$ and $\Phi(h+dh,\mu_l,\varphi_1)$ are eigenfunctions by use of the WKBZ approximations. We defined that

$$\Delta\alpha = -\int_h^{h+dh}\sqrt{k^2(z)-\mu_l^{\ 2}}\,dz$$

$$\hbar = \frac{\Phi_{n+1}}{\Phi_n}\cdot\frac{\left\{Bb_{h+dh}^{\ 4/3}-Db_{h+dh}^{\ 2/3}\left[k^2(h+dh)-\mu_l^{\ 2}\right]+\left[k^2(h+dh)-\mu_l^{\ 2}\right]^2\right\}^{1/8}}{\left\{Bb_h^{\ 4/3}-Db_h^{\ 2/3}\left[k^2(h)-\mu_l^{\ 2}\right]+\left[k^2(h)-\mu_l^{\ 2}\right]^2\right\}^{1/8}}$$

where B = 2.152, D = 1.619, $b_h = \left|\frac{dk^2(z)}{dz}\right|_h$, $b_{h+dh} = \left|\frac{dk^2(z)}{dz}\right|_{h+dh}$, then from equations (8) and (9) the phase-shift function for the normal mode Ⅱ is

$$\varphi_1(\mu_l) = 2\arctan\left(\hbar\csc(\Delta\alpha)-\cot(\Delta\alpha)\right) \quad (10)$$

In summary, the phase-shift function of the upper boundary reflection coefficient can be expressed as

$$\varphi_1 = \begin{cases}\dfrac{\pi}{2}+\arctan\left(\dfrac{Ai(t)}{Bi(t)}\right)+\arctan\left(\dfrac{Ai'(t)}{Bi'(t)}\right) & \mu_l > k_0 \\ 2\arctan\left(\hbar\csc(\Delta\alpha)-\cot(\Delta\alpha)\right) & \mu_l \le k_0\end{cases} \quad (11)$$

3 Implementation and examples

To illustrate the computational speed and accuracy of the theory, sound transmission losses in the two-axis underwater channel are calculated in this section. The bottom parameters are: bottom speed 1 680 m/s, bottom density 1.8 g/cm^3, bottom absorption 0.6 dB/λ. The sound speed profile is shown in Fig.3, the sea depth is 5000 m and the depth of the surface channel is 75 m.

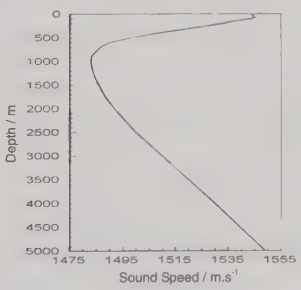

Fig.3 The sound speed profile

The transmission losses for the frequency 200 Hz are calculated by KRAKEN and BDRM [7]. They are shown from Fig.4 to Fig.6, and the transmission losses calculated by KRAKEN and BDRM agree with each other well. The CPU time of BDRM is 0.9 s, while the CPU time of KRAKEN is 24.6 s. And this shows that the application of the BDRM theory in the two-axis underwater channel is effective.

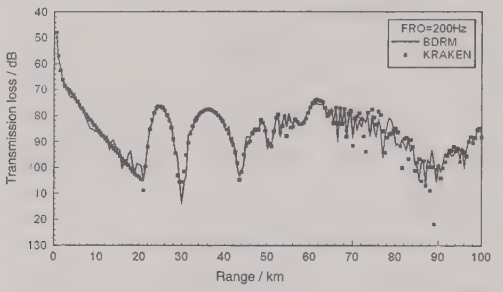

Fig.4 TL vs range, source depth 30 m, receiving depth 30 m

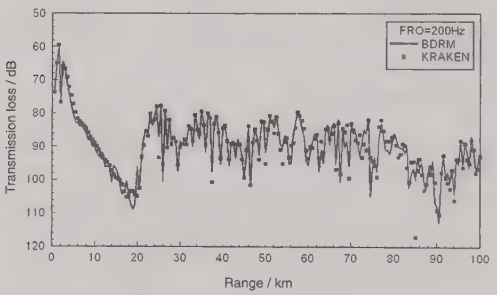

Fig.5 TL vs range, source depth 30 m, receiving depth 300 m

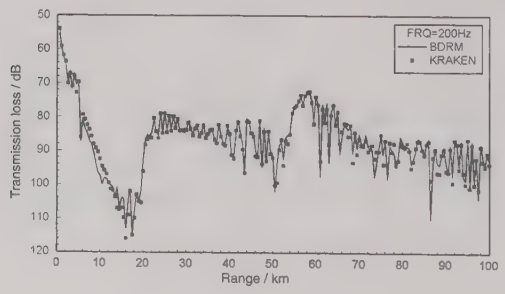

Fig.6 TL vs range, source depth 300 m, receiving depth 300 m

4 Conclusion

Computation of the upper boundary reflection coefficient is very important to calculating the eigenvalues and the WKBZ eigenfunctions. A new method for computing the upper boundary reflection coefficient is proposed in this paper. And we also apply the beam-displacement ray-mode theory to

calculate the transmission losses in the two-axis underwater channel for different frequencies, and the results of comparison with KRAKEN show that applying the BDRM theory to predict the transmission losses in the two-axis underwater channel is effective. What needs to be pointed out is that, because the BDRM and KRAKEN approaches consider only the modes whose phase speeds are less than the bottom speed, the transmission losses from the range 5 to 21 km are a little big.

References

[1] Yan J, Zhang R. The WKBZ mode approach to sound propagation in two-axis underwater channel [J]. Acta acoustica, 1997, 22(3): 209.

[2] Zhang R, Li F. Beam-displacement ray-mode theory of sound propagation in shallow water [J]. Science in China (Series A), 1999, 42(7): 740.

[3] Zhang R, He Y, Liu H. Applications of the WKBZ adiabatic mode approach to sound propagation in the Philippine Sea [J]. J. Sound & Vib., 1995,184(2): 439.

[4] Murphy E L. Modified ray theory for bounded media [J]. The Journal of the Acoustical Society of America, 1974, 56 (6).

[5] Miller J F, Wolf S N. Modal Acoustic Transmission Loss: A Transmission-Loss Computer Program Using Normal-Mode Model of the Acoustic Field in the Ocean[J]. Washington DC: Applied Ocean Acoustics Branch, Naval Research Laboratory, 1980, August 27.

[6] Li F. Beam-displacement ray-mode theory and its application in shallow water[J]. National Laboratory of Acoustics, 2000.

[7] Porter M B. The KRAKEN Normal Mode program[J]. Washington D.C.: Naval Research Laboratory, 1992.

BDRM 理论在双轴海洋声道中的应用

张林，笪良龙，卢晓亭

（海军潜艇学院战术水声数据中心，青岛 266071）

摘 要：由于表面声道与深海声道间的耦合效应，声波在双轴海洋声道中的传播比较复杂，因此求解双轴海洋声道中的声场就比较困难。在 WKBZ 本征函数的基础上，推导出了参考界面相位修正的一致表达式，并将浅海声传播的波束位移射线简正波（BDRM）理论应用于计算双轴海洋声道中的声场，进行了数值模拟并与传统简正波方法进行比较，结果表明应用 BDRM 理论计算的传播损失具有很高的精度和速度，可以对双轴海洋声道内声传播问题进行分析和预报。

关键词：BDRM 理论；双轴海洋声道；传播损失

Research into Uncertainty in Measurement of Seawater Chemical Oxygen Demand by Potassium Iodide-Alkaline Potassium Permanganate Determination Method

ZHANG Shiqiang, GUO Changsong

National Ocean Technology Center, Tianjin 300111, *China*

Abstract: Using the glucose and L-glutamic-acid to prepare the standard substance according to the ratio of 1:1, and the artificial seawater and the standard substance to prepare a series of standard solutions, the distribution pattern of uncertainty in measurement of seawater COD is obtained based on the measured results of the series of standard solutions by the potassium iodide-alkaline potassium permanganate determination method. The distribution pattern is as follows: Uncertainty in measurement is big and not constant at the high end, but small and constant at the low end.

Keywords: potassium iodide-alkaline potassium permanganate determination; COD; uncertainty in measurement

Introduction

Chemical oxygen demand (COD for short) refers to the amount of oxidant converted into the oxygen required for oxidizing the reducing substances in a liter of water under given conditions of reaction. According to China's national standards (GB17378.4) [1], the potassium iodide-alkaline potassium permanganate method is the standard method for determining the COD in seawater. A known excessive amount of potassium permanganate in used as the oxidant, and the solution under alkaline conditions is heated and boiled for 10 minutes to oxidize the reducing substances in the water sample. Then, potassium iodide to reduce the excessive amount of potassium permanganate and manganese dioxide under sulfuric acid conditions. The free iodine produced will be titrated by the sodium thiosulfate standard solution. The COD value of the sample can be calculated by the amount of the sodium thiosulfate standard solution used.

GB17378.4 does not specify the measuring uncertainty and range of this method, and no literature regarding the measuring uncertainty and range of this method is available. Some literature specifies that the measuring range of another method for measuring the COD in seawater --- the sodium oxalate-alkaline potassium permanganate method --- is: 0.5 mg/L-4.5 mg/L. The lower measurement limit is 0.5 mg/L. Measurement is repeated on the sample whose COD value is 2.5 mg/ L. It is calculated that the related standard deviation within the laboratory is 4.0 % (standard deviation equal to 0.10 mg/ L) and

Received on March 22, 2007

the related standard deviation between laboratories is 6.3 % (standard deviation equal to 0.16 mg/ L)[2]. However, this literature does not point out the error distribution pattern of this method throughout the whole range of measurements. Assessment of the uncertainty in the measurement of seawater COD by the potassium iodide-alkaline potassium permanganate method requires an accurate understanding of the measuring range of this method as well as the distribution pattern of uncertainty in the measurement within this range. This paper will make an exploration into this issue.

1 Experimental method

Sample: Use glucose and L-glutamic-acid to prepare the "standard substance" according to the ratio of 1:1. Use artificial seawater (with a salinity of 35) to dissolve and dilute it to prepare a series of standard solutions of the "standard substance" with a concentration of 1.50 mg/L, 3.00 mg/L, 6.00 mg/L, 9.00 mg/L, 12.00 mg/L and 15.00 mg/L respectively. These solutions will serve as the testing samples.

Formula of artificial seawater: 31 g sodium chloride (analytical reagent), 4 g magnesium sulphate ((analytical reagent), adding distilled water until the volume reaches 1 liter.

Blank solution: using distilled water as blank solution.

Method of testing: China's national standard method (GB17378.4), with the test repeated under reproducible conditions.

2 Analysis of experimental results

2.1 Experimental results

Tab. 1 Experimental Results (Unit: mg/L)

Concentration of standard sample	Measured value	Average value	Standard deviation	Related standard deviation
0.00	0.01;0.00;-0.02;-0.02;0.01;0.00;	0.00	0.014	/
1.50	0.59;0.61;0.73;0.72;0.77;0.68;	0.68	0.071	10.4%
3.00	1.49;1.35;1.45;1.45;1.45;1.41;	1.43	0.048	3.2%
6.00	2.70;2.89;2.78;2.83;2.88;2.87;	2.82	0.074	2.6%
9.00	3.80;3.74;3.91;3.87;3.71;3.80;	3.80	0.076	2.0%
12.00	4.73;4.80;4.85;4.69;4.57;	4.73	0.108	2.3%
15.00	5.09;5.18;5.23;5.31;5.46;5.30;	5.28	0.127	2.4%

2.2 Measuring range of the potassium iodide-alkaline potassium permanganate determination method

As can be seen in Fig.1, which is a curve drawn according to the experimental results of a series of

standard solutions, the measured value of COD has a nonlinear relationship with the standard substance concentration. Especially in the section where COD value is above 4 mg/L, the curve is bent (see Fig.1). This is consistent with relevant reports. This is mainly because when measuring high-concentration samples, the amount of Potassium Permanganate consumed is too large and its ability of oxidation declines. At the section where COD value is bigger than 4 mg/L, along with increase in the COD value of the samples, the curve bends downwards, the sensitivity of measurement decreases and the absolute error of measurement rises sharply (see Fig.2). Different grades of seawater quality differ from each other only by 1 mg/L in terms of the COD index [5]. As a result, a relatively high degree of accuracy is required for the measurement of seawater COD. In order to accurately assess the grade of seawater quality, the expanded uncertainty of seawater COD measurement should be less than 0.20 mg/L (the expanded factor k=2). In other words, the standard uncertainty should be less than 0.10 mg/L.

As can be directly seen from Fig.2, the COD value of samples whose standard uncertainty (standard deviation) is about 0.10 mg/L should be between 3.80 mg/L and 4.73 mg/L. Based on the test results presented in Tabl.1, it can be calculated by means of the interpolation method that the COD value of the sample with a standard uncertainty of 0.10 mg/L is 4.50 mg/L. Therefore, it can be determined that the upper measurement limit of the potassium iodide-alkaline potassium permanganate method in measuring seawater COD is 4.50 mg/L in order to ensure that the expanded uncertainty is less than 0.20 mg/L (k=2).

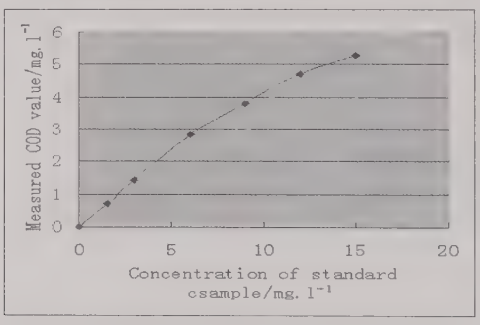

Fig.1 Standard curve of the potassium iodide-alkaline potassium permanganate determination method based on actual experimental results

It should be specially pointed out that the uncertainty in the measurement of the potassium iodide-alkaline potassium permanganate determination method for the distilled water (with a COD value of 0.00 mg/L) is very small. The standard deviation is only 0.014 mg/L. It is the point with the smallest uncertainty among all measuring points. This is more than sufficient for meeting the requirement that the standard uncertainty is less than 0.10 mg/L. Therefore, the lower measurement limit of the potassium iodide-alkaline potassium permanganate determination method for measuring seawater COD is 0.00 mg/L.

To sum up, in order to meet the requirement that the standard uncertainty is less than 0.10 mg/L, the measuring range of the potassium iodide-alkaline potassium permanganate determination method for

measuring seawater COD is 0.00 mg/L-4.50 mg/L. The author of this paper has made some investigation and research about areas in the north part of East China Sea. The COD value of seawater in these areas is usually about 1 mg/L. Only in aquatic breeding areas, port areas and around sewage discharge outlets is the COD value somewhat higher, but it generally does not exceed 5 mg/L. Such is also the case in areas in the south part of East China Sea as well as in the South China Sea [6-8]. Therefore, the potassium iodide-alkaline potassium permanganate determination method can meet the requirements for measuring seawater COD in terms of both the measuring range and the measuring uncertainty.

GB17378.4 does not specify whether the samples can be diluted. In the actual operation, high-concentration samples (COD value above 4 mg/L) are all tested after being diluted. This means dilution is the acquiesced method. Only by allowing dilution of high-concentration samples can a relatively good linear relationship be ensured between the measured COD value of high-concentration samples and that of low-concentration samples. When dilution of samples is allowed, theoretically speaking, there is no upper measurement limit. However, along with dilution of samples and increase in the measuring range, the error of measurement will also be multiplied according to the multiply factor of dilution. In practice, the amount of potassium permanganate consumed is generally controlled within 1/2 of the amount of dosage. That is, the actual measured value is controlled within 4 mg/L. Samples whose COD value exceeds 4mg/L should be diluted with distilled water. Samples between 4 mg/L and 8 mg/L should be diluted according to the ratio of 1 ∶ 1 (sample: distilled water). Meanwhile, the error of measurement will double. Samples between 8 mg/L and 12 mg/L should be diluted according to the ratio of 1 ∶ 2 (sample: distilled water). Meanwhile, the error of measurement will increase by two times, and so on and so forth. Dilution by such ratios is just the ideal state. In fact, there does not exist a unique and appropriate ratio of dilution. Therefore, when the concentration of the sample is relatively high, the results of measurement of the same sample may be different for the different ratios of dilution adopted. For a sample whose COD value is 20 mg/L, dilution ratios ranging from 5 to 8 are all appropriate, but the results of measurement may be different. For the same sample, the measured value for a high dilution ratio is usually relatively greater than that for a low dilution ratio. Dilution of seawater sample also lowers the concentration of chlorine ion in the sample. This destroys the properties of the original seawater sample and increases the measuring uncertainty.

Therefore, the dilution method should be adopted for the measurement of high-concentration samples (COD value above 4 mg/L), but the ratio of dilution should not be too high, at most 1 ∶ 2 (sample: distilled water). Therefore, the upper measurement limit when adopting the dilution method can be expanded to 12 mg/L. The standard uncertainty at this time reaches 0.30 mg/L.

3.3 Distribution of uncertainty of the potassium iodide-alkaline potassium permanganate determination method

Distribution diagrams of uncertainty in measurement (see Fig.2 and Fig.3) are made based on standard deviation data and results of calculation and inference. Among these, the values of standard uncertainty (standard deviation) for samples whose COD value is below 6 mg/L are the statistical results of

the actually measured data, and the values of standard uncertainty (standard deviation) for samples whose COD value is above 6 mg/L are the results of calculation and inference based on the actually measured data.

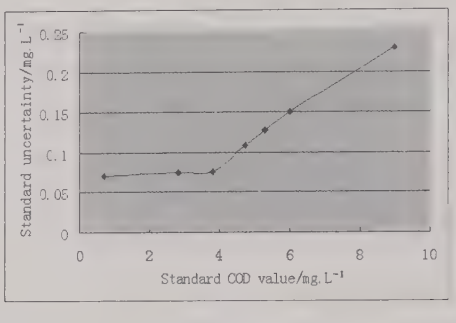

Fig.2 Distribution of uncertainty of the potassium iodide-alkaline potassium permanganate determination method

As can be seen from Fig.2, change in the measuring uncertainty is not significant when COD is below 4 mg/L, and the value remains between 0.07 mg/L and 0.08 mg/L. When COD is above 4 mg/L, the measuring uncertainty rises sharply whether the samples are diluted or not. Especially when the samples are diluted, the uncertainty in measurement increases by the ratio of dilution. See the calculated values of the high-concentration section in Fig.2.

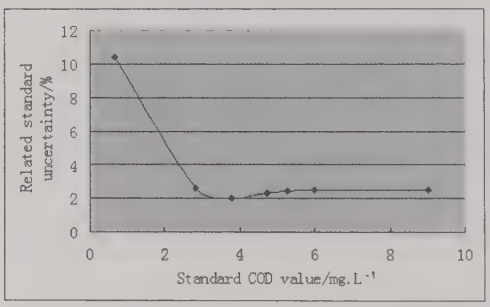

Fig.3 Distribution of related uncertainty of the potassium iodide-alkaline potassium permanganate determination method

As can be seen from Fig.3, the related uncertainty does not change much and remains at about 2 % when COD is above 3 mg/L. However, as COD becomes smaller below 3 mg/L, the related uncertainty rises sharply. Therefore, uncertainty in measurement has a distribution pattern as given in Fig.4. That is, the uncertainty in measurement is big and not constant at the high end, while it is small and constant at the low end. The curve has the shape of a horn. Related uncertainty is just the opposite. It is small and constant at the high end, but big and not constant at the low end. Therefore, the actual conditions can be better reflected if the uncertainty in measurement by the potassium iodide-alkaline

potassium permanganate determination method is represented in different sections. In other words, the low end is represented by the absolute uncertainty; and the high end is represented by the relative uncertainty.

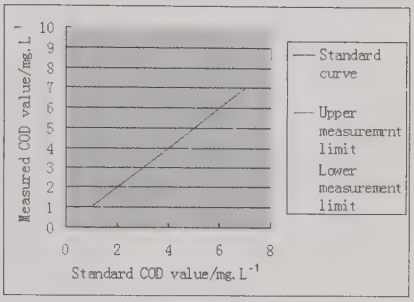

Fig.4 Distribution pattern of uncertainty of the potassium iodide-alkaline potassium permanganate determination method

When dilution of samples is allowed, the expanded uncertainty of the potassium iodide-alkaline potassium permanganate determination method is as reported in Tab.2.

Tab.2 Expanded uncertainty of the potassium iodide-alkaline potassium permanganate determination method

Measuring range	Expanded uncertainty (k=2)
0.00 mg/L - 4 mg/L	0.20 mg/L
> 4 mg/L	5 % of measured result

4 Discussion

Measurement of COD is a typical conditioned reaction. That is, the results of measurement vary along with differences in conditions such as the type of oxidant used, concentration, dosage, ambient temperature, reaction temperature, speed of temperature rise, speed of temperature decrease and time of reaction [3, 4]. GB17378.4 has rigorous specifications regarding the type of oxidant used, concentration and dosage, but its specifications for ambient temperature, reaction temperature, speed of temperature rise, speed of temperature decrease and time of reaction are not as rigorous. The reaction temperature specified in GB17378.4 is 100 ℃ heated to boiling. The speed of temperature rise is higher than the 100℃ boiling water bath and therefore the test takes less time. But it is the major source of uncertainty in measurement for this method. In addition, difficulty in determining the starting moment of boiling is another major source of uncertainty in measurement for this method.

This paper does not adopt the method of assessing the uncertainty in measurement of the potassium iodide-alkaline potassium permanganate determination method by decomposing the

uncertainty into various factors according to the source of uncertainty and then re-synthesizing the factors. Instead, this paper adopts a comprehensive experiment method (A-type assessment), which enables the factors contributing to the uncertainty in measurement to play their role in the experiments and assess the uncertainty in measurement by means of experimental results.

Acknowledgements

The project is supported by the National High Technology Research and Development Program (No. of research topic 2001AA635110).

References

[1] GB17378.4 -1998. The specification for marine monitoring Party 4: Seawater analysis.

[2] Method of Analysis of Environmental Monitoring of State Environmental Protection Administration of China [M]. Beijing: China Environmental Science Press, 1986, 151-153.

[3] Wei Fusheng et al. Guide for Method of Analysis Water and Seawater [M]. Beijing: China Environmental Science Press, 1989, 225-240.

[4] Fu Yunna, Xu Guanghuan. The Investigation of Factors for Influence on alkalinity potassium permanganate determination of COD in Sea Water [J]. Marine Science Bulletin, 1997, 16(5): 43-47.

[5] GB3097-1997 Sea water quality standard.

[6] Cai Qinghai. Distribution of COD in the Sea Areas around Islands in the Southern Fujian [J]. Marine Science Bulletin, 1998, 17 (5): 40-45.

[7] Meng Wei. Qin Yanwen et al. Analysis of Nitrogen, Phosphorus Nutrients and COD in Waters of Yangtze River Estuary [J]. Environmental Science, 2004, 25 (6): 65-68.

[8] Yang Meilan. Lin Qin et al. The Distribution Characteristics of the Concentration of COD in Kaozhouyang Bay [J]. Journal of Zhanjiang Ocean University, 2001, 21 (4): 27-31.

碘化钾碱性高锰酸钾法测量海水化学需氧量不确定度的研究

张世强，郭长松

（国家海洋技术中心，天津 300111）

摘 要：葡萄糖与谷氨酸以 1:1 的比例配制成标准物质，用人工海水和标准物质配制成系列标准溶液，根据碘化钾碱性高锰酸钾法对系列标准溶液的测量结果，获得了海水 COD 测量不确定度在全量程范围内的分布规律，即测量不确定度在高端大不恒定，在低端小恒定。

关键词：碘化钾碱性高锰酸钾法；化学需氧量；测量不确定度

Changes of Water Temperature and Harmful Algal Bloom in the Daya Bay in the Northern South China Sea

YU Jing [1, 2, 3], TANG Danling [1, 2], WANG Sufen [1, 2], LIAN Jiansheng [1], WANG Youshao [4]

1. *Remote Sensing and Marine Ecology / Environment Group (RSMEE), Key Laboratory of Tropical Marine Environmental Dynamics (LED), South China Sea Institute of Oceanology, Chinese Academy of Sciences, Guangzhou* 510301, *Guangdong, China; Lingzistdl@126.com*
2. *Graduate School of the Chinese Academy of Sciences, Beijing* 100039, *China;*
3. *South China Sea Fisheries Research Institute, Chinese Academy of Fishery Sciences, Guangzhou* 510300, *Guangdong, China;*
4. *LED, South China Sea Institute of Oceanology, Chinese Academy of Sciences, Guangzhou* 510301, *Guangdong, China;*

Abstract: Economic development around the Daya Bay, China has profoundly affected the marine environment in the bay area in recent years, particularly since the operation of Daya Bay Nuclear Power Station (DNPS) in 1994. This study analyzed the changes of water temperature and harmful algal blooms (HABs) for two periods: 1983-1993 and 1994-2004, using *in situ* and satellite data. Results showed that yearly mean surface water temperature (SWT) and Chl-*a* concentration (Chl-*a*) increased by 1.1 ℃ and 1.9 mg/m^3, respectively, after 1994. The monthly occurrence of HAB was found to have increased also. HABs appeared only in spring and autumn before 1994, but occurred all the year round after 1994. SWT, Chl-*a* and HABs all increased significantly in May. Those changes were associated with environmental changes in this area, such as thermal discharge from the DNPS and enhancement of eutrophication from human activities around the Daya Bay.

Keywords: water temperature; Harmful Algal Bloom; Chlorophyll *a*; nuclear power station; Daya Bay, China

Introduction

Economic development around the Daya Bay has expanded rapidly since the operation of the first large-capacity commercial nuclear power unit in China (Daya Bay Nuclear Power Station, DNPS) in 1994 (Fig.1A, B). The second nuclear power station (Ling Ao Nuclear Power Station, LNPS) near DNPS also started its first-stage operation in early 2003 (Fig.1A). Other industries such as petrochemical, plastic, printing and harbors are also present. Cage aquaculture along the coastal waters in the bay increased dramatically in recent years and reached 20500 cages in 2004 (http://www.huizhou.gov.cn/).

Investigation in the Daya Bay showed the high temperature effluent from the power station was one

Received on November 13, 2006

of the main artificial impacts. Increase of water temperature and nutrient supply from land-sources may stimulate Harmful Algal Blooms (HABs) [1-4] (Fig.1C, HAB photo was available from: http://www.gdofa.gov.cn/asp/home/index.asp). HABs are regarded as a serious problem throughout the world and have also caused considerable economic loss in the Daya Bay. For example, a HAB caused fish mortality of about 75 tons in March 1983. Another two HABs occurring in August 2000 and August 2003 resulted in losses of about US $370,000 and US $41,000, respectively (http://www.china-hab.cn).

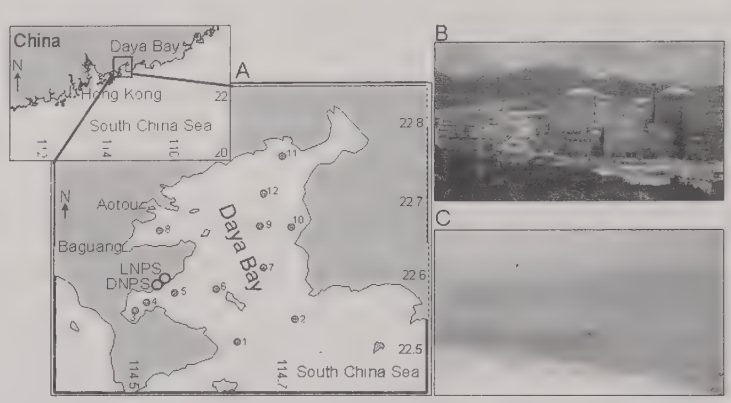

Fig.1 (A) Daya Bay map with Daya Bay Nuclear Power Station (DNPS) and Ling Ao Nuclear Power Station (LNPS) in Dapeng Cove (DC).

The small box indicates the location of Daya Bay in the South China Sea.

Twelve survey stations (indicated by shaded circles) are shown in the Daya Bay.

(B) Photo of DNPS. (C) A Harmful Algal Bloom in the Daya Bay in June 2004.

Daya Bay is an ideal area in which to study and assess impacts of thermal discharge and environmental changes on algal blooms because of its semi-closed shape, suitable size and long-time observation data. It has already received much attention for its environmental changes [5-9]. In this study, we have interest in: What are changes in the surface water temperature (SWT) after the DNPS operation in 1994? How do the changes of water temperature affect Chlorophyll *a* concentration (Chl-*a*) and HAB frequency? In order to answer these questions, historical observations (1970-2005) and satellite remote sensing data (1997-2004) were used to analyze the changes of SWT, Chl-*a* and HAB frequency after the DNPS operation.

1 Research area and methods

1.1 Research area

Daya Bay is located at 22.5ºN-22.9º N, 114.5ºE-114.9º E, covering an area of about 550 km^2 with an irregular coastline and more than 50 islands inside the bay area (Fig.1A). It is rather shallow, with a maximum depth of 21 m and a mean depth of 11 m. Located in a sub-tropical region, Daya Bay's annual

mean air temperature is about 22 °C, with the coldest months in January-February (15 °C) and the hottest months in July-August (28 °C). As a semi-enclosed bay, currents in the Daya Bay are dominated by tides, and the water circulation with the SCS is fairly slow. No major rivers discharge into the Daya Bay [6, 8].

1.2 In situ data collection and analysis

All available data of SWT, Chl-*a* and HABs were collected from relevant references [7, 10-13] and Daya Bay environmental research reports over more than 30 years (1970-2005). Our institute, South China Sea Institute of Oceanology (SCSIO), has also made a series of research surveys over 12 stations in the Daya Bay since 1982 (Fig.1A). These surveys have been conducted in spring (April), summer (July), fall (October) and winter (January) every year, and include measurements of seawater temperature, salinity, pH, biomass of the biota and etc [8].

In this study, we have collected a total of 3188 data from January 1970 to June 2005, including SWT (2331 data during 1970-2005), Chl-*a* (790 data during 1984-2005) and HAB frequency (67 data during 1983-2004). All these data were processed to yield monthly mean values for the entire Day Bay, to compare between two periods: before and after the DNPS operation in 1994.

1.3 Satellite SeaWiFS data

The Sea-viewing Wide Field-of-view Sensor (SeaWiFS) Project provides quantitative data on global ocean bio-optical properties through satellite remote sensing (http://oceancolor.gsfc.nasa.gov/SeaWiFS/). We processed monthly average SeaWiFS-derived Chl-*a* data (1997-2004) with ~1 km spatial resolution for the Daya Bay using the Ocean Color 4-band algorithm [14] through the SeaWiFS Data Analysis System [15] (SeaDAS). Color bars with different scales were used to show Chl-*a* concentrations and distribution in different seasons.

2 Results

2.1 Increase of surface water temperature (SWT)

Comparison for monthly data between the two periods (before and after 1994) showed an increase in SWT (Fig.2A). Before 1994, the lowest SWT was 16.5 °C (January) and the highest SWT was 29.0 °C (July); after 1994, the lowest SWT increased to 17.2 °C (March) and the highest SWT reached 29.7 °C (July and August). The yearly mean SWT was 23.3 and 24.4 °C before and after 1994, respectively, with an increase of 1.1 °C (Fig.2A).

2.2 Changes of Chl-*a* concentration

Chl-*a* concentration increased in every month after 1994 (Fig.2B). Before 1994, the highest Chl-*a* concentration was 2.9 mg/m^3 (June) and the lowest was 1.4 mg/m^3 (January). After 1994, the highest Chl-*a* concentration was found to be 7.2 mg/m^3 (May) and the lowest was 2.3 mg/m^3 (February). The yearly mean Chl-*a* concentration increased from 1.9 mg/m^3 before 1994 to 3.8 mg/m^3 after 1994 with an elevation of 1.9 mg/m^3 (Fig.2B).

Satellite ocean color images derived from SeaWiFS showed the spatial distribution of Chl-*a* in the Daya Bay in January, March, July and October during 1997-2004 (Fig.3). For a better display, color bars with different scales were used to show Chl-*a* in different seasons. High Chl-*a* concentrations were observed in the waters near DNPS in July (indicated by red arrow in Fig.3C), as well as in the coastal waters northwest of Daya Bay (indicated by red circles in Fig. 3) all the year round.

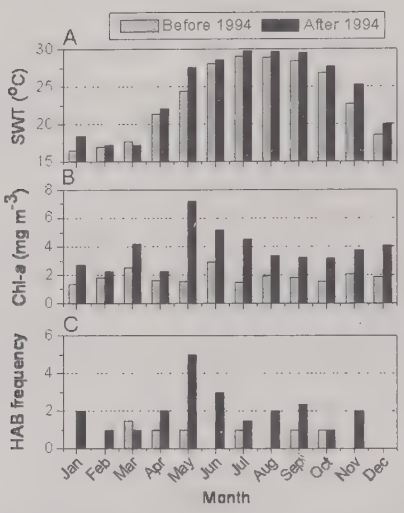

Fig.2 Comparison of (A) surface water temperature (SWT), (B) Chlorophyll *a* (Chl-*a*) and (C) Harmful Algal Bloom (HAB) frequency between two periods: before and after 1994.

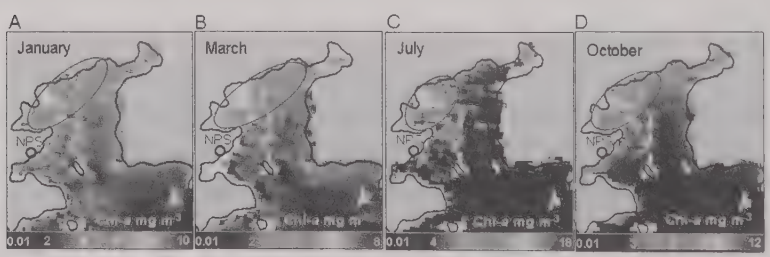

Fig.3 SeaWiFS-derived monthly average Chl-*a* images with ~1km spatial resolution during 1997-2004. (A) January; (B) March; (C) July; (D) October

The black circle indicates the location of nuclear power station (NPS) including DNPS and LNPS.

Red circles indicate cage aquaculture waters in the northwest of Daya Bay.

Red arrow indicates waters with high Chl-*a* concentrations near to the NPS.

2.3 Seasonal change of HAB frequency

Comparison of HAB seasonality between the two periods (before and after 1994) showed HABs lasted for longer seasons after 1994 (Fig.2C). During 1983-1993, HABs appeared mainly in spring and

autumn months; while during 1994-2004, HABs occurred all the year round with the largest increase in May. The occurrence frequency of HAB also increased in most of the months after 1994 (Fig.2C).

2.4 Analysis of water temperature, Chl-a and HAB frequency

In order to understand the relation between the changes of SWT, Chl-*a* and HAB frequency, we compared the difference in monthly SWT (Delta SWT) and Chl-*a* concentration (Delta Chl-*a*) between the two periods: before and after 1994 when DNPS began operation (Fig.4).

Delta SWT (change of monthly mean SWT before and after 1994) ranged from -0.5 ℃ (March) to 3.2 ℃ (May), indicating SWT increased in each month except in March (Fig.4A). Delta SWT was relatively high in winter and spring months (November to May except March) compared to summer months (June to September). Delta Chl-*a* (change of monthly mean Chl-*a* before and after 1994) increased during the DNPS operation, with the largest value of 4.5 mg/m^3 (May) and the smallest value of 0.1 mg/m^3 (April) (Fig.4A). As was shown in (Fig.4A), Delta SWT and Delta Chl-*a* displayed a similar trend in most of the months. Delta HAB (change of monthly mean HAB frequency before and after 1994) ranged from -0.5 (March) to 4 (May) (Fig.4B). Delta SWT showed some positive correlation with Delta HAB (Fig.4B) and Delta Chl-*a* (Fig. 4A). The peak and lowest values of Delta SWT and Delta HAB occurred in the same months (Fig.4).

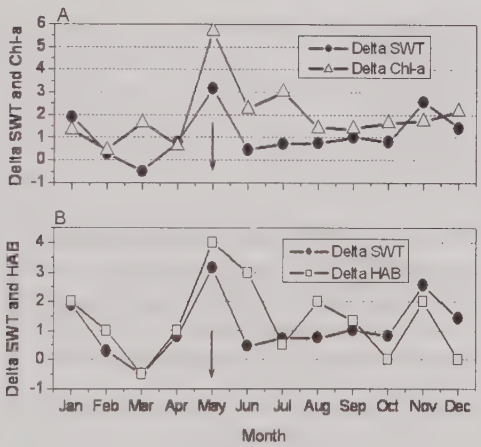

Fig.4 Monthly variations of change in the surface water temperature before and after 1994 (Delta SWT), change in Chl-*a* before and after 1994 (Delta Chl-*a*) and change in HAB frequency before and after 1994 (Delta HAB).

(A) Delta SWT and Delta Chl-*a*; (B) Delta SWT and Delta HAB.

Arrows indicate the month when peak values appeared.

3 Discussion

3.1 Temperature increase and thermal discharge

Our previous study observed the SWT difference between the plume and non-plume area was about

1.5 ℃ in winter and 1 ℃ in summer and fall in the Daya Bay [9]. An early comparison near DNPS between 1991 and 1994 showed that SWT increased by 0.3 ℃ [5]. The present study for a longer period from 1970 to 2005 observed the yearly mean SWT increased by 1.1 ℃ after DNPS operation in 1994 (Fig.2). Daya Bay is a semi-enclosed bay, so its water circulation with the South China Sea is rather slow [8]. And the bay generally has a more amplified response to environmental changes than open water bodies [16-17]. All of these may have contributed to the increases of SWT in the Daya Bay.

We found that changes of SWT (Delta SWT) were less in summer months (June to September) and more in winter months (November to February) (Fig.4), consistent with our previous study for 1998-1999 in the Daya Bay [9]. In summer, the water was stratified under the dominance of weaker southwest monsoon, impact of the high temperature water was limited to the upper layer of water near the discharge point. Therefore, for the entire bay area, the increase of SWT was found less in summer months. But for the area near the outlet of DNPS, the increase of SWT was more significant. During winter, the waters were vertically mixed under the influence of the strong northeast monsoon and SWT in the entire bay area decreased [8]. Therefore, the increase of SWT induced by the thermal discharge in the local waters was more significant.

3.2 Increase of Chl-*a* and HABs related with temperature and eutrophication

Temperature is one of the important environmental variables that affect the survival, growth and reproduction of aquatic organisms [3, 18]. In this study, we verified the close relation between water temperature and Chl-*a* (and HABs) in such a small bay as Daya Bay. Both of Delta SWT and Delta Chl-*a* (or Delta HAB) showed a positive correlation in most of the months (Fig.4), indicating that temperature may have stimulated the algal growth, and thus HAB occurences. Relevant study showed the water temperature increase from the power station would create conditions favorable for the algal growth [19]. In our satellite Chl-a images (Fig. 3C), waters with high Chl-*a* concentrations were observed near DNPS, indicating that the thermal discharge from the DNPS may help the algal growth.

Before 1990, the nutrient level in the Daya Bay was rather low [8]. But in the past decade, increasing cage aquaculture enhanced local eutrophication, particularly for the coastal waters northwest of Daya Bay (Fig. 5) (cage aquaculture data were from http://www.huizhou.gov.cn/). Total inorganic nitrogen ($TIN=NO_3$-N+NO_2-N+NH_4-N; mg/L) also enhanced from 0.021 (1986) to 0.068 mg/L (1999) and kept a relatively high level after 1999 (Fig.5). Satellite Chl-*a* images showed high Chl-*a* areas in the aquaculture waters (Fig.3), indicating the nutrient was partially from cage aquaculture. The nutrient situation in the Daya Bay has experienced a remarkable change in the past 2 decades: N/P ratio increased from 1.5 to 59.8 and the limiting nutrient factor has changed from N to P [7]. The nutrient status has changed from the low level in the 1980s to the middle or even eutrophicated level in some areas of the bay at present. Eutrophication has become an important factor contributing to the annual occurrences of HAB, and it is at least partially responsible for the increase in the frequency and areal extent of HABs.

It was noticed that SWT, Chl-*a* concentration and HAB frequency increased a lot in May after 1994 (Fig.4), indicating May may be a sensitive month for marine ecology and environment. More investigations

and analysis are needed to understand it.

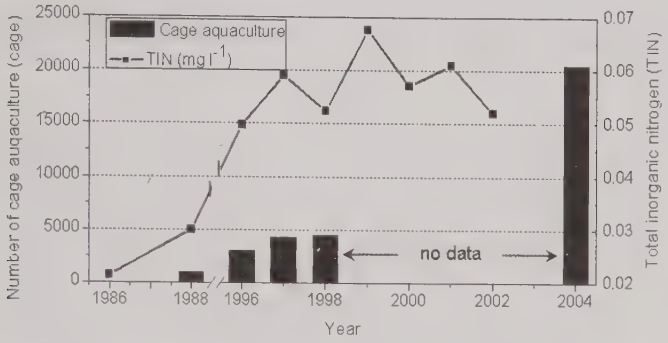

Fig.5 Variation of cage aquaculture and total inorganic nitrogen (TIN) in the Daya Bay from 1986 to 2004

4 Summary

This study analyzed historical observation data for 1970-2005 and satellite remote sensing images for 1997-2004.

(1) Surface water temperature and Chl-*a* concentration increased in the Daya Bay, partly because of the thermal discharge from the DNPS.

(2) HAB frequency increased remarkably after 1994, particularly in May, which was associated with the increasing of water temperature and eutrophication around the Daya Bay.

(3) The marine environment in the Daya Bay has been influenced by human activities.

Acknowledgements

This study was jointly supported by the following funds awarded to Professor Danling TANG: (a) Guangdong Natural Science Foundation (05102008 and 04001306), China; (b) Key Innovation Project of Chinese Academy of Sciences (CAS) (KZCX3-SW-227-3); (c) "One Hundred Talents Program" of CAS (Ybrjh0403). Authors are grateful to projects of South China Sea Fisheries Research Institute, Chinese Academy of Fishery Sciences (2007TS10 and 2007ZD03), High-tech Research and Development Program of China (2006AA100303), Chinese Ecosystem Research Network (http://www.cerndata.ac.cn), Dr. Guifeng WEI of Jinan University and the Key Innovation Project of CAS (KZCX3-SW-214).

References

[1] Tang D L, Kawamura H, Luis A J. Short-term variability of phytoplankton blooms associated with a cold eddy on the North-western Arabian Sea [J]. Remote Sensing of Environment, 2002, 81(1): 82-89.

[2] Tang D L, Kester D R, Ni I –H et al. In situ and satellite observations of a harmful algal bloom and water condition at the Pearl River Estuary in late autumn 1998 [J]. Harmful Algae 2003, 2(2): 89-99.

[3] Tang D L, Kawamura H, Dien T V et al. Offshore phytoplankton biomass increase and its oceanographic causes in the South China Sea. Marine Ecology Progress Series, 2004, 268: 31-41.

[4] Tang D L, Kawamura H, Nhu-Doan H et al. Remote sensing oceanography of a harmful algal bloom off the coast of southeastern Vietnam. Journal of Geophysical Research, 2004, 109, C03014, dio:10.1029/2003JC002045.

[5] Huang X N, Zhu Z H, Xu M C et al. Variation of water temperature in the southwestern Daya Bay before and after the operation of Daya Bay nuclear power plant. In: Pan J P, Wang Z D, Annual Research Reports (II): Marine Biology Research Station at Daya Bay. Science Publishing House, Beijing, China, 1998, 102-112.

[6] Wang W Q, Lu M L, Huang S G. Analysis on relationship among total generation rate of oxygen, biological factors and environment in Daya Bay [J]. Acta Oceanologica Sinica, 1996, 18(2): 57-65.

[7] Wang Y S, Wang Z D, Huang L M. Environment changes and trends in Daya Bay in recent 20 years [J]. Journal of Tropical Oceanography, 2004, 5(23): 85-95.

[8] Xu G Z. 1989. Environments and resources of Daya Bay [M]. Anhui Science Publishing House, Hefei, China.

[9] Tang D L, Kester D R, Wang Z D et al. AVHRR Satellite remote sensing and shipboard measurements of the thermal plume from the Daya Bay, Nuclear Power Station, China. Remote Sensing of Environment, 2003, 84(4): 506-515.

[10] Huang H H, Wang Z D, Zhang Z B et al. Preliminary study on the regional division of the distributions of Chlorophyll-a and nutrients at Daya Bay in autumn [J]. Marine Science Bulletin, 1999, 18: 32-38.

[11] Lin Y S. Researches on phytoplankton near the Daya Bay Nuclear Power Station. In: Jin Q Z, Researches on Daya Bay ecosystem (I), MBRSD (Marine Biology Research Station at Daya Bay), Chinese Academy of Sciences [M]. China Meteorological Press, Beijing, China, 1999, 59-69.

[12] Chen J F, Qi Y Z, Xiao Y Z et al. A new red tide species found *Peridinium quinquecorne Abe* in South China Sea [J]. Marine Environmental Science, 2000, 19: 20-23.

[13] Chen J F, Xu N, Wang Z H et al. Dynamics of *Pseudo-nitzschia spp.* and environmental factors in Daya Bay, the South China Sea [J]. Acta Scientiae Circumstantiae, 2002, 22: 743-748.

[14] O'Reilly J E, Maritorena S, Siegel D A, et al. Ocean color chlorophyll a algorithms for SeaWiFS, OC2, and OC4: Version 4. In: Hooker, S.B., Firestone, E.R., SeaWiFS post launch calibration and validation analyses (Part 3). NASA Goddard Space Flight Center, Greenbelt, Maryland, America, 2000, 9-23.

[15] Baith K, Lindsay R, Fu G et al. SeaDAS: data analysis system developed for ocean color satellite sensors. Eos, 2001, 82: 202.

[16] Fox M F, Kester D R, Andrews J E et al. Seasonal warming of Narragansett Bay and Rhode Island Sound in 1997: Advanced very high resolution radiometer sea surface temperature and in situ measurements [J]. Journal of Geophysical Research-Oceans, 2000, 105: 22071–22082.

[17] Mustard J F, Carney M A, Sen A. The use of satellite data to quantify thermal effluent impacts [J]. Estuarine, Coastal and Shelf Science, 1999, 49: 509-524.

[18] Poornima E H, Rajadurai M, Rao T S et al. Impact of thermal discharge from a tropical coastal power plant on phytoplankton [J]. Journal of Thermal Biology, 2005, 30: 307-316.

[19] Mallin M A, Stone K L, Pamperl M A. Phytoplankton community assessments of seven southeast U.S. cooling reservoirs [J]. Water Research, 1994, 28(3): 665-673.

南中国海北部大亚湾水温和赤潮的变化

余景[1,2,3]，唐丹玲[1,2]，王素芬[1,2]，练建生[1]，王友绍[4]

(1. 中国科学院南海海洋研究所热带海洋环境动力学重点实验室，遥感与海洋生态环境学科组，广东 广州 510301，Lingzistdl@126.com；2. 中国科学院研究生院，北京 100039；3. 中国水产科学研究院南海水产研究所，广东 广州 510300；4. 中国科学院南海海洋研究所热带海洋环境动力学重点实验室，广东 广州 510301)

摘　要：近年来，大亚湾周边的经济和人口快速发展；自 1994 年大亚湾核电站运转以来，大亚湾的海洋环境和生态状况尤其受到关注。本研究利用实测和卫星遥感数据比较和分析了大亚湾水温和藻华在 1983—1993 和 1994—2004 两个时期的变化情况。结果表明：大亚湾核电站运转后（1994—2004）比运转前（1983—1993），年平均表层水温和表层叶绿素 *a* 含量分别升高 1.1 ℃ 和 1.9 mg/m^3；月平均有害赤潮（HAB）的发生次数也有增加；有害赤潮在 1994 年以前只出现在春季和秋季，而在 1994 年以后则全年都有发生；表层水温、叶绿素和有害赤潮发生次数都在 5 月份增加最明显。这些水环境和生态变化与来自大亚湾核电站的热排放以及由于人类活动增加导致的水体富营养化有关。

关键词：水温；有害赤潮；叶绿素 *a*；核电站；大亚湾

Effect of Fouling on Feeding, Oxygen Consumption and Waste Excretion of Pearl Oyster *Pinctada martensii* in Daya Bay Cultivation

SU Zhenxia, YAN Yan, HUANG Liangmin

1. *LED and LAMB, South China Sea Institute of Oceanology, Chinese Academy of Sciences, Guangzhou* 510301, *Guangdong, China;*
2. *Graduate School of the Chinese Academy of Sciences, Beijing* 100039, *China*

Abstract: Biofouling is a particular problem in the pearl oyster culture. It may reduce the growth and survival rates of the cultured species. Foulers are often themselves filter feeders, and are therefore potential competitors for food resource with the cultured species. Fouling organisms may also reduce the oxygen supply. A study was conducted to measure the impact of foulers on feeding, oxygen consumption, and waste excretion. POM, ammonia, phosphate and oxygen concentration were measured in various treatments (cultured species, foulers). This study showed that fouling organisms had significant effect on food uptake, oxygen consumption and waste excretion. The clearance rate, ammonia and phosphate release rate, oxygen consumption rate of the fouled pearl oyster were greater than those of the clean pearl oysters. Other foulers that settled on cages or buoys also contributed much to phytoplankton depletion, oxygen consumption and concentration increase of ammonia and phosphate in water. Therefore, this study showed us that foulers were important competitors in the pearl oyster cultivation of Daya Bay in November 2005.

Keywords: pearl oyster; fouler; oxygen consumption rate; clearance rate; ammonia excretion rate; phosphate excretion rate

Introduction

Cultivation of the pearl oyster, *Pinctada martensii* in the Daya Bay, China, began in the 1960s[1-2] .To date, most researches have concentrated on the research of genetics, seeding, larval biology, farming biology, pearl formation and culture, and pearl species improvement and growth techniques[3-14]. However, there is little published information on the physiological research such as feeding, oxygen consumption and excretion of this species.

Pearl oyster cultures are constantly submerged and become fouled by ascidians, barnacles, bryozoans, filter-feeding gastropods and bivalves. Zheng Chengxing and Zheng Dongqiang (1990, 1991) described various species of fouling organisms attached to the adult *Pinctada martensii*. In the Daya Bay, common members of the pearl oyster culture fouling community included the ascidians *(Styela plicata*,

Received on September 10, 2006

Styela canopus, and *Symplegma oceania),* the barnacle *(Balanus reticulates*, *Balanus cirratus*, and *Balanus trigonus)*, the bivalves *(Ostrea radix*, *Ostrea crenulifera* and *Perna viridis).* However, these studies were concerned with the identification of fouling species rather than determining any effects they may have had on *Pinctada martensi.*

Most fouling organisms are sedentary filter feeders [16-25] settling on the culture equipment or directly on bivalves shells. For fouling organisms that settle on shells, their presence not only competes for food but also increases the weight of shells substantially, which may restrict the opening of the valves and affect feeding [22]. Some fouling organisms such as sponges and burrowing worms can even bore through the shell and damage and weaken the shell or grow between the shells and prevent the pearl oyster from closing completely [26-35]. For species grown in nets or cages, the settlement of fouling organisms not only competes for food but also greatly reduces or restricts the water flow. Consequently, less food is available to individuals and growth is decreased [22-24]. Labor and maintenance costs can also increase greatly.

The aim of this study was to evaluate the uptake of food, release of waste, and the consumption of oxygen by pearl oyster and associated foulers found on culture cages, and also to examine whether the presence of foulers on pearl oyster shell increases the use of oxygen, excretion of ammonia and phosphate, and depletion of phytoplankton.

1 Material and methods

1.1 Sample collection and acclimation

In November 2005, pearl oyster cages were collected from the Daya Bay pearl oyster *Pinctada martensii* culture farm and then transported to the laboratory. Foulers and pearl oysters were carefully removed by hand from cages and placed in individual glass tanks. Foulers included ascidians *Styela plicata*, the barnacle *Balanus reticulates*, the bivalves *Ostrea radix* , *Perna viridis* (fouling mussels *Perna viridis* were collected from buoys). Cultured species of pearl oyster included two different groups: one group was pearl oysters cleaned of fouling organisms; the other was fouled by fouling organisms. Before experiments all groups were maintained in glass tanks for 12-48 h as recommended by Widdows (1993). During acclimation, they were fed daily with laboratory cultured *Platymonas* sp.

1.2 Physiological measurements

1.2.1 Oxygen Consumption (OC) and Ammonia (N) and Phosphate (P) Excretion Rates

Before the experiment, acclimated specimens were kept unfed for 24 h and then individually transferred into glass respiration chambers. Each chamber contained filtered oxygen-saturated sea water and an organism of a particular species. To ensure steady oxygen consumption, specimens were acclimated in the chambers until their valves opened (approximately 10 min). Five considered replicates of each group were performed and a control chamber with no organisms. Specimens were left undisturbed in the chamber for 1~2 h. Oxygen in the water was measured by the Winkler method [37]. Oxygen

Consumption (mgO_2/ (h·ind)) was calculated by the following formula:

$$OC\ (mgO_2/(h\cdot ind)) = V\cdot (O_0 - O_t) / t$$

Where O_t is the oxygen concentration in water (mg/L)) at the end time t, O_0 is the oxygen concentration in chamber without organisms and V is the volume of the respiratory chamber (L). t is the incubation time (h).

The ammonia and phosphate analysis was carried out by collecting water samples from the respiration chambers and from the control chamber without animals. Samples of 500 mL sea water were frozen and ammonia and phosphate concentrations (mg/L) were later determined using the method described in GB 17378.4-1998.

The ammonia and phosphate excretion was calculated by subtracting ammonia and phosphate concentration values of the control chamber from those of experimental chambers. Ammonia and phosphate excretion were expressed in mg / (h·ind).

1.2.2 Clearance Rate (CR)

Individual clearance rate was measured using a statistic experimental system, following the methodology described by Coughlan (1969). 3 L beakers were used for experimental measurements plus one (control) beaker not containing animals.

All beakers containing filtered seawater received a diet of 10-12.4 mgPOM/L of laboratory-cultured *Platymonas* sp. Individual test organisms were placed in each beaker, allowing 15 min for them to open their valves. The test organisms were allowed to filter for 0.5-1 h. Each experiment was conducted on five separate similar size individuals. after which, the final algae concentration was determined. This was done by collecting a water sample of 500 mL from the control and experimental beaker at the end time. Each water sample was filtered onto pre-ashed and pre-weighed Whatman GF/C 47-mm filters, rinsed with distilled water, dried at 70 °C for 24 hours, weighed, and then ashed in a 500 °C muffle furnace for 24 hours and reweighed.

The clearance rate for each individual was calculated using the following formula:

$$CR = (V/t)^* \text{Ln}\ (C_0/C_t)$$

Where: CR, clearance rate; V, volume of water; C_0 and C_t, concentrations at the beginning and end of the test interval t.

1.3 Statistical analyses

Among fouled and clean pearl oyster treatments one factor ANOVA was used to compare differences in clearance rate, oxygen consumption rate, and ammonia and phosphate excretion rate. Significance of all tests was accepted at $p<0.05$.The statistical software SPSS was used.

2 Results

Fouled pearl oysters and the cleaned ones had significant difference in clearance rate (P<0.01), ammonia excretion (P<0.001) rate, phosphate excretion (P<0.001) rate and oxygen consumption rate (P<0.001). The fouled pearl oysters had the highest values of algal intake, oxygen consumption and waste excretion (Figs.1, 2, 3, 4).

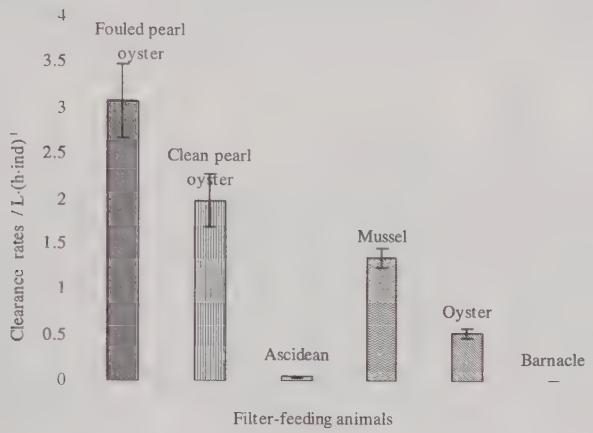

Fig.1 Clearance rates of experimental animals carried out in November 2005

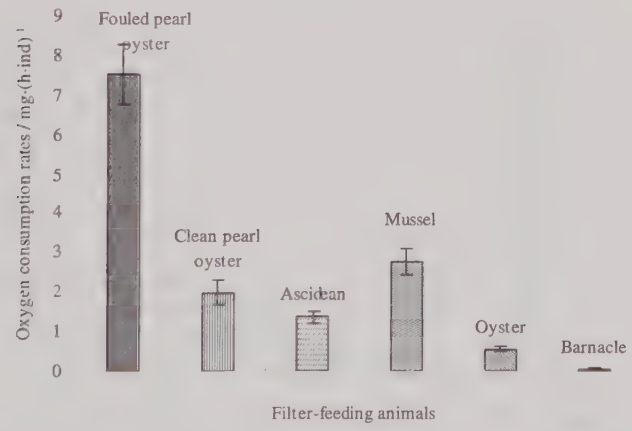

Fig.2 Oxygen consumption rates of experimental animals carried out in November 2005

Foulers such as ascidian *Styela plicata*, the barnacle *Balanus reticulates*, the bivalves *Ostrea radix*, and *Perna viridis* also showed a significant uptake of algal, and release of ammonia and phosphate (Figs.1, 3, 4). The foulers *Perna viridis* consumed seven tenths and *Ostrea radix* about three tenths of the algal consumed by cleaned pearl oysters. The foulers *Perna viridis* excreted five tenths, *Styela plicata* four

tenths, *Ostrea radix* three tenths of the ammonia compared to the cleaned pearl oysters. The foulers *Perna viridis* excreted more phosphate than cleaned pearl oysters, ascidian *Styela plicata* three tenths, oyster *Ostrea radix* two tenths of the phosphate compared to the cleaned pearl oysters.

Foulers also showed a significant consumption of oxygen (Fig.2). *Perna viridis* consumed one point four times the cleaned pearl oysters, ascidian *Styela plicata* seven tenths, the oyster *Ostrea radix* three tenths of oxygen consumption compared to the cleaned pearl oysters.

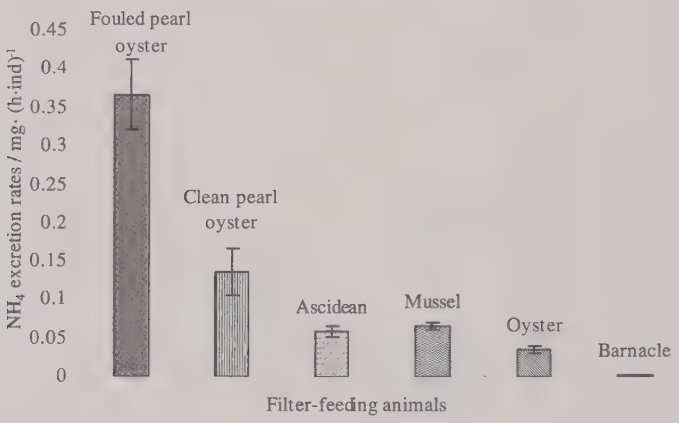

Fig.3 NH_4 excretion rates of animals from the experiment carried out in November 2005

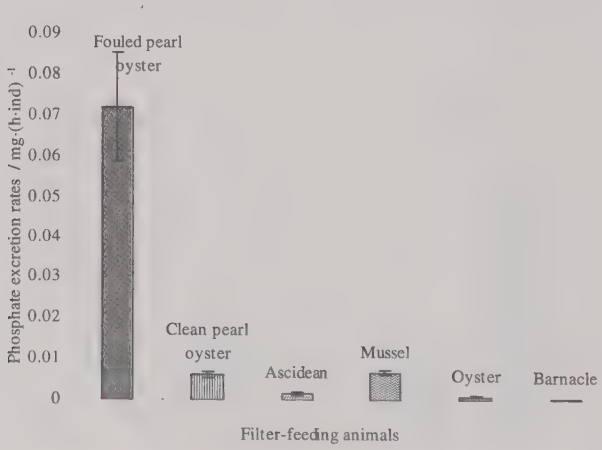

Fig. 4 Phosphate excretion rates of animals from the experiment carried out in November 2005

3 Discussion

The clearance rate experiment was conducted in the statistic system and *Platymonas* sp was the only food. In the natural situation, pearl oyster and other foulers not only filter phytoplankton but also other sources of organic and inorganic matter. So in the natural situation, the clearance rate will be bigger than

this experiment's result.

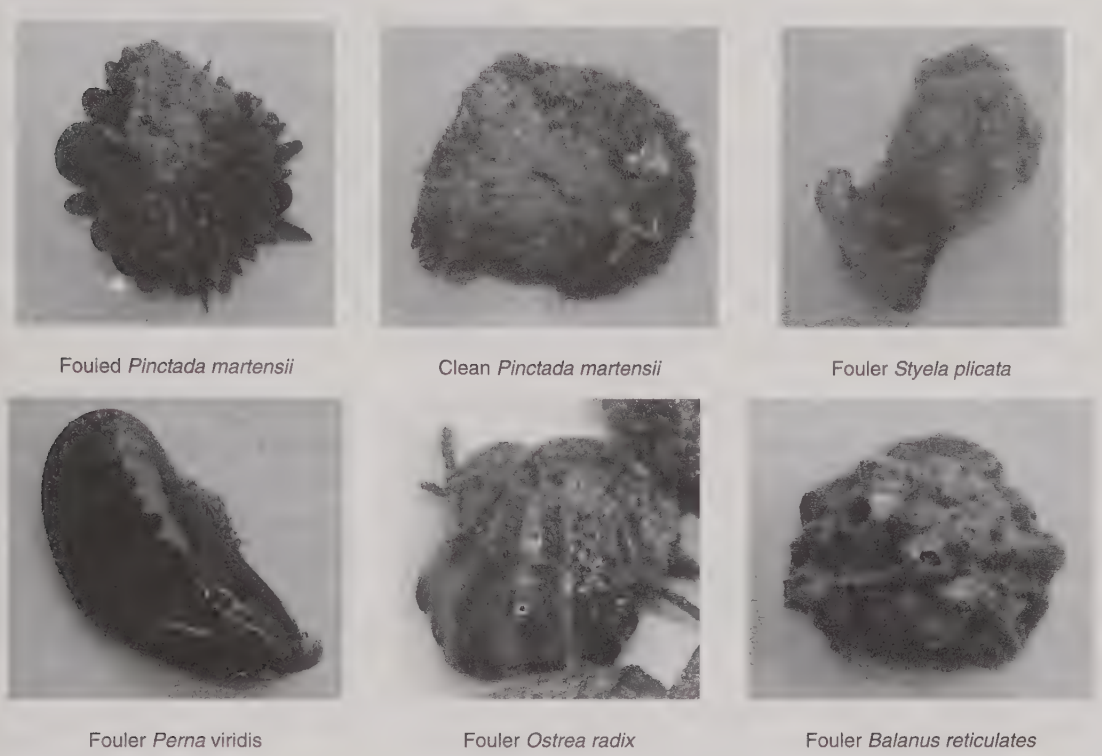

Fig.5 Pictures of experimental organisms

Results from this study showed that the foulers settling on pearl oyster shells seem to be important. Their presence increased algae uptake, ammonia and phosphate release, and oxygen consumption. This is due to the relatively high abundance of foulers. According to investigation, the quantity of foulers, mainly mussel spats that settled on one experimental fouled pearl oyster shell, is up to 100. The presence of so many foulers on the pearl oyster shell may compete for food or oxygen with the pearl oyster, especially when food and oxygen are not abundant.

The quantity of foulers that settled on culture cages in November 2005 was also very large and their biomass was absolutely greater than that of cultured species. According to investigation, ascidians, barnacles, oysters as the main fouling species intensively settled on farming cages, and mussels also settled on suspended buoys and ropes in great quantity. According to the investigation of two-layer cages, the quantity of ascidians was up to 100 or so per cage. The quantity of smaller oyster spats was also astonishing, they distributed densely on the cages. The quantity of barnacles was also very large, they settled not only on the pearl oyster shell, but also on the shell of other fouling animals. Their presence may have impacted on the whole farming area. When the culture density is high and the oxygen supply is scarce, the foulers may compete for food and oxygen with the cultured organisms, the growth and survival

rates will be reduced, which may threaten the aquaculture industry.

Daya Bay belongs to the subtropical sea area and its pearl oyster farm is one of the biggest farms in China. There is a long history in farming *Pinctada martensii*. Fouling organisms settled all the year around and the peak fouling period is from May to August, and October to November is the second peak fouling period. Foulers closely related to the pearl oyster growth mainly included oyster, ascidian, barnacle et al. Oyster and ascidian had a long growth period and the interval of April to June was the prosperous fouling period. In November, they were also usually found settling on cages firmly and difficult to remove. Barnacle had a smaller body size and settled in the whole year. Its peak fouling period was from May to August [2, 15]. To ensure the normal growth of pearl oyster, the impact of fouling cannot be neglected. The cages and pearl oyster shells should frequently be cleaned on condition that their mortality is not affected.

This study indicates that the presence of foulers on the pearl oyster shell increases the food depletion, ammonia and phosphate concentration in the water, and the consumption of oxygen in the peak fouling period. The types and abundance of fouling organisms on pearl oyster shells and cages vary temporally. In other months, when the fouling community is different, the impact of fouling organisms on the pearl oyster may be different. In the Daya Bay, a subtropical farming area, filter-feeding foulers are in the majority, so the impact of fouling organisms should be taken into account when considering the carrying capacity of the pearl oyster culture system.

Acknowledgements

The author thanks the staff of Marine Biology Research Station at the Daya Bay of the Chinese Academy of Sciences for their technical support and instrument supply.

References

[1] Jin Q Z, Zhou B C. The research of biofouling control on pearl culture of *Pinctada Martensii* [J]. Tropical Oceanology, 1983, 2(2): 141-147.

[2] Zheng C X, Huang Z G, li C Y, et al. Fouling organisms on mariculture farming in DAYA Bay, China [J]. Chinese journal of applied ecology, 1991, 2(2): 146-152.

[3] Jin Q Z, Li H, He H. Effects of pearl-growth-hormone on pearl culture of *Pinctada Martensii* [J]. Tropical Oceanology, 1998, 17(4): 43-50.

[4] Jin Q Z. Research of increasing pearl growth [J]. The research and exploitation of Nanhai, 1997, 1: 12-16.

[5] Li H, Jin Q Z, Guo C L, et al. Study on the feeding rate and feeding rhythm of larvae and juveniles of pearl oyster, *Pinctada Martensii* [J]. Tropical Oceanology, 1997, 16(3): 41-48.

[6] Du X D, Li G L, Liu Z G, et al. Genetic diversity of two wild populations in *Pinctada martensii* [J]. Journal of Fishery Sciences of China, 2002, 9(2): 100-105.

[7] Li G L, Du X D, Ye F L. Biochemical genetic variations of two wild populations of pearl oyster *Pinctada Martensii* [J]. Journal of Tropical Oceanology, 2002, 21(4): 63-68.

[8] He M X, Jiang W G. The advances of genetics and breeding in *Pinctada Martensii* [J]. Transactions of Oceanology and Limnology, 2000, 1: 75-82.

[9] He M X, Shen Q, Lin Y G, et al. Inducement of tetraploid *Pinctada martensii* in eggs from triploid [J]. Journal of Fisheries of China, 2000, 24(1): 22-27.

[10] Xie Y K. The Normal Growth of the Pearl Oyster Spats [J]. Guangxi Science, 1999, 6(2): 152-153.

[11] Lin Y G, Jiang W G. A preliminary study on comparisons between triploid and diploid in the cultured pearls of pearl oyster, *Pinctada martensii* [J]. Tropic Oceanology, 1993, 12(3): 90-94.

[12] Shen Y P, Zhang X Y, He H P. Developmental stages of the gonad of pearl oyster, *Pinctada martensii* dunker [J]. Journal of Wuhan University, 1992, 4: 103-109.

[13] Jiang W G, Li G, LinY G, et al. Observation on the gonad of triploidy in *Pinctada martensii* [J]. Tropic Oceanology, 1990, 9(1): 24-30.

[14] Shen Y P, Zhang X Y. An ultrastructural study on oogenesis of pearl oyster *Pinctada martensii* dunker [J]. Journal of Wuhan University, 1993, 5: 101-108.

[15] Zheng D Q, Huang Z G. Fouling organisms on mariculture cages in Daya Bay, China [J]. Journal of Fisheries of China, 1990, 14(1): 15-24.

[16] LeBlanc A R, Landry T, Miron G. Fouling organisms of the blue mussel *Mytilus edulis*: their effect on nutrient uptake and release [J]. Journal of Shellfish Research, 2003, 22(3): 633-638.

[17] Lodeiros C, García N. The use of sea urchins to control fouling during suspended culture of bivalves. Aquaculture, 2004, 231: 293-298.

[18] Ross K A, Thorpe J P, Brand A R. Biological control of fouling in suspended scallop cultivation. Aquaculture, 2004, 229: 99-116.

[19] Peterson J K, Riisgård H U. Filtration capacity of the ascidian Ciona intestinalis and its grazing impact in a shallow fjord [J]. Mar Ecol Prog Ser, 1992, 88: 9-17.

[20] Arawaka KY. Competitors and fouling organisms in the hanging culture of the pacific oyster, *Crassostrea gigas* (Thunberg) [J]. Mar. Behav. Physiol., 1990, 17 (2): 67-94.

[21] Lesser M P, Shumway S E, Cucci T, et al. Impact of fouling organisms on mussel rope culture: interspecific competition for food among suspension feeding invertebrates [J]. J. Exp. Mar. Biol. Ecol., 1992, 165 (1): 91-102.

[22] Lodeiros C J M, Himmelman J H. Influence of fouling on the growth and survival of the tropical scallop, *Euvola (Pencten) ziczac* (L. 1758) in suspended culture [J]. Aquaculture Res., 1996, 27 (10): 749-756.

[23] Taylor J J, Southgate P C, Rose R A. Fouling animals and their effect on the growth of silver-lip oysters, *Pinctada maxima* (Jameson) in suspended culture [J]. Aquaculture, 1997, 153 (1): 31-40.

[24] Claereboudt M R, Bureau D, Côté J, et al. Fouling development and its effect on the growth of juvenile giant scallops (*Placopecten magellanicus*) in suspended culture [J]. Aquaculture, 1994, 121(4): 327-342.

[25] Cayer D, MacNeil M, Bagnall A G. Tunicate fouling in Nova Scotia aquaculture: A new development [J]. J. Shellfish Res., 1999, 18(1):327.

[26] Baxter J M. The incidence of *Polydora ciliata* and *Cliona celata* boring the shell of *Patella vulgata* in Orknay [J]. J. Mar. Biol. Assoc. UK, 1984, 64: 728-729.

[27] Bergman K M, Elner R W, Risk M J. The influence of *Polydora websteri* borings on the strength of the shell of the sea scallop *Placopecten magelllanicus* [J]. Can. J. Zool., 1982, 60: 2551-2556.

[28] Blake J M, Evans J W. Polydora and other related genera as borers in mollusc shells and other calcerous substrats [J]. Veliger, 1972, 15: 235-249.

[29] Caceres-Martinez J, De Oca P M M, Vasquez-Yeomans R. Polydora sp. infestation and health of the Pacific Oyster Crassostrea gigas cultured in Baja California, NW Mexico [J]. J. Shellfish Res., 1998, 17 (1): 259-264.

[30] Curtin L. Mudworm menace in oyster farms. NZ Shellfish Newsl, 1986, 31: 10-11.

[31] Handley S J, Bergquist P R. Spionid polychaete infestations of intertidal pacific oysters *Crassostrea gigas* (Thunberg), Mahurangi Harbour, northern New Zealand [J]. Aquaculture, 1997, 153: 191-205.

[32] Lleonart M, Handlinger J, Powell M. Spionid mudworm infestation of farmed abalone (*Haliotis spp.*) [J]. Aquaculture, 2003, 221: 85-96.

[33] Schleyer M H. Shell-borers in the oyster, *Striostrea magaritacea*: pest or symbionts? [J] Symbiosis, 1991, 10: 135-144.

[34] Tinoco-Orta G D, Caceres-Martinez J. Infestation of the clam *Chione fluctifrage* by the burrowing worm *Polydora sp.* nov. in laboratory conditions [J]. J. Invert. Pathol., 2003, 83: 196–205.

[35] Wargo R N, Ford S E. The effect of shell infestation by *Polydora sp.* and infection by *Haplosporidium nelsoni* (MSX) on the tissue condition oysters *Crassostrea gigas* [J]. Estuaries, 1993, 16: 229–234.

[36] Widdows J. Marine and estuarine invertebrate toxicity tests. In: Calow, P. (Ed.), Handbook of Ecotoxicology, vol. 1. Blackwell Scientific Publications, London, 1993, pp 145-166.

[37] GB 17378.4-1998. The specification for marine monitoring Part 4: Seawater analysis [M]. Chinese Standard Publications, Beijing: 150-159.

[38] Coughlan J. The estimation of filtering rate from the clearance of suspension [J]. Mar. Biol., 1969, 2: 356-358.

污损生物对大亚湾养殖珍珠贝的滤食、呼吸和排泄的影响

苏振霞，严岩，黄良民

（1. 中科院南海海洋研究所热带海洋环境动力学重点实验室，应用海洋生物学重点实验室，广东 广州 510301；2. 中科院研究生院，北京 100039）

摘　要：污损生物是影响贝类养殖业生产效率的重要因素。污损生物不仅附着在养殖网笼上，而且也大量附着在养殖生物的贝壳上。大部分污损生物是滤食性捕食者，这些污损生物与养殖生物竞争食物，氧气与空间导致贝类生长速度减慢，死亡率提高。本实验以大亚湾养殖网笼里的珍珠贝及附着的污损生物为对象，研究有污损生物附着的珍珠贝及没有污损附着的珍珠贝在滤食，耗氧及排泄上的差异，同时对网笼上附着的污损生物优势种的滤食，呼吸及排泄也进行了测定，用以说明污损生物对养殖生物滤食，耗氧和排泄的影响。研究结果表明，有污损附着的珍珠贝及没有污损附着的珍珠贝在滤食率，耗氧率和氮磷排泄率上存在明显差异，有污损附着的珍珠贝的滤食率，NH_4-N 和 PO_4-P 的排泄率要高于没有污损附着的珍珠贝。同时在网笼上附着的优势污损生物的滤食，耗氧和排泄也不容忽视，他们对食物的滤食，溶氧的消耗及氮磷排泄的贡献也很大。本研究结果表明，不管是附着在养殖生物贝壳上还是附着在网笼上的污损生物与养殖生物之间存在食物及氧气的竞争，污损生物对水中氮、磷浓度的提高贡献也很大，因此在养殖中，污损生物的影响不容忽视。

关键词：珍珠贝；污损生物；氧消耗率；滤食率；氨排泄率；磷排泄率

Preliminary Study of Microzooplankton Grazing and Community Composition in the North of South China Sea in Autumn

SU Qiang[1], HUANG Liangmin[1], TAN Yehui[1], XU Runlin[2], LI Tao[1], XU Zhanzhou[1], ZHANG Janlin[1] QIU Dajun[1]

1. *South China Sea Institute of Oceanology, Chinese Acdademy of Sciences, Graduate School of the Chinese Academy of Sciences, Led, Lamd, Guangzhou* 510301, *Guangdong, China;*
2. *Zhongshan University, Gugangzhou* 510275, *Guangdong, China*

Abstract: Microzooplankton community composition in the north of South China Sea was investigated during autumn (between September and October), 2004. Dilution technique using chlorophyll *a* (Chl *a*) was employed to estimate grazing rates and grazing pressure. The results showed that Polymenophorea Oligotrichida was the dominant group with 16 species, and there were 4 species in Oligotrichina and 11 species in Tintinnina. The ciliates abundance ranged from 9 to 102 ind/m^3. Instantaneous growth rates of phytoplankton (k) varied from 0.03 / d to 2.13 / d. Grazing rates of microzooplankton(g) ranged between 0.01 / d and 1.06 / d. The grazing pressure on initial phytoplankton stock (P_i) and primary production (P_p) was 0.089 % - 65.23 % and 33.63 % - 86.04 %, respectively. The grazing of microzooplankton was mainly limited by ciliates abundance. Results of grazing pressure on primary production indicated that microzooplankton played an improtant role in transmitting primary production in the north of South China Sea.

Keywords: Microzooplankton; Grazing pressure; Dilution technique; South China Sea

1 Introduction

Microzooplankton has never been taken seriously in the research on marine ecology for a long time because of their small size, which was mostly under 200 μm. As the consumer of phytoplankton abundance and primary production, microzooplankton research has been the subject of many studies [1] since the dilution technique for estimating microzooplankton grazing was given by Landry in 1982 [2]. Indeed, we already knew that 10 % - 75 % of daily primary production and 0 % - 65 % phytoplankton standing stock were consumed by microzooplankton[3], and their grazing pressure on primary production could even be over 100 %[4]. Moreover, these studies also showed microzooplankton played an improtant role in regulating bacteria abundance and regenerating nutrients [5]. As the consumer of small bacteria and nanophytoplankton and the food of larger mesozooplankton, microzooplankton acted as trophic intermediates among them [6]. Therefore, the study of microzooplankton grazing was necessary to understand the complex system of bacteria, phytoplankton and zooplankton. There have been some basic

Received on July 17, 2007

studies about microzooplankton grazing in China, but reports on the north of South China Sea were not enough yet.

In this paper we estimated microzooplankton grazing and composition in the north of South China Sea during autumn (between September and October) in 2004. Microzooplankton grazing experiments were conducted at 6 stations to provide basic data for a thorough study on ecosystem structure, especially microbial loop, and energy transfer in the South China Sea.

2 Materials and methods

2.1 Sampling station

Microzooplankton grazing experiments were conducted during autumn in 2004 at 6 experiment stations in the north of South China Sea (Fig.1), including 1 neritic station and 5 oceanic stations. Temperature, salinity, Chlorophyll *a* (Chl *a*), microzooplankton composition and abundance were investigated at the same time.

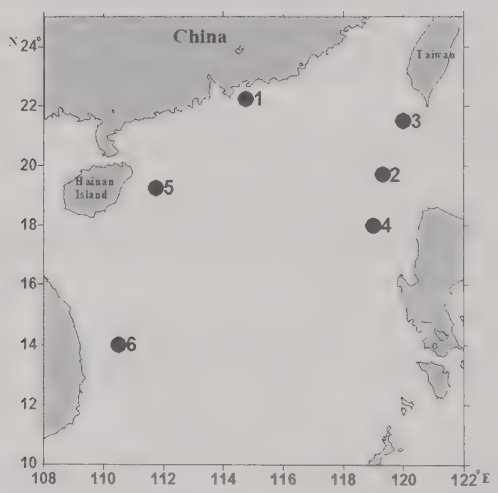

Fig.1 Sampling stations in the north of South China Sea

2.2 Sampling

Water samples were obtained with a 5 L bottle from subsurface, and the sampling depth was shown in Tab.3. We sampled 20 L water in each station, including 1 L water for washing experiment vessels, 500 mL for Chl *a* collection, 5 L water for microzooplankton species identification preserved by formaldehyde (final conc. 1%) and other water for dilution experiments. The incubation volume was 1 L.

2.3 Dilution experiment

The whole experiment was based on the dilution technique [2]. The experiment filters and incubation bottles (Whatman) were soaked in 10 % HCL over 10 h, which were washed by seawater before

incubation experiments [7]. The remaining seawater was poured through 200 μm screening to remove large zooplankton and suspended particles. Particle free water (PFW) for dilution was prepared by filtering seawater through GF/F 0.7 μm filters (Whatman) below 13.33 kPa vacuum. These seawater and PFW were mixed in transparent bottles to give mixtures of 75 %, 50 %, 25 % and 0 % of PFW, and a set of parallel treatment was conducted at the same time. Incubation bottles were put gently into an aquarium for 24 h, which was covered in mesh to reduce light and cooled with tap water to keep temperature close to natural conditions. We used Chl *a* for phytoplankton abundance [8], and took 900mL water for collecting Chl *a* by GF/F 0.7 μm filters (Whatman) at the start and end of incubation, respectively. Filters were kept frozen at -20 ℃ and determined with a Turner Designs Fluorometer Model-10 AU in laboratory.

2.4 Temperature and salinity

Temperature and salinity were obtained by employing the submersible CTD.

2. 5 Chl *a* collection and determination

Water sample for Chl *a* was pre-filtered through a 200 μm screening to remove larger zooplankton and suspended particles. 500 mL subsample was filtered through cyclopore 20 μm, cyclopore 3 μm and GF/F 0.7 μm filters (Whatman) below 13.33 kPa vacuum to collect size fractionation of Chl *a*. Filters were kept frozen at -20 ℃ for determination. In laboratory, filters were transferred to a small glass tubescontaining 10 mL 90 % analytical acetone, and extracted for 12 - 24 h. The whole process was under the obscuration conditions, and limited to 30 minutes. Fluorescence of acetone extracts before and after acidification with one drop of 10 % HCl was measured with a Turner Designs Fluorometer Model-10 AU.

2.6 Microzooplankton species identification

In this paper we only identified ciliates species in microzooplankton samples, and identification samples with formaldehyde (final conc. 1 %) were stored at room temperature in dark for determination. Samples over 24 h standing were taken off upper water and left 30 mL for identification and count.

2.7 Dilution experiment data analysis

Instantaneous growth rates of phytoplankton(*k*) and grazing mortality rates of microzooplankton (*g*) could be expressed as the following equation according to the theory of dilution technique[1].

$$(1/t)\ln(P_t / P_0) = k - g \qquad (1)$$

Where *t* was the incubation time, and P_t and P_0 were the phytoplankton abundance at time *t* and 0. We used Chl *a* concentrations for phytoplankton abundance [9] in this study.

Equation (1) changed as follows under any diluted condition (Dilution factor, *d*).

$$(1/t)\ln(P_t / P_0) = k - dg \qquad (2)$$

We could calculate *k* and *g* according to 4 dilution factors because *t* and *d* were already known and

P_0 and P_t could be determined.

The grazing pressure on initial phytoplankton stock(P_i) and primary production(P_p) were calculated according to equations given by ZHANG Wuchang and WANG Rong in 2001[7].

$$P_i = 1 - e^{-gt} \times 100\ \% \quad (3)$$

$$P_p = (e^{kt} - e^{(k-g)t}) / (e^{kt} - 1) \times 100\ \% \quad (4)$$

3 Results

3.1 Temperature and salinity

Teperature and salinity at the station 6 were not determinated due to a failure of CTD. The range of temperature and salinity in the sample depth was from 28.41 ℃ to 29.32 ℃ and from 31.29 to 33.91, with an average of 28.85 ℃ and 32.96 ℃, respectively. Vertical profiles of temperature and salinity were shown in Fig.2. Station 1 was near the coast and was influenced by freshwater with a great variation of saliniy. Thermocline appeared in other stations except for the station 3, which may be related to some physical factors.

3.2 Chl *a* concentration

Chl *a* concentration at the station 6 was not determinated due to a failure of CTD. Chl *a* concentrations ranged from 0.093 to 0.306 mg/m^3, with an average of 0.225 mg/m^3. The results of Chl *a* size fractionation collection were shown in Fig.3. Picophytoplankton appeared the highest concetration, followed by nanophytoplankton, and microphytoplankton was lowest in every station. Chl *a* at the stations 2, 3 and 4 were so different in close range, which indicated an appearance of uneven water distribution.

3.3 Species composition and abundance

Seventeen species of ciliates were identified representing 10 genuses in all stations (Tab.1). Polyhymenophora Oligotrichida were dominant groups with 16 species, followed by Tintinnina with 11 species and Oligotrichida with 4 species. Some species appearing in samples were not pelagic ciliates, such as *Aspidisca* sp., which belonged to the benthic species.

Species richness of ciliates ranged from 3 species at the station 6 to 9 species at the station 5, with the average below 7 species. Ciliates abundance was between 9 ind/m^3 and 102 ind/m^3, with an average of 45.5 ind/m^3 (Tab.2). The lower species richness and abundance may be related to the sample volume, which would be better in 10 - 30 L.

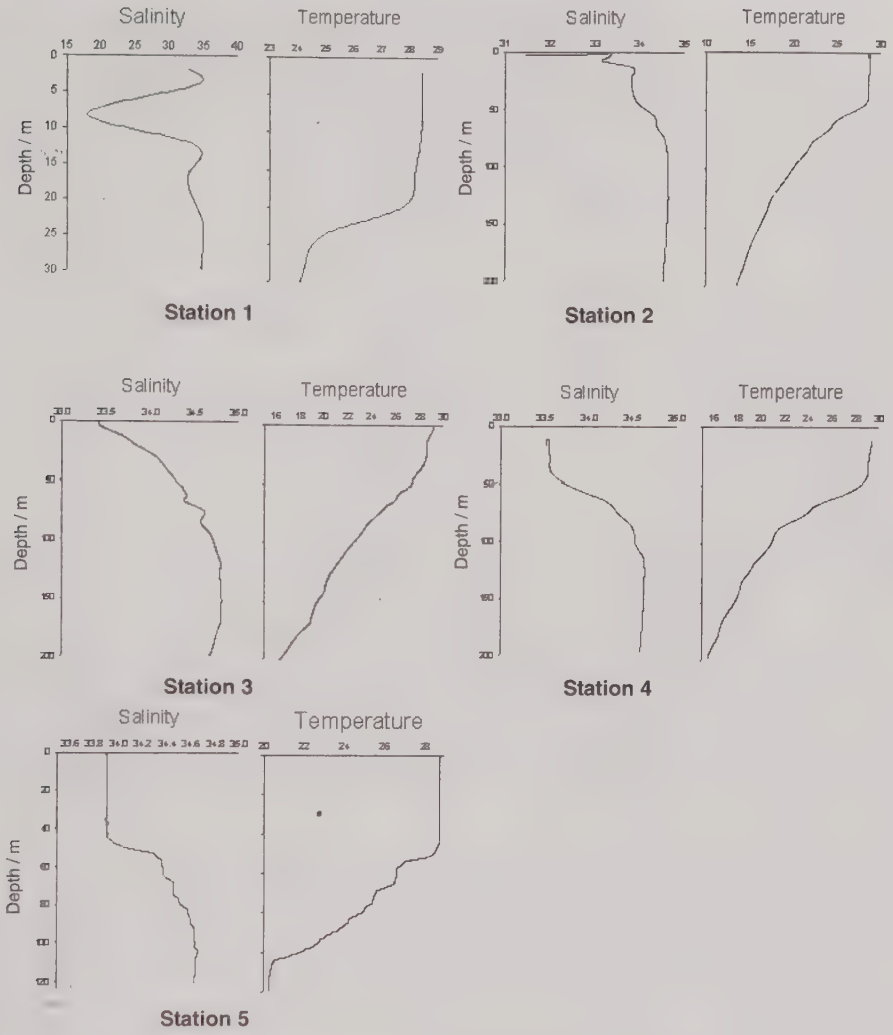

Fig. 2 Vertical profile of temperature and salinity

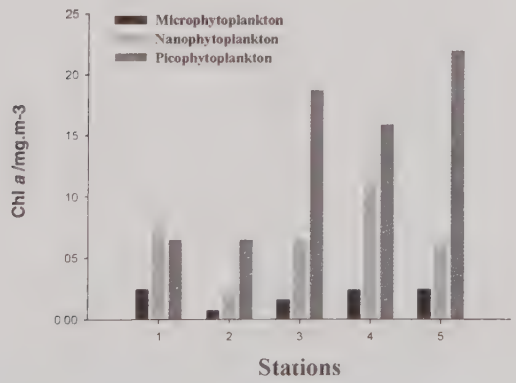

Fig.3 Size fractionation of Chl *a* and total concentration in every station

Tab.1 A list of ciliates in the samples

Ciliophora	*Amphorella*
Oligohymenophorea	*Amphorella amphora*
Peritrichida	*Dadyiella*
Vorticella	*Dadyiella ganymedes*
Vorticella marina	*Undella*
Polymenophorea	*Undella ostenfeldia*
Oligotrichida	*Dictyocystamexicann*
Strombidium	*Dictyocysta mexicann*
Strombidium conicum	*Climatocylis*
Strombidium tintinnodes	*Climatocylis scalaroides*
Strombidium sp.	*Parundella*
Lohmanniellar	*Parundella* sp.
Lohmanniellar orifirmis	*Eutinnus*
Tintinnopsis	*Eutinnus apertus*
Tintinnopsis major	*Salpingella*
Tintinnopsis sp.	*Salpingella minutissima*
Codonellopsis	Hypotrichida
Codonellopsis sp.	*Aspidisca*
	Aspidisca sp.

Tab.2 Composition and density of ciliates in all the stations

Ciliates species	Stations					
	1	2	3	4	5	6
Amphorella amphora					+	
Aspidisca sp.			+			
Climatocylis scalaroides				+	+	
Codonellopsis sp.					+	
Dadyiella ganymedes				+	+	+
Dictyocysta mexicann		+	+	+		
Eutinnus apertus					+	
Lohmanniella ovifirmis	+	+	+	+	+	+
Parundella sp.			+			
Salpingella minutissima				+		
Strombidium conicum	+	+	+	+	+	
Strombidium tintinnodes						+
Strombidium sp.	+			+		
Tintinnopsis major					+	
Tintinnopsis sp.	+	+				
Undella ostenfeldia				+	+	
Vorticella marinema	+	+				
Species richness	5	5	5	8	9	3
abuncance (ind/m^3)	102	57	33	27	45	9

Annotation: + means appearance.

3.4 Microzooplankton grazing

Results at Station 5 were not listed because the value of r^2 was lower than 0.4 [10] (Tab.3). The highest instantaneous growth rates of phytoplankton and grazing rates were 2.13 /d and 1.06/d, and they all appeared at the station 1, followed by the station 2. Grazing pressure on the initial phytoplankton stock ranged from 0.89 % to 65.23 %, and grazing pressure on the primary production was between 33.63 % and 86.04 %.

Tab.3 Results of microzooplankton grazing at 5 stations

Stations	Depth / m	r^2	k / d	g / d	P_i / %	P_p / %
1	10	0.62	2.13	1.06	65.23	74.02
2	75	0.51	0.15	0.12	11.11	82.28
3	75	0.64	0.06	0.05	4.79	86.04
4	75	0.55	0.03	0.01	0.89	33.63
6	75	0.81	0.04	0.02	2.38	61.63
	average		0.48	0.25	16.88	67.52

Our research findings on the four parameters were at low level compared with other researches (Tab.4), which may be related to the ocean environments characteristic of South China Sea.

Tab.4 Results of microzooplankton grazing in other regions

Regions	Times		K /d	G /d	P_i /%	P_p/%
Northern San Francisco Bay[11]	1993-1994		-	0.06-0.69	-	44-122
Bellingshausen Sea[12]	1994		-	-	3-40	21-271
Equatorial Pacific[13]	1995		0.2-0.7	0.2-1.0	70-105	123-133
Southern Bight of the North S ea[14]	1998		0.13-0.67	0.27-1.14	24-68	53-341
Barents Sea[15]	1999	<200 μm	0.19-0.45	0.14-0.34	20-50	69-85
		<20 μm	0.24-0.46	0.16-0.42	18-50	77-91
		<8 μm	0.25-0.47	0.22-0.44	23-57	88-96
East China Sea[8]	2002		-	0.28-1.13	35.14-811.69	74.04-203.25
Jiaozhou Bay[4]	2003 spring		0.18-0.44	0.12-1.47	17.56-92.19	31.77-467.88
	2003 summer		0.38-0.71	0.27-0.60	34.60-83.04	71.28-98.80
Xiamen Waters[16]	2003.05		2.41-2.43	0.78-1.32	54.23-73.20	59.59-80.26
	2003.08		1.94-2.43	0.91-1.32	59.65-94.47	69.62-99.43
Daya Bay[17]	2004.12		0.18-1.19	1.00-2.08	76-287	101-445
	2005.03		0.16-1.14	0.33-1.74	47-258	70-330

4 Discussion

4.1 Chl *a* Concentration, Ciliates Abundance and Microzooplankton Grazing

We took Chl a concentration, ciliates abundance and microzooplankton grazing together and made an analysis (Fig.4), and the results in station 6 were not listed because of the absence of Chl *a* concentration data. The results of ciliates abundance and microzooplankton grazing indicated a very close relationship between them. Grazing rates and grazing pressure on the initial phytoplankton stock increased with ciliates abundance. These results suggested that in the north of South China Sea microzooplakton abundance was the dominant limiting factor of microzooplankton grazing, and the dominant group was ciliates, which determinated microzooplankton grazing levels. The results of Chl *a* concentration and microzooplankton grazing indicated that microzooplankton grazing effects of Chl were different in every station. For example, at the stations 1 and 2, it maybe reached a higher grazing level with water Chl *a* concentration increasing due to the higher ciliates abundance. While at the stations 3 and 4, phytoplankton abundance, as food sources, were abundant for consumer, and microzooplankton grazing would not increase with Chl *a*.

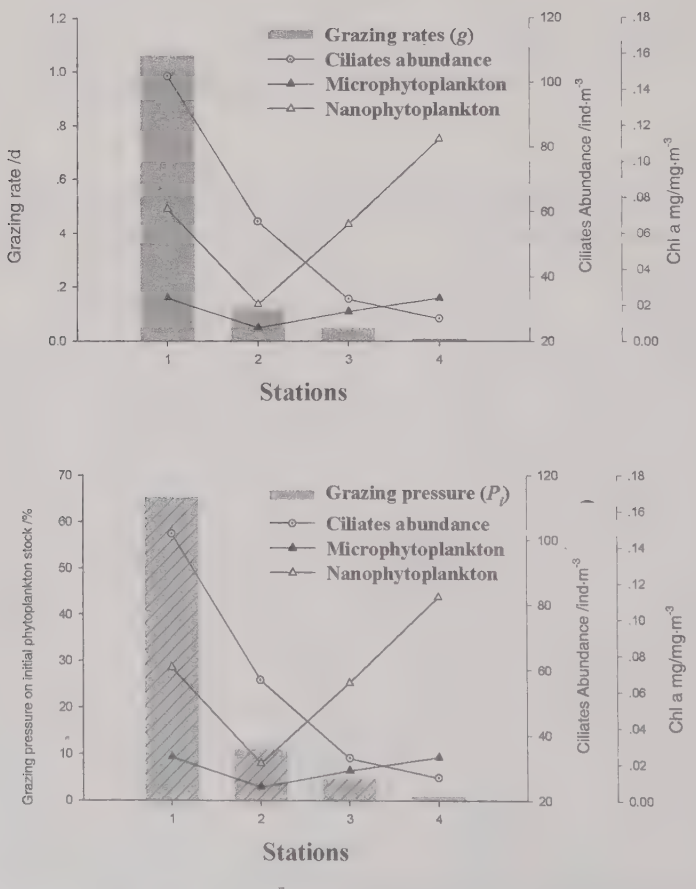

Fig. 4 Chl *a* concentration, ciliate abundance, microzooplankton grazing rates and pressure

4.2 Microzooplankton's role in energy transfer

Microzooplankton was important consumers of phytoplankton production in open ocean [18], and also played a significant role in grazing bacterial populations and regenerating nutrients. The fate of phytoplankton production was determined directly by grazing phytoplankton standing stocks by microzooplankton, or indirectly through the consumption by larger zooplankton [19]. Our results indicated that microzooplankton grazing on primary production was all significant in neritic and oceanic environments. However, microzooplankton grazing results at the station 1 and the station 3 should be noted. The highest instantaneous phytoplankton growth rate and microzooplankton grazing rate appeared at the station 1, but the result of grazing pressure on primary production ranked third among 5 data (Tab. 3), while the highest grazing pressure on primary production appeared at the station 3 with lower phytoplankton growth rate and microzooplankton grazing rate. These suggested that phytoplankton production transfer by microzooplankton grazing was a complex process restricted by several factors. The high growth rates and high grazing rates maybe indicated high loss in engery transfer. The high efficient engery transfer required the balance between phytoplankton growth and microzooplankton grazing. A deep research in these fields would help us to understand marine ecosystems and global carbon cycles, and provide necessary scientific basis for the rational development and utilization of marine resources.

5 Conclusion

The results showed that the dominant group of microzooplankton was Polyhymenophora Oligotrichida in the north of South China Sea in autumn. In neritic environments the higher ciliates abundance appeared with higher microzooplankton grazing rates and grazing pressure, which was mainly determined by microzooplankton abundance. Future studies with focus on several depths in various seasons would be carried out, and it may be more worth devoting our efforts to the grazing on each other among the microzooplankton, the grazing on bacterioplankton, and other direct use of the grain organic matter and so on.

Acknowledgements

The paper was supported by the National Science Fund of China (40531006), NSFC-GD (U0633007) and the Creative Group Program of the Chinese Academy of Sciences (KZCX2-YW-213).

Reference

[1] Landry M R, Hassett R P. Estimating the grazing impact of marine microzooplankton [J]. Marine Biology, 1982, 67: 283-288.

[2] Mazumder A, McQuen D J, Taylor W D, et al. Micro- and mesozooplankton grazing on natural picoplankton and nanoplankton in contrastiong plankton communities produced by planktivore manipulation and fertilization [M].

Archives der Hydrobiologie, 1990, 118: 257-282.

[3] Pierce R W, Turner J T. Ecology of planktonic ciliates in marine food webs [J]. Review Aquatic Sciences, 1992, 6: 139-181.

[4] ZHANG Liyong, SUN Jun, LIU Dongyan, et al. Studies on growth rate and grazing mortality rate by microzooplankton of size-fractionated phytoplankton in spring and summer in the Jiaozhou Bay, China [J]. Acta Oceanologia Sinica, 2005, 24(2): 85-101.

[5] McManus G B, Fuhrman J A. Control of marine bacterioplankton populations: Measurement and significance of grazing [J]. Hydrobiologica, 1988, 159: 51-62.

[6] Gifford D J. The protozoan-metazoan trophic link in pelagic ecosystems [J]. Journal of Protozoologica, 1991, 38: 81-86.

[7] ZHANG Wuchang, WANG Rong. Grazing pressure of microzooplankton on phytoplankton and primary production in marine ecosystem [J]. Acta Ecologica Sinica, 2001, 21(8): 1 360-1 368.

[8] SUN Jun, LIU Dongyan, WANG Zhongling, et al. Microzooplankton herbivory during red tide-frequent-occurrence period in spring in the East China Sea [J]. Chinese Journal of applied Ecology, 2003, 14(7): 1 073-1 080.

[9] Burkill P H, Mantoura R F C, Llewellyn C A, et al. Microzooplankton grazing and selectivity of phytoplankton in coastal waters [J]. Marine Biology, 1987, 93: 581-590.

[10] ZHANG Wuchang, WANG Rong. Microzooplankton and their grazing pressure on phytoplankton in Bohai Sea [Z]. Oceanologia Et Limnologia Sinica, 2000, 31(3): 252-258.

[11] Murrell M C, Hollibaugh J T. Microzooplankton grazing in northern San Francisco Bay measured by the dilution method [J]. Aquatic Microbial Ecology, 1998, 15: 53-63.

[12] Burkill, P H, Edwards E S, Sleigh M A. Microzooplankton and their role in controlling phytoplankton growth in the marginal ice zone of the Bellingshausen Sea [R]. Deep-Sea Research, 1995, 42: 1 277-1 290.

[13] Verity P G, Stoecker D K, Sieracki M E, et al. Microzooplankton grazing of primary production in the equatorial Pacific [R]. Deep-Sea Research II, 1996, 43 (4-6): 1 227-1 256.

[14] Stelfox-Widdicombe C E, Archer S D, Burkill P H, et al. Microzooplankton grazing in Phaeocystis and diatom-dominated waters in the southern North Sea in spring [J]. Journal of Sea Research, 2004, 51: 37– 51.

[15] Peter G, Verity P, Wassmann M E, et al. Grazing of phytoplankton by microzooplankton in the Barents Sea during early summer [J]. Journal of Marine Systems, 2002, 38: 109-123.

[16] LIU Yuan, HUANG Bangqin, CAO Zhenrui, et al. Grazing pressure of microzooplankton on phytoplankton in Xiamen Waters [J]. Marine Environmental Science, 2005, 24(1): 9-12.

[17] WANG Xuefeng, LI Chunhou, JIA Xiaoping, et al. Study on the microzooplankton herbivory in winter and spring in the Daya Bay [J]. Marine Environmental Science, 2006, Z(1): 44-47.

[18] Stelfox-Widdicombe C E, Edwards E S, Burkill P H, et al. Microzooplankton grazing activity in the temperate and sub-tropical NE Atlantic: Summer 1996 [Z]. Marine Ecology Progress Series, 2000, 208: 1-12.

[19] Wassmann P. Retention versus export food chains: processes controlling sinking loss from marine pelagic systems [J]. Hydrobiologia, 1998, 363, 29-57.

南海北部秋季微型浮游动物摄食和种类组成的初步研究

苏强[1]，黄良民[1]，谭烨辉[1]，徐润林[2]，李涛[1]，许战洲[1]，张建林[1]，邱大俊[1]

（1. 中国科学院南海海洋研究所 Led, Lamb，广东 广州 510301；2. 中山大学，广东 广州 510275）

摘 要：2004 年 9 月到 10 月间在南海北部海区对微型浮游动物的种类组成进行了调查，同期运用现场稀释法，以叶绿素 *a* 为监测对象，估计了该海区内微型浮游动物摄食率和摄食压力的水平。结果表明，南海北部海区纤毛虫群体中以多膜纲寡毛目为主，有 16 种，其中寡毛亚目纤毛虫 4 种，砂壳亚目纤毛虫 11 种。各站纤毛虫丰度比较低，在 9 ~ 102 ind/m^3 之间。浮游植物瞬时增长率（k）在 0.03/d ~ 2.13/d 之间；微型浮游动物的摄食率（g）在 0.01/d ~ 1.06/d 之间。微型浮游动物对浮游植物现存量的摄食压力（P_i）在 0.089% ~ 65.23%之间，对初级生产力的摄食压力（P_p）在 33.63 % ~ 86.04%之间。微型浮游动物的摄食水平主要受其丰度的影响，同时微型浮游动物对浮游植物现存量和初级生产力的摄食压力显示，在南海北部海区微型浮游动物在初级生产力传递方面具有重要的科学意义和研究价值。

关键词：微型浮游动物；摄食压力；稀释法；南海

New Species of Punctariaceae (Phaeophyta) from China

LUAN Shujun, LUAN Rixiao, WANG Xuri, SHEN Caizhi

Dalian Natural History Museum , Dalian 116023, *Liaoning, China*

Abstract: This paper demonstrates three species of Punctariaceae, newly-recorded in China, i.e. *Desmotrichum balticum* Kuetzing, *Myriotrichia clavaeformis* Harvey and *Punctaria projecta* Yamada.

Keywords: Punctariaceae; newly-recorded species; *Desmotrichum balticum*; *Myriotrichia clavaeformis*; *Punctaria projecta*

Introduction

Punctariaceae belongs to Phaeophyta, Phaeophyceae, Dictyosiphonales. Researchers have different opinions on how to divide the genus, and they haven't achieved a uniform result at present. Some believe there are up to 20 genuses (Smith, 1951) [1], while others claim there are only several genuses (Fletcher et al, 1987) [2], so the species vary very much correspondingly. The species reported in this paper are mainly according to the standard established by Taylor (1957) [3] and Smith [1] etc.

The earliest report on the categories of Punctariaceae is *Punctaria latifolia* Greville, which was found in Qingdao and reported by Zeng Chengkui and Li Liangqing [4] in 1935; Zeng Chengkui and Zhang Junpu [5] reported *P. plantaginea* (Roth) Greville in 1962; In 2000, the authors [6] of this paper reported *Pogotrichum yezoense* (Yamada and Nakamura) Sakai and Saga, *Punctaria Hesperia* Setchell and Gardner and *P. occidentalis* Setchell and Gardner. There are totally 2 genuses and 5 species up to now. This paper reports *Desmotrichum balticum* Kuetzing, *Myriotrichia clavaeformis* Harvey and *Punctaria projecta* Yamada. The specimens are stored in the ocean research laboratory of the Chinese Academy of Sciences.

1 Materials and methods

1.1 Sampling and fixing

Materials (specimens) were collected from the ocean, and then were put into the stable conserving liquid (Ingredients' volume proportions: seawater 60 %, alcohol 36 %, formaldehyde 4 %, glycerin 1 %, a little saleratus) immediately after they were collected.

Received on March 6, 2007

1.2 Making slice and observing

Take the specimens out of the conserving liquid, rinse them with tap water, then choose part of the algae (2.1, 2.2) and slice them (2.1, 2.3) on the carrier glass, drip the volume percent 10 % glycerin liquid, put the cover glass, observe and measure the related data and plot under the light microscope.

2 Results

2.1 *Desmotrichum balticum* Kuetzing

Desmotrichum balticum Kuetzing 1849: 470 [7]; Levring 1937: 65 [8]; Taylor 1957: 164 [3].

Dsemotrichum balticum f. *paradoxum* Gran 1897: 37.

Punctaria baltica (*Kuetzing*) Batters 1902: 26.

Desmotrichum scopulorum Reinke 1888: 18.

The frond is filemot and pale brown, simple or tufted, 0.5-1.5 cm tall, the monolayer cells' basal disc epiphytic on other algae at the basal part which is composed of creeping filaments. The creeping filaments' cells are 5.5-10 μm long, 5.5-10 μm wide. The erect protonema are linear or speculate, the lower parts are usually composed of uniseriae cells, while the middle and the top parts are composed of pluriseriate cells in flat leaf shape. They are 20-100 μm thick, 25-1200μm wide, which are composed of 2-4 layers of cells, some even have more than 6 layers. Both margins are accidented, like blunt serrations. There are not many differences between inner and outer cells of the transection. The cells are rectangular or square, 12-25 μm long, 12-20 μm wide. The epidermal cells are rectangular, 12-16 μm , 12-25 μm wide. Hairs develop and scatter on the top, along the leaf margins or on the leaves singly. The cells are 50-120 μm long, 10-12 μm wide. The length is 5-12 times the width. They live in the basal region, there are 3-7 disperse cells. Chromatophores are discoid, scatter sparsely.

The plurilocular sporangia satterea, from ovoid to conital, 30-60 μm long, 15-25 μm wide, pedicelled or sessile, grow along the blade margins or on the blades. Some are on the basal disc. The sessile plurilocular sporangia are mostly buried among the layers of the thallus. The pedicelled usually grow on the basal disc or under the thallus. The unilocular sporangia are unknown.

Habit and locality: Epiphytic on *Chaetomorpha aerea* on the tide pools in the intertidal zone, grow mixed with *Ectocarpus confervoides*, get mature in spring or summer. The specimens were collected from Lianyungang City, Jiangsu Province (AST 9990175).

Distribution: North Atlantic, North-eastern America.

Type locality: North Europe.

Desmotrichum was established by Kuetzing in 1845. Some researchers (Fletcher, 1987) [2] united it

with *Punctaria* in *Punctaria* based on their similar features, while we insist that *Desmtrichum* should be retained because *Desmotrichum* has the following distinguished characters: the rhizoid-shaped creeping filaments cling to the stroma; the uniseriae cells usually distribute at the basal part of the erect filament, which are cylindrical; there are some branches at the base; the middle and the top parts are membranaceous; the margins are anomalous; the hair is simple along the blade margins or on the blades. the *Punctaria* base has a plate-like sessile organ; the erect front is leaf-like and has no branches; the margins are slightly smooth; the hairs are tufted.

There is no uniform opinion on whether *D. balticum* and *D. undulatum* can exist independently. Rosenvinge & Lunt (1947) [9] and Fletcher (1987) [2] believed they were synonymous, while Levring (1937) [8] and Taylor (1957) [3] claimed they were different. The main differences include: *D. balticum* is not more than 1.5 cm tall; some have branches at the base; the plurilocular sporangia are pedicelled, while *D. undulatum* is over 1.5 cm tall; has no branches; the plurilocular sporangia are sessile. We agree with Levring and Taylor because there are many differences between them, they should represent two different species.

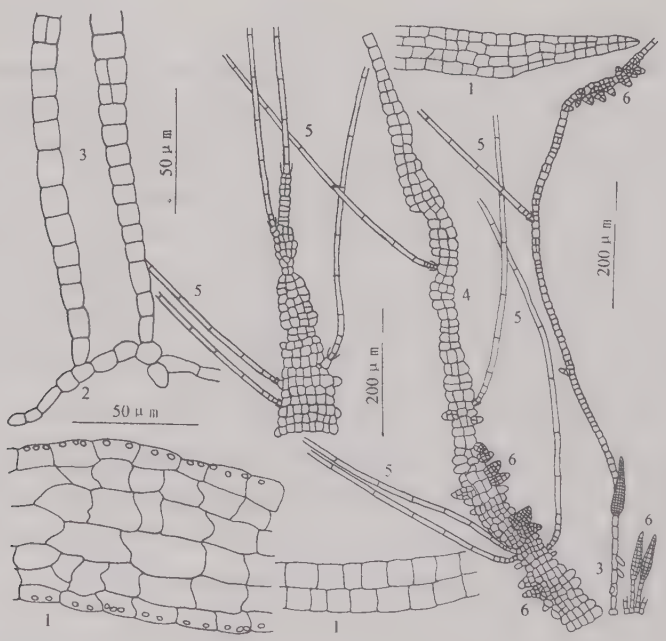

Fig. 1 ***Desmotrichum balticum*** **Kuetzing**

1. transection of the frond; 2. creeping filament; 3. lower part of the frond; 4. upper part of the frond; 5. hairs; 6. plurilocular sporangia

2.2 *Myriotrichia clavaeformis* Harvey

Myriotrichia clavaeformis Harvey 1834: 300; Levring 1937: 70 [8]; Rosenvinge and Lund

1941: 50 [10]; Taylor 1957: 161, pl. 10, (Figs.4-7) [3]; Fletcher 1987:174, pl. 4c-e, (Figs.38-39)[2].

Myriotrichia repens Hauck 1879: 242; Levring 1937: 70 [8]; Rosenvinge and Lund 1941: 48[10]; Taylor 1957: 160 [3].

Dichosporangium repens (Hauck) Hauck 1885: 339.

Myriotrichia filiformis Harvey 1841; 44; Levring 1937: 70 [8]; Taylor 1957: 161 [3].

The frond is brown, 0.7-1 mm tall, epiphytic on the hosts. The base is composed of creeping branched filaments. A few short rhizoids extend to the cortexes and plurilocular sporangia. The creeping filament cells are anomalistic, which are 10-25 μm long, 8-12 μm wide. The length is 1.3-3.6 times the width. The erect filaments grow on the creeping filaments, which have prominent main stems, and have no branches or have some short branches at the middle and top parts. The main axis cells' septum constricts, some cells divide longitudinally. The middle and top parts are slightly thick, become slim basally. The basal cells are 30-45 μm long, 15-16 μm wide. The length is 2-4 times the width. The middle and top cells are 17-30 μm long, 16-25 μm wide. The length is 0.75-1.8 times the width. The hairs are on the top of the main axis or on the lateral base of short branches. There is a growing region at the base, having 4-6 meristematic cells. The middle and top cells are 60-200 μm long, 10-12 μm wide. The length is 6-20 times the width. The chromatoplasm is discoid.

The unilocular sporangia are solitary, opposite or thickly whorled, only a few on the creeping filaments, which are orbicular, oval or long-obovate, and 35-80 μm long, 32-50 μm wide. Most of them are sessile, some have one pedicel. The plurilocular sporangia are unknown.

Habit and locality: Epiphytic on the *Scytosiphon lomentarius* on the tide pools in the lowtidal zone, grow mixed with *Ectocarpus* sp. Grow in the early summer. The specimens were collected from Changhai County, Liaoning Province (DNHM83-1293).

Distribution: the east and west coasts of North Atlantic.

Type locality: Germany.

The holotype and original paper couldn't be found. We mainly based ourselves on the reports written by Levring (1937) [8], Rosenvinge and Lund (1941) [10], Taylor (1957) [3] and Fletcher (1987) [2].

The primary characters of *Myriotrichia* are: the basal creeping filaments are composed of uniseriae cells; some rhizoids stretch to the hosts' tissues from the base; the erect filaments are epiphytic on the creeping filaments, which is cylindrical and solid; the lower part is composed of uniseriae cells, the middle and top parts are composed of multiserial cells because of the cells' longitudinal division; there are many short radiate branches with hairs on the main axis; unilocular sporangia and plurilocular sporangia are in the same body; the unilocular sporangia are adnational, opposite or whorled, and orbicular or oval; the plurilocular sporangia are adnational, simple or gregarious, uniserial or multiserial, cylinder or spindly. The cladistic location of this genus is controversial, Levring (1937) [8], Rosenvinge and Lund (1941) [10] and

Fletcher (1987) [2] referred *Myriotrichia* as one genus of Myrotichiaceae, while Taylor claimed *Myrotrichia* belongs to Punctariaceae. We agree that *Myrotrichia* belongs to Punctariaceae based on its characters.

Myriotrichia clavaeformis is similar to *M. densa* Batters, the main differences are: the former's lateral branchlet is not or seldom ramose, the main axis usually exposes; while the latter's main axis has many dichotomous lateral branchlets.

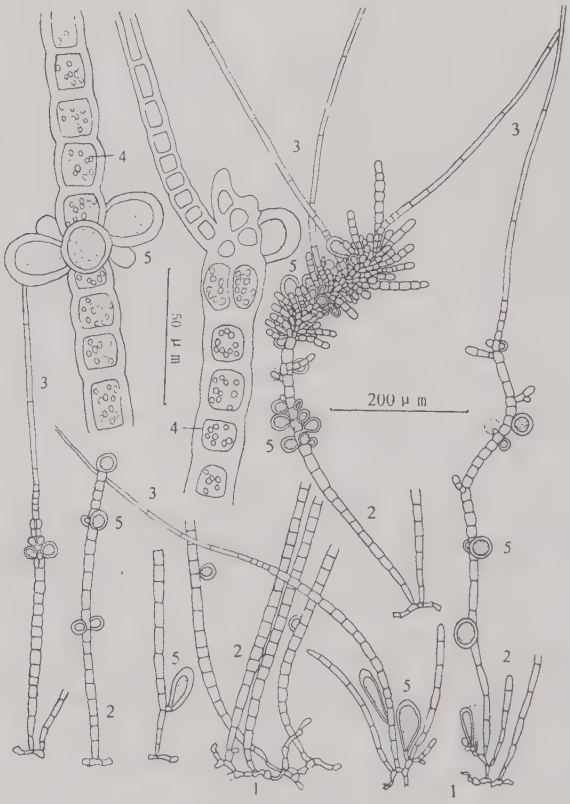

Fig. 2 *Myriotrichia clavaeformis* Harvey

1.creeping filament; 2.erect filament; 3.hairs; 4.chromatophore; 5.unilocular sporangia

2.3 *Punctaria projecta* Yamada

Punctaria projecta Yamada 1968: 372, (Figs.1-2) [11]; Yoshida et al. 1998: 294, (Figs. 1-16E) [12].

The frond is brown but turns to olive green after dried. They are tufted and epiphytic on other algae, foliaceous or lanceolate. Its holdfast is discoid, its base is narrowly cuneate, both margins are slightly rugate. Its top is often broken and blunt round. It is 4-8 cm tall, 0.5-2 cm wide and 110-170 μm thick. It consists of cortexes and medullae. There are totally 4-5 layers of cells. The cortex is on the outer, its cells have chromatophore. The transections are 10-25 μm long and 10-20 μm wide. The medulla is inside the cortex, the cell sizes diverse greatly. They are rectangular or sub-round. The transections are 20-75 μm

long and 15-50 μm wide. The hairs are tufted. They are formed by cortical cells' division, and the cells are 55-125 μm long and 8-15 μm wide. The length is 5.5-13 times the width. The base has a growing region and 6-15 meristematic cells.

The plurilocular sporangia and the unilocular sporangia are in the same body or in different bodies. They are both formed by cortex cells. The plurilocular sporangia are simple or aggregate in 2-3, irregularly subulate. Some are slightly curving, 35-55 μm long and 16-27 μm wide, pedicelled or sessile. The unilocular sporangia are oval, sessile, 40-55 μm long and 16-27 μm wide.

Habit and locality: Epiphytic on *Laurencia* sp. and *Sargassum* sp. between low and mid tidal zones. The specimens were collected from Lianyungang City, Jiangsu Province (AST9990139).

Distribution: Japan.

Type locality: Miyazu, Japan.

Punctaria projecta is similar to *P. Hesperia* Setchell and Gardner (1924: 3) [13] in shape. The main differences are: the thallus of *P. projecta* Yamada is 110-170μm thick; the plurilocular sporangia are irregularly subulate, 35-55 μm long; pedicelled or sessile. The latter is 60-70 μm thick; some are even 100 μm . The plurilocular sporangia are short-taper shaped or oval, sessile, 25-38 μm long.

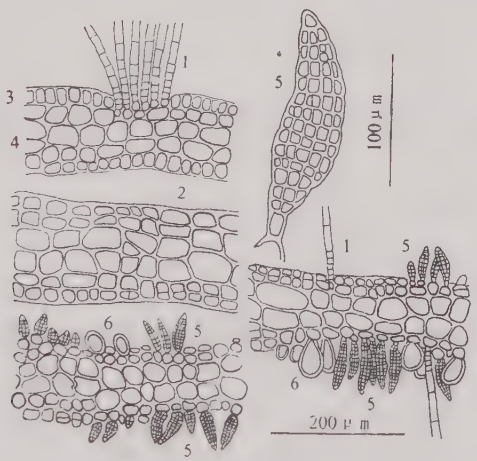

Fig. 3 *Punctaria projecta* Yamada

1.hairs; 2.transection of the frond; 3.surface layer; 4.medulla;
5.plurilocular sporangia; 6.unilocular sporangia

References

[1] Smith G M. Manual of Phycology. Waltham, Mass [M]. USA: Chronica Bot. Company. 1951, 119-158.

[2] Fletcher R L. Seaweeds of the British Isles… Volume 3. Fucophycea (Phaeophyceae) [M]. Part I. London: British Museum Natural History, 1987, 166-215.

[3] Taylor W R. Marine algae of the northeastern coast of North America [M]. Revised edition. Univ. Mich. Press, Ann Arbor., 1957, 161-165.

[4] Tseng C K, Li L C. Some marine algae from Tsingtao and Chefoo, Shantung [J]. Bull. Fan. Mem. Inst. Biol. (Bot.) 1935, 6(4): 183-235.

[5] Zeng C K, Zhang J P. Analysis of the coastle algae area of western Yellow Ocean, Ⅰ. The temperature characters of the algae area [Z]. Ocean and lake marsh, 1962, 4(1-2): 49-59.

[6] Luan R X, Chu Z G, An J L et al. Al. Three newly-recorded Punctariaceae [Phaeophyta] [J]. Botany taxonomy bulletin. 2000, 38(4): 392-397.

[7] Kuetzing F T. Species algarum [M]. Brockhaus, Leipzig, 1849: 470.

[8] Levring T. Zur Kenntnis der Algenflora der norwegischen Westkueste [M]. Acta Univ. Lund. 1937, 33: 65-70.

[9] Rosenvinge L K, Lund S. The marine algae of Denmark. Contributions to their natural history, Vol. Ⅱ. Phaeophyceae. Biol. Skr. 1947, 4: 1-99.

[10] Rosenvinge L K, Lund S. The marine algaeof Denmark. Ⅱ.Det, Kongelige Danske Vidensk. Selskab. Biol. Skr., 1941, 1(4): 48-55.

[11] Yamada Y. Two new marine algae from Japan [J]. J. Jpn. Bot.,1968, 43: 372-377.

[12] Yoshida T, Kitayama T, Tanaka J, et al. Marine Algae of Japan [M]. Tokyo: Uchida- Rokakuho, 1998: 290-299.

[13] Setchell W A and Gardner N L. Phycological contributions [J], Ⅶ. Univ. Calif. Publ. Bot., 1924, 13: 1-13.

中国点叶藻科（褐藻门）新记录种

栾淑君，栾日孝，王旭日，沈才智

（大连自然博物馆，辽宁 大连 116023）

摘　要：报道中国点叶藻科的新记录种，波罗丝毛藻 *Desmotrichum balticum*，棍状毛丝藻 *Myriotrichia clavaeformis*，突起点叶藻 *Punctaria projecta*。

关键词：点叶藻科；波罗丝毛藻；棍状毛丝藻；突起点叶藻

Coral Reef and High Sea Level at Luhuitou, Hainan Island during the Holocene

HUANG Deyin[1, 2, 3], SHI Qi[3], ZHANG Yechun[3]

1. *Guangzhou Institute of Geochemistry, Chinese Academy of Sciences, Guangzhou* 510640, *Guangdong, China;*
2. *Guangdong Institute of Eco-Environment and Soil Sciences, Guangzhou* 510650. *Guangdong, China;*
3. *South China Sea Institute of Oceanology, Chinese Academy of Sciences, Guangzhou* 510301, *Guangdong, China*

Abstract: According to the field survey and ^{14}C dating at Luhuitou, southern Hainan Island, a subsiding area, the authors conclude the high sea level history recorded by coral reef in the Holocene. At least 4 sea level high-stands can be identified from the distribution of coral reef ages: 7300 - 6000 cal.aBP, 4800 - 4700 cal.aBP, 4300 - 4200 cal.aBP and 3100 - 2900 cal.aBP. The highest sea level occurred around 7300 - 6700 cal.aBP, and biological-morphological zones took their shape during the stage. The later coral reefs developed in ponds, depressions, and developed outwards on both sides of Luhuitou peninsula. The modern coral reefs are developing in out reef flat and reef-front slope. Moreover, the time of high sea levels in the northern South China Sea recorded by coral reefs in the Luhuitou peninsula can link up with that in other parts of South China Sea. That means the high sea levels in the South China Sea during the Holocene, which are relative to the warming climate, have the global background.

Keywords: coral reef; high sea level; Luihuitou; Holocene

1 Introduction

The elevation of sea level resulted from global warming has attracted more and more attention, especially in many countries and areas along the coast. According to the third assessment report of Intergovernmental Panel on Climate Change (IPCC), the sea level will rise 0.09 - 0.88 m above the present, and the rising will last for some hundred years [1]. It is obvious that the study on high sea level in the Holocene could help to predict the changes of the sea level in future.

The development of coral reef is restricted strictly by the sea level [2], and the development of coral reefs is a good indicator to record the changes of sea level [3]. There are three vegetal patterns of coral reefs responding to the sea level rise: keep-up, catch-up or give-up [4], and the reef flat developed from massive *Porites* with the patterns of keep-up or give-up is the indicator of up-limit of living coral during the past sea level high-stands or low location of spring tide. According to the results of study on coral reefs in Nansha Archipelago, Xisha Archipelago, Leizhou Peninsula and Hainan Island, the massive *Porites* with a diameter of more than 0.5 m ordinarily lives 1m below the low location of spring tide. So the coral reefs formed from massive *Porites* above the low location of spring tide must have developed during the high

Received on May 10, 2007

sea level stage in the stable geotectonic or subsiding area. According to this, Nie studied the high sea level in the Holocene recorded by the coral reefs in the South China Sea [5, 6].

Luhuitou peninsula（109º 29′ E，18º 12′ N）situates at the southern Hainan Island, and lies at the northern edge of tropics. The coral reefs are influenced by the sea level and sea temperature, and are sensitive to the environmental changes. Luihuitou is one of the key areas in which to study the interaction between sea and land. The authors found in the field survey that the old reef flat is under the sand bank or lagoon sediment zones,and its configuration is controlled directly by the dynamics of sea water. Furthermore, the main compositions of sand bank from top to bottom are coral grit, which shows that the sediments are marine facies. This is consonant with the data of L1 bore at Shuiweiling（109º 28′ 30″ E，18º 12′ 32″ N）[7, 8]. The ages of multiple sea level high-stands in the Holocene are discussed according to the data of calibrated ^{14}C ages from many original *porites* sampled at the Luhuitou peninsula in this study.

2 Sampling

The coral reefs are distributed on both sides of Luhuitou peninsula, i.e., Sanya Bay and Xiaodonghai. There are 3 main parts: southeastern Sanya Bay reefs, southwestern Xiaodonghai reefs and Northeastern Xiaodonghai reefs, but there are no coral reefs in the southern peninsula due to the strong dynamics of sea water, which made it hard for the coral to settle down and live stably (Fig.1).

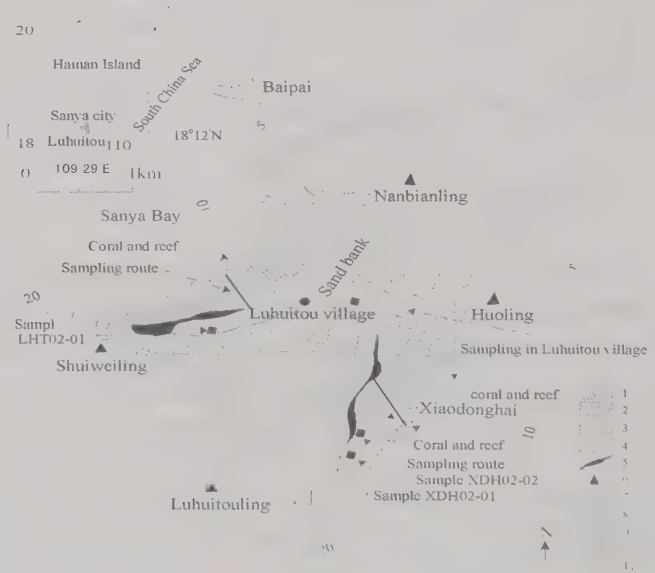

Fig.1 Distribution of coral reefs and locality of sampling at Luhuitou

1.Living coral zones; 2.Coral reef flat; 3.Sand bank; 4.Lagoon sediment zones; 5.Beachrock; 6.Hill; 7.Siliceous limestone; 8.Quartzose conglomerate; 9.Granite; 10.Quaternary marine sediment; 11.Bathymetric contour

The sampling localities are dispersive, and many are sampled from regenerative reefs, beachrock and coral grit in some former studies [9, 10]. The errors of measured ages of them are large because of the environmental reconstruction, and most of ages are not calibrated according to the environmental impact factor of ^{14}C age. In this study, the pristine *Porites* on the reef flats were concentratively sampled along the vertical route with coast on both sides of Luhuitou, and the diameters, of sampled coral reefs are more than 1m, and were not transited, and were less eroded during late period. All samples were sampled from the edge of beach to the reef-front slope according to the different biological-geomorphological zones (Figs.1, 2, 3). This method could avoid repeated sampling at the same geomorphological zone, and the ages of samples could reflect the sea level high-stands in the Holocene. Sixteen pristine *Porites* were sampled on the reef flat, and 2 pristine *Porites* in the reef-pond.

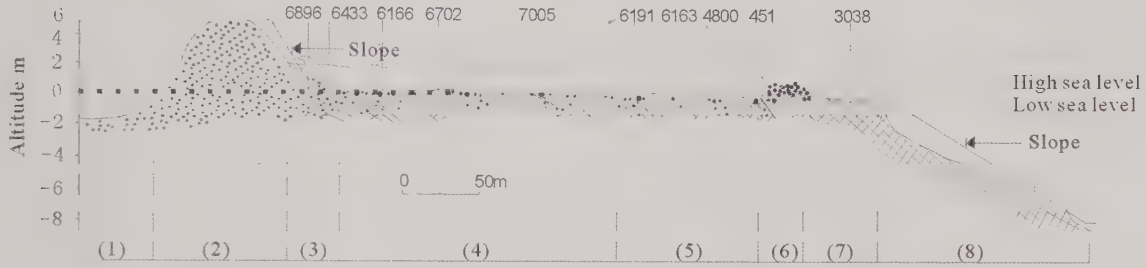

(1) Depression (2) Sand bank (3) Sand flat-beach (4) Inner reef flat (5) Middle reef flat
(6) Protuberant reef ridge (7) Outer reef flat (8)Ling coral cluster on reef front slope

Fig.2 The locality and calibrated ^{14}C age of coral reefs sampled in Xiaodonghai (cal.aBP, 0aBP = AD 1950)

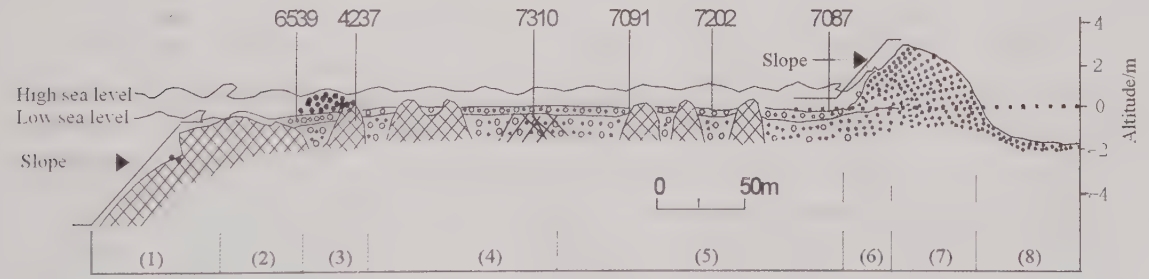

(1) Depression (2) Sand bank (3) Sand flat-beach (4) Inner reef flat (5) Middle reef flat
(6) Protuberant reef ridge (7) Outer reef flat (8)Ling coral cluster on reef front slope

Fig.3 The locality and calibrated ^{14}C ages of coral reef sampled in the Sanya Bay (cal.aBP)

3 Calibration of ^{14}C ages

The coral samples were washed with clean water in order to remove the salinity and impurity at

laboratory. Then the samples were dried and machined into 200 g per fraction, and their ^{14}C ages were measured at the Key Laboratory of Western China's Environmental Systems (Ministry of Education), Lanzhou University after labeled. The data are listed in Tab.1.

Tab.1 The measured and calibrated ^{14}C ages of pristine Porites at Luhuitou, Hainan Island

Sample label	Sample locality	^{14}C ages /aBP	calibrated ages /cal.aBP	Distribution of Caliburated ages /cal.aBP	Probability of distribution /%
LC02—01	Luihuitou village 18º12.716'N, 109º29.477'E	5836±78	6452	6559-6381	100
LC02—02	Luhuitou village 18º12.716'N, 109º29.477'E	5374±52	5989	6083-5945	100
XDH02—01	Southwestern Xiaodonghai 18º12.153'N, 109º29.663'E	6254±45	6896	6982-6831 6813-6807	97.3 2.7
XDH02—02	Southwestern Xiaodonghai 18º12.222'N, 109º29.694'E	5806±62	6433	6513-6371 6361-6358	99.1 0.9
XDH02—03	Southwestern Xiaodonghai 18º12.423'N, 109º29.800'E	5510±62	6166	6237-6079 6062-6058	98.3 1.7
XDH02—04	Southwestern Xiaodonghai 18º12.395'N, 109º29.813'E	6037±61	6702	6757-6627	100
XDH02—05	Southwestern Xiaodonghai 18º12.357'N, 109º29.830'E	6304±53	7005	7129-7126 7039-6944	1.4 98.6
XDH02—06	Southwestern Xiaodonghai 18º12.345'N, 109º29.858'E	5481±59	6191	6268-6150 6125-6118	96.5 3.5
XDH02—06'	Southwestern Xiaodonghai 18º12.334'N, 109º29.854'E	5488±61	6163	6205-6046	100
XDH02—07	Southwestern Xiaodonghai 18º12.322'N, 109º29.871'E	4305±68	4800	4829-4690	100
XDH02—08	Southwestern Xiaodonghai 18º12.313'N, 109º29.885'E	448±44	451	486-412	100
XDH02—09	Southwestern Xiaodonghai 18º12.310'N, 109º29.894'E	2933±52	3038	3108-2956	100
LHT02—01	Sanya Bay 18º12.670'N, 109º29.358'E	6381±64	7087	7157-7001	100
LHT02—02	Sanya Bay 18º12.705'N, 109º29.409'E	6453±64	7202	7259-7132 7105-7097	96.6 3.4
LHT02—03	Sanya Bay 18º12.708'N, 109º29.407'E	6373±62	7091	7159-7006	100
LHT02—04	Sanya Bay 18º12.735'N, 109º29.408'E	6591±56	7310	7366-7263	100
LHT02—05	Sanya Bay 18º12.777'N, 109º29.530'E	3890±38	4237	4297-4173	100
LHT02—06	Sanya Bay 18º12.755'N, 109º29.455'E	5867±73	6539	6625-6462	100

Note: Measured and calibrated ^{14}C ages: 1σ

Because of the effects of many environmental factors of ^{14}C radioactive concentration changes, the

measured ^{14}C ages have different errors, which resulted in that they need be calibrated accordingly. In order to calibrate the measured ^{14}C ages, the conventional software of R.C.P.4.3(RADIOCARBON CALIBRATION PROGRAM)[11] is used to amend the storage effect in this study, and the measured ages are transformed into calendar ages (cal.aBP, 0 aBP = AD 1950). Each distribution range of calibrated ^{14}C ages is small, the mean is 140 a, the minimum is 74 a, and the maximum is 178 a. So, the calibrated data of pristine *Porites* are highly representative and reliable.

All the measured and calibrated ^{14}C ages are distributed in the Holocene and dispersed in different periods. Most of ages are in 7300 - 6000 cal.aBP, and 12 sample ages on coral reefs are in this stage. Furthermore, 7 sample ages are in 7000 - 6000 cal.aBP, a few samples are in the last 6000 cal.aBP, and there is no sample age in 3000 - 1000 cal.aBP, but only 1 sample is in the last 1000 cal.aBP. All the samples collected from coral reefs are arranged and plotted in Fig.4. It is shown that the ages distributed in 7300 - 6000 cal.aBP is prominent, and the others were spasmodically distributed before 4800 cal.aBP.

Fig.4 The series of ages of coral reef

4 The high sea level in the Holocene recorded by the coral reef at the Luhuitou peninsula

About 81 % of the ages of the samples collected on reef flat is 7300 - 6000 cal.aBP, indicating that the coral reefs were developed very well and the pattern of biological-geomorphological zones was basically shaped in this period. Similar to the development of coral reefs in the Leizhou Peninsula, the coral reefs developed in this stage were not covered by the latter [3], indicating that the later sea levels were not higher than this period's. The coral reefs developed in later different stages were formed in depressions, such as reef-pools and reef-tunnels. Moreover, they developed outwards on both sides of the peninsula, but the present-day coral reefs develop at outer reef flat and reef-front slope. This is consonant with the highest sea level recorded by the coral reefs in the Leizhou Peninsula, and also with the development of the coral reefs in both peninsulas [3].

It is usually considered that the high sea levels correspond to the warming stages during the Holocene. All sample ages are distributed in the megathermal of Holocene except for the sample XDH02-08 [12]. Fig.5 shows the comparison between the calibrated ^{14}C ages and the Holocene temperature changes recorded by spore and pollen in China [14]. In this study, the sea level high-stands are divided into 5 stages according to the distribution of sample ^{14}C ages and the character of sea level

changes in the northern South China Sea [12-14].

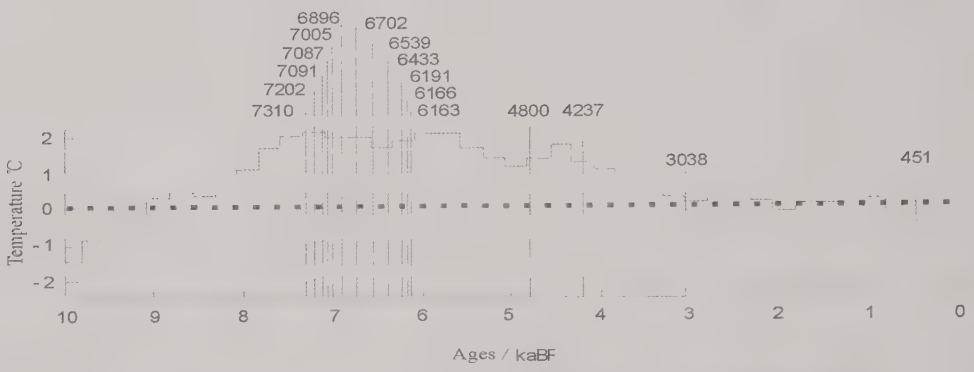

Fig.5 The sample ages and temperature curve in China during the Holocene [14]

The first stage (7300 - 6000 cal.aBP) Wang [15] considers that it was ordinary for the sea along the China coast in this period, and the transgression was prevalent. It is the megathermal of Holocene in 8000 - 6000 aBP [14]. It is also consonant with the sea level high-stands recorded by the coral reef in the Leizhou Peninsula [3]. Yu considers there were some relatively lower sea level fluctuations during 7200 - 6700 cal.aBP, and it was 3.42 m more than the elevation of the relative sea level (subsiding of crust or elevation of sea level) [16]. Maybe it was the first sea level high-stand in the Holocene according to the fact that the coral reefs were not covered by the later developed coral reefs and the temperature changes in past China [13]. The ages of LC02—01and LC02—02 are all in this period, which were sampled in a reef-pond about 5 m deep at the Luhuitou village. It is shown that the coral reefs were developed widely among Luhuitou Ling, Huo Ling and Nanbian Ling. This is a proof that the sea level high-stand existed at that time. The high sea level around 7000 cal.aBP is also recorded by sediments in the Song Hong (Red River) delta, Vietnam [17].

The second stage (4800 - 4700 cal.aBP） It is reflected by the sample XDH02-07, which is the outcome of less fluctuant warm-humid climate after a sharp temperature reduction around 6000 – 5000 cal.aBP. Furthermore, the age of it is close to the maximum of temperature increment after the second new glacial stage recorded by Dunde ice core. It was also a high temperature stage in China in the Holocene [13]. The sea level high-stand in this stage was also consonant with the third high sea level recorded by the coral reefs in the Leizhou Peninsula. In addition, the sea level in the Penghu Islands in 4700 aBP was 2.4 m higher than that at present according to the study of Chen et al [18].

The third stage (4300 - 4200 cal.aBP) It is reflected by the sample LHT02-05(4237 cal.aBP), which was sampled on the outer reef flat at the Sanya Bay and is also the outcome of less fluctuant and warm-humid climate before 4000 aBP[12, 13]. The high sea level in this stage was consonant with the "Guizhou transgression" in the South China Sea (the ^{14}C age is around 4600 - 3300 aBP) [15]. The obvious temperature increment around 4600 - 3600 cal.aBP was unveiled by the Jinchuan peat [19]. The sea level in the Pearl River Delta was also rising in 4500 - 3200 aBP [14]. Furthermore, the sea level around 4500 -

4300 aBP, which is recorded by sediment of Abatan River and evolution of mangrove in southwestern Bohol, Philippines, was 1 - 0.7 m higher than that at present, and the relative stable high sea level lasted until around 2500 aBP [20].

The fourth stage (3100 - 2900 cal.aBP) It is reflected by the sample XDH02-09 (3038 cal.aBP), which was sampled on the front of outer reef flat at Xiaodonghai. The sea level high-stand in this stage was consonant with the temperature increment around 3000 - 2900 aBP recoded by Dunde ice core, and there was a temperature reduction after that until the end of the megathermol of Holocene [12]. Maybe it corresponds to the second transgression in Guangzhou(^{14}C age is around 3000 - 2500 aBP)discussed by Luo [21]. The sea level was rising around 3200 - 2800 aBP in the Pearl River Delta, and the magnitude was about from -1.0 m to +1.5 m [14]. The sea level high-stand was stable in southwestern Bohol in Philippines at that time [20].

The fifth stage(~ 450 cal.aBP) It is reflected by the sample XDH02-08 (451 cal.aBP), which was sampled on the outer middle-reef flat adjacent to the protuberant reef ridge, and the last high sea level is maybe recorded by it. The medieval warming stage was around 930-1240 aAD, and it was the small ice age after 1 400 a. The sea level high-stand was maybe at the end of medieval warming stage.

The terraces and coral reefs at some islands along the Vietnam coast show that they were sea level high-stands in 5060 - 6800 aBP, 3375 - 4100 aBP, 2170 - 2435 aBP and 900 - 1200 aBP (^{14}C age) [22]. They are transformed into calendar ages by Yu, and are considered that they are consonant with the 5 sea level high-stands recorded by coral reefs in the Leizhou Peninsula [3]. Zhao thinks they were the sea level high-stands around 2500 - 1500 cal.aBP and middle Holocene according to the precise U-series dating of coral reefs from the Leizhou Peninsula, and the sea levels were 3 - 4 m higher than that at present [24]. Ma thinks it was a prosperous stage for the development of coral reef at Xisha Archipelago and northern South China Sea, and the sea level was 3 - 4 m higher than the sea line [24]. Moreover, Maeda also considers sea level high-stands existed in different stages in the Holocene according to the study on the coral reef terraces and tidal notches in Ilocos, Palawan and Samar along the Philippine coast.

The sea level high-stand exists widely in Vietnam and Philippine maritime space, Xisha Archipelago, northern South China Sea and Taiwan Straits recorded by paleo-coral reefs, indicating that the formation of the high sea level has the global background, at least in the South China Sea, which is correlated with the warming climate. Furthermore, the climate had a 1 000 a periodic change in the Holocene, it is important to recover the history of the sea level high-stand [26] and to predict the change trend of the sea level along the coast of South China.

The modern biological-geomorphological zones of coral reef had been already formed in the northern South China Sea around 7300 - 6000 cal.aBP according to the study on coral reef. Maybe the outline of modern coastline of South China Sea was also formed at that stage, and the distribution of landform was similar to that at present [3, 23].

It is noticed that there existed the megathermal of Holocene in 7300 - 6000 cal.aBP, and the sea

level high-stand lasted for a long time. Furthermore, the XDH02—08 is young relatively, which was at the beginning of the small glacial age. Maybe it is more reasonable that the high sea level is much older, i.e., it must be around Middle Ages, and the sea level high-stand around the warming period of Middle Ages is also recorded by coral reef in the Leizhou Peninsula [3]. The high sea level at this stage should be studied deeply because of the limitation of the technology of ^{14}C dating [27].

5 Conclusions

a) There were 4 sea level high-stands at least in the northern South China Sea in the Holocene (7300 - 6000 cal.aBP, 4800 - 4700 cal.aBP, 4300 - 4200 cal.aBP, 3100 - 2900 cal.aBP and ~ 450 cal.aBP). The highest sea level in 7300 - 6000 cal.aBP was the first stage, and no other was higher than it, and the temporal span was larger than the others.

b) 7300 - 6000 cal.aBP was the prosperous stage for the development of coral reef, and the biological-geomorphological zones had been formed basically. Later on coral reefs developed in reef-ponds or depressions in different periods and expanded outwards on both sides of Luhuitou peninsula after that. The modern coral reefs developed at the outer reef flat and reef-front slope.

c) Similar to the coral reef in the Leizhou Peninsula, the reflected high sea level stage could link up or correspond to the others in the South China Sea, which shows that the sea level high-stands have the global background, at least in the South China Sea. Furthermore, they are correlated with the warming climate.

Acknowledgements

The authors thank Dr. Kufu Yu and Dr. Gangjian Wei for their assistance in revising this paper. We gratefully acknowledge the financial supports from the National Natural Science Foundation of China (Grant No. 49976015).

References

[1] Gao F, Sun C Q, Qu J S. The new cognition on the change of the global climates ~ IPCC WGI. Third Assessment Report: Summary to Policymakers [J]. Advances in Earth Science, 2001, 16(3): 442-445.

[2] Woodroffe C, Mclean R. Microatolls and recent sea level change on coral atolls [J]. Nature, 1990, 344: 531-534.

[3] Yu K F, Zhong J L, Zhao J X, et al. Biological-geomorphological zones in a coral reef area at southwest Leizhou Peninsula unveil multiple sea level high-stands in the Holocene [J]. Marine Geology & Quaternary Geology, 2002, 22(2): 27-33.

[4] Neuman A C, Macintyre I. Reef response to sea level rise: keep-up, catch-up or give-up. Proceedings of the 5th International Coral Reef Congress (3), Tahiti.1985:105-110.

[5] Nie B F, Chen T G, Liang M T, et al. The coral reef and the high sea level in Leizhou Peninsula in the Holocene [J].

Chinese Science Bulletin, 1997, 42(5): 511-514.

[6] Nie B F. The coral reef records during high sea level in the Nansha archipelago for the last 5000 years. The Papers of the Study on Geology & Geophysics and Atolls in Nansha Archipelago and Its Neighboring Sea Zones(2) [M]. Beijing: Science Press, 1994, 115-125.

[7] Chen J R, Chen X S, Zhao X T, et al. Study on sea level in the Holocene change at Luihuitou area of Hainan province. The Geology Study in the South China Sea (3) [M]. Guangzhou: Science and Technology of Guangdong Press, 1991, 77-86.

[8] Zhao X T, Chen X S, Zhen F. Development of the coral reefs and tombolo of Luhuitou peninsula, Sanya city, Hainan province [J]. Quaternary Sciences, 1996, (1): 48-56.

[9] Zhao X T, Zhang J W, Li G Y. Development of the Holocene coral reefs along the southern coasts of Hainan Island [J]. Geology Science, 1983, (2): 150-159.

[10] Zhang M S, Liu J, Li H, et al. Basic characteristics and formation time of peripheral coral reefs in Hainan Island [J]. Marine Geology & Quaternary Geology, 1990, 10 (2): 25-43.

[11] Stuiver M., Reimer P J, Bard E, et al. INTCAL98 Radiocarbon age calibration 24,000 - 0 cal BP. Radiocarbon, 1998, 40: 1 041-1 083.

[12] Shi Y F, Wang Z C, Wang S M. Major events of the climate variations during the megathermal of Holocene in China [J]. Science in China (Series B), 1992, (12): 1 300-1 308.

[13] Wang S W, Gong D Y. Climate in China during the four special periods in Holocene [J]. Progress in Natural Science, 2000, 10(4): 325-332.

[14] Li P R, Qiao P N, Zheng H H, et al. The Environment Evolution of the Pearl River Delta in the Last 10 000 Years [M]. Beijing: Ocean Press, 1991, 59-68.

[15] Wang Y. Oceanography in China [M]. Beijing: Science Press, 1996, 169-170.

[16] Yu K F, Liu T S, Shen C D, et al. High-frequency climatic oscillations recorded in a Holocene coral reef at Leizhou Peninsula, South China Sea [J]. Science in China (Series D), 2002, 45(12): 1 057-1 067.

[17] Tanabe S, Hori K, Saito Y, et al. Sedimentary facies and radiocarbon dates of the Nam Dinh-1 core from the Song Hong (Red River) delta, Vietnam [J]. Journal of Asian Earth Sciences, 2003, (21):503-513.

[18] Chen Y G, Liu T K. Sea level changes in the last several thousand years, Penghu Islands, Taiwan Strait [J]. Quarternary Resarch, 2000,53: 277-284.

[19] Hong Y T, Jiang H B, Tao F X, et al. Jinchuan peat $\delta^{18}O$ record of temperature in the past 5 ka [J]. Science in China (Series D), 1997, 27(6): 526-530.

[20] Berdin R D, Siringan F P, Maeda Y. Holocene relative sea-level changes and mangrove response in southwest Bohol, Philippines [J]. Journal of Coastal Research, 2003, 19(2): 304-313.

[21] Luo Z S. Recent level changes in Guangzhou [J]. Tropical Geography, 1983, (2): 25-31.

[22] Korotky A M, Razjigaeva N G, Ganzey L A, et al. Late Pleistocene-Holocene coastal development of islands of Vietnam [J]. Journal of South Asian Earth Sciences, 1995, 11(4): 301-308.

[23] Zhao J X, Yu K F. Timing of Holocene sea-level highstands by mass spectrometric U-series ages of a coral reef from Leizhou Peninsula, South China Sea [J]. Chinese Sciences Bulletin, 2002, 47(4): 348-352.

[24] Ma Z B, Xiao J L, Zhao X T, et al. Precise U-series dating of coral reefs from the South China Sea and the high sea level during the Holocene [J]. Journal of Coastal Research, 2003, 19(2): 296-303.

[25] Maeda Y, Siringan F, Omura A, et al. Higher-than-present Holocene mean sea levels in Ilocos, Palawan and Samar, Philippinges [J]. Quaternary International, 2004, 115-116:15-26.

[26] Campbell I D, Campbell C, Rutter N W, et al. Later Holocene ~1500 yr climatic periodicities and their implications [J]. Geology, 1998, 26(5): 471-473.

[27] Yu K F, Zhao J X, Shi Q, et al. New insights into biological- geomorphological-sedimentary zones and environment records at the south west reef bracelet of Yongshu reef, Nansha Islands [J]. Marinegeology & Quaternarygeology, 2003, 23(4): 1-7.

海南岛鹿回头珊瑚礁与全新世高海平面

黄德银[1]，施祺[2]，张叶春[2]

（1. 中国科学院广州地球化学研究所，广东 广州 510640；2. 中国科学院南海海洋研究所，广东 广州 510301）

摘 要：通过实地考察和资料分析，海南岛南部全新世以来以沉降活动为主要特征，鹿回头珊瑚礁能够反映全新世以来的海平面变化，鹿回头岸礁礁坪面上的原生珊瑚礁是全新世高海平面时期的产物。全新世以来南海北部至少存在过 4 期相对高海平面阶段：7300 ~ 6000、4800 ~ 4700、4300 ~ 4200 和 3100 ~ 2900 cal.aBP。其中 7300 ~ 6000 aBP 是整个全新世最高海平面时期，也是鹿回头珊瑚礁发育的繁盛期，基本形成了现代珊瑚礁的地貌格局，后来不同时期发育的珊瑚礁是在此时期形成的礁塘或礁坑等低洼地中形成，并在鹿回头半岛两侧向外发展，现代珊瑚礁则发育于全新世珊瑚礁的外礁坪和礁前斜坡带。另外，鹿回头珊瑚礁反映的南海北部全新世高海平面时间与南海其他地区高海平面时间可以衔接或对应，说明南海地区全新世高海平面具有全球背景，至少在南海是一致的，且与气候变暖紧密相联。

关键词：珊瑚礁；高海平面；全新世；海南岛鹿回头

An Overview of the Concept of Regional Sediment Management

LEI Huaiyan [1,2], Serif BASOGLU [1], SHI Yuezhong [1], LIN Binghuang [1], GONG Chenlin [1]

1. *College of Oceanography and Environmental Sciences of Xiamen University, State Key Laboratory of Marine Environment Science, Xiamen University, Xiamen* 361005, *Fujian, China;*
2. *Key Laboratory of Gas Geochemistry, CAS, Lanzhou* 730000, *Gansu, China*

Abstract: In this article we described the concept of "regional sediment management" (RSM), and identified opportunities for and impediments to implementing regional approaches to sediment management, and also summarized the background information and applications of RSM. Furthermore, we considered the needs of RSM studies and, suggested the framework for developing RSM strategies, and described the specific studies for the Xiamen region.

Keywords: RSM; resource; coastal zone; dredging

Introduction

In this article we described the concept of "Regional Sediment Management" (RSM), its background and application within the coastal engineering concept, and issues associated with its implementation in the future.

The need for RSM is based on the recognition of the regional implications of dredging and other activities in the littoral zone, as well as the appreciation for sand as a resource as much as water which is a resource experiencing competing demands, along with both quantity and quality issues. RSM is an approach to managing projects involving sand and other sediments that incorporates many of the principles of integrated watershed (including riverine system) resources management, applying them primarily in the context of coastal watersheds. It also supports many of the recommendations on improving the dredged materials management. Examining RSM implementation through demonstration efforts can provide lessons not only on improved business practices, techniques and tools necessary for managing resources on a regional scale, but also in terms of roles and relationships important to the integrated water resources management.

1 History of RSM

RSM originated in the notion of coordinating dredging activities in the coastal zone for the purpose of retaining sand in the littoral system in the interest of promoting more balanced, natural system processes, and reducing project costs. In 1994, the U. S. Coastal Engineering Research Board (CERB) was tasked

Received on April 9, 2006

with developing future directions for civil works coastal engineering and supporting R&D (research and development). Recommendations from the CERB task force included, among other things, adopting a "system approach to coastal sediment management".

As a result, a working group on the sediment resources management was formed to develop implementation recommendations.

The concept of RSM was later introduced at the U S. Marine Transportation System National Conference in 1998 [1]. The theme for the 67th CERB (1998) was "Regional Sediment Management," and the CERB reexamined the concept along with the proposal for an RSM demonstration project within the Mobile District. Recommendations for pursuing RSM were made by the CERB at its 1997 meeting. The CERB recommended taking a "system approach to effective sediment resource management", noting that:

(1) Current cost-benefit analysis and engineering considerations treated navigational concerns of coastal engineering separately from the associated impacts of down drift beaches, with the result that it was often more expensive, and less acceptable to repair the down drift beaches than it would have been to maintain the original natural flow of sand.

(2) The challenges of projects in bays and harbors make a systems approach essential to managing sediment in an environmentally sensitive manner.

(3) Benefits of taking this system approach could include enhanced public participation and agency collaboration in planning and management, and reduced adverse impacts on the nearshore system.

(4) Costs (first costs and long-term maintenance costs) could be reduced over both the short and long terms.

2 Implications of dredging

Particularly navigation jetty and navigation-channel projects along the riverine system or boundaries between riverine- littoral marine systems are generally old, having been constructed without knowledge of potential regional impacts and contemporary needs and values associated with the resource management. Advances in understanding of coastal sediment processes, and observation of impacts from earlier projects reveal a number of regional impacts associated with navigation projects. Large jetties, deep channels, and sand management practices that obstruct or otherwise prevent the natural movement of sand along the coast can be detrimental to beaches and other aspects of coastal systems. These effects can extend miles from the project and across many regional boundaries.

Main implications of dredging without considering "Operation and Management" (O&M) under the RSM concept are the changes or effects of the sediment budget -which is an accounting of the sources and sinks (or gains and losses) of littoral material in a defined area- and impacts on the natural environment or the ecosystem in the vicinities, even in the coastal region. From the coastal engineering point of view, main causes and effects of this type of dredging are outlined below.

2.1 Creation of new depositional environment and changes of bottom sediment composition

Deepening of the bottom and increasing of the slope increase the sedimentation rates in the dredged areas. The diagram in Fig. 1 shows how the quality of the sediment changes with depth. The red curve is the bottom profile, running from land at the 10 m height on the left, to a depth of -45 m, on the right. The colored areas show the relative composition (0 - 100 %) of the sea sand. Close to the coast, the sand consists mainly of fine sand, which is capable of being moved by wind, thus forming part of the dune system. Fine sand also moves easily in the water, and up a steep dredged slope. It is also easily moved away from the coast. Further out, the sand is mainly of medium size, easily moved by waves. Then an area comes of mainly coarse sand, which is not easily moved by waves from the coastal zone, and is left behind at the coast, while its finer sand component was winnowed out by the wave action toward deeper waters. Then suddenly, the composition changes to fine sand and a substantial amount of mud comes in. This is the area where even large waves cannot move the sand towards the coast, and the mud is soaked up by the fine sand. Deeper still where the waves are very seldom felt, the mud can settle out on top. Eventually, the bottom of the dredged areas becomes entirely muddy.

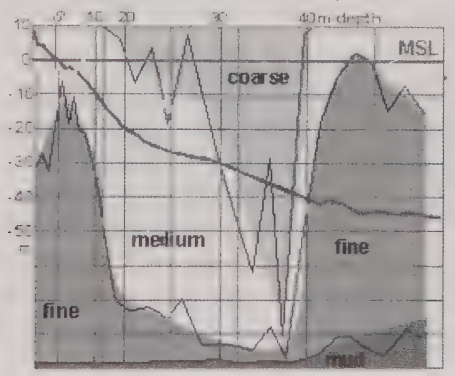

Fig.1 Relationship between sediment types vs. depth

2.2 Changes of current velocities for erosion/accretion, sedimentation and transport

The diagram in Fig.2 depicts the relationships between water velocity and grain size with relevance to erosion/accretion, transport and sedimentation. It defines the behavior of sediment in water, under the influence of currents and waves. Notice that the scales span an enormous range of four decades! Vertically, from bottom to top, the grain size increases, and colored bands have been drawn to mark clay, silt, sand, granules and pebbles. The straight line is the theoretical drag, as defined by Stokes' equation, which excludes turbulence. The two curves left and right of it have been derived from actual measurements. Water velocity needs to exceed the right-hand curve before the cohesive (packed-together) material begins to move. It is interesting to note that silt and clay, once settled as a 'cake', are hard to dislodge. The left-hand curve shows at which velocities particles settle out. Again silt and clay need extremely tranquil conditions before doing so. For the coarse material, the erosion and sedimentation curves follow the theoretical straight line. The diagram shows that pebbles can be moved

only by strong wave action, or by fast flowing currents. In order to form beaches, the grains must be moved easily but also stay put - two conflicting properties. Sand from about 0.2 mm to boulders of 100 mm or larger (the area between the straight ends), would do this. Silt and clay, however, would not. Boulder beaches form only on very exposed shores, whereas beaches of fine sand form on more sheltered shores. Mud flats, on the other hand, form only at the most sheltered places inside enclosed harbors. Furthermore, particularly in the navigational channels and jetties while causing the deposition of muddy material, combination of changes of natural current velocities due to sudden slope variations with the turbulence created by vessels' propellers export the sand to the less deep areas will not only alter the coastline configurations, but also create shoals and bars, and increase the deposition of mud within the harbor.

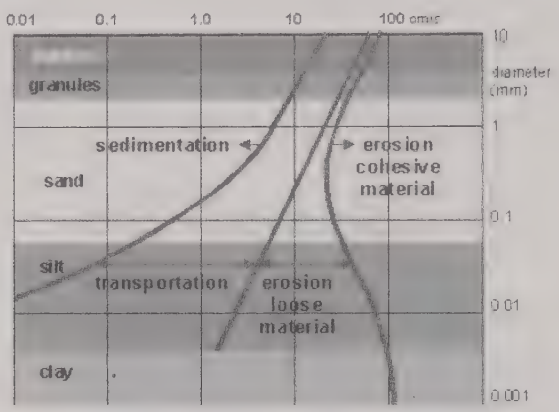

Fig.2 The relationship between erosion/accretion, transport and sedimentation due to changes in current velocities and particle size

2.3 Environmental consequences of dredging

This type of local or project-specific scale dredging will have negative impacts on the environment or the overall ecosystem. A main effect of dredging is stirring. For instance, skimming the bottom 30 cm daily will cause an area of 1 km^2 disturbed by the stirring.

As it is illustrated in Fig.3, firstly, this will cause a direct habitat disturbance to bottom living communities. Secondly, during the dredging, a plume of silt will develop, both over the bottom and near the surface. It will pollute the sea water for some time, and promote plankton blooms from the released nutrients. Poisons such as heavy metals and hydrogen sulphate, locked up over time within the sea soil, are released again. This will cause either death of some of the bottom fauna, or alteration within the bottom living communities on the one hand, and transportation of polluted plumes by currents, waves or tidal actions to elsewhere on the other.

Furthermore, during the offshore disposing of dredged material suspended load with contaminated materials will be generated by the surface dust plume. Some of this contaminated suspended load will be

carried by the transporting agents (current, wave, tide) to the nearshore areas. This would cause pollution of the beaches and nearshore waters.

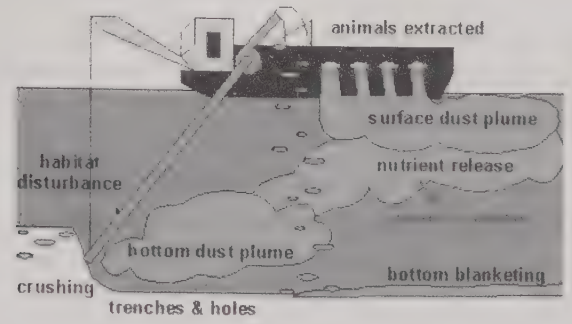

Fig.3 Environmental consequences of dredging

2.4 Overall/combined effects of the local or project-specific dredging

The overall or combined negative effects and its consequences of local or project-specific dredging in the navigation channels or jetties off the riverine system are given below.

(1) Rapid sediment transport toward the newly dredged sites, and its accumulation and settling.

(2) Increase of both erosion in the coastal headlands, and offshore shoaling and nearshore bar formation.

(3) Physical, chemical, and biological changes by disturbing the sea bottom.

(4) From an ecological perspective, bottom fauna could suffer permanently from disturbance.

(5)Increase of the pollution stress in the coastal zone and coastal areas.

(6) As it is proven elsewhere, increase of the dredging costs (first costs and long-term maintenance costs) year by year.

For instance, in the USA the yearly average for total dredging for the 10-year period 1992-2001 was $641 million, to dredge an average of 269 million cubic yards. The average total dredging cost for the last three years was $834 million. The average O&M dredging under the RSM plan for the same three-year period is about $559 million and 228 million cubic yards. That means, the three year cost of the dredging under local or project-specific works are $281 million more than the RSM planned dredging. (These figures are in real dollars, not adjusted for inflation.) Source: Annual Continuing Analysis of Dredging Data; US Corps of Engineers, 2003.

3 Current concept of regional sediment

Regional sediment management (RSM) is a "system-based approach" that seeks to solve sediment-related problems by designing solutions that fit within the context of a regional strategy.

(1) RSM involves making local project decisions in the context of the sediment system and forecasting the long-range implications of management actions.

(2) RSM recognizes that sediment management actions have potential economic and ecological implications beyond a given site, beyond originally intended effects, and over long time scales (decades or more).

(3) RSM is the integrated management of littoral, estuarine, and riverine sediments to achieve balanced and sustainable solutions to satisfy the sediment-related needs. This approach provides opportunities to achieve greater effectiveness and efficiency.

As it was mentioned earlier, the concept of RSM originated in the notion of coordinating dredging activities in the coastal zone for the purposes of retaining sand in the littoral system in order to foster more balanced, natural system processes, and reduce project costs. RSM applies a system perspective to problem solving, managing sand as a regional resource, and integrating the portfolio of coastal engineering programs and projects related to the sediment in a given region. It is intended to advance application of sustainability principles, by

(1) Recommending approaches that can reasonably accommodate multiple objectives,

(2) Promoting consideration of the competing demands for sediment resources (ecological and socio-economic),

(3) Recognizing "sediment as a resource", RSM involves maintaining or promoting the natural exchange of sediment within the boundaries of the physical natural system,

(4) Identifying sand and sediment processes as important components of coastal and riverine systems that are integral to economic and environmental vitality,

(5) Considering effects beyond the immediate timeframe, and

(6) Achieving acceptable tradeoffs and cost efficiencies.

Concurrently, RSM involves recognizing the multiple, often competing demands for sediment in a region, and that the systems involved are often modified by multiple factors.

RSM is intended to integrate planning, engineering and operations activities within coastal, estuarine, and riverine systems, and broaden the problem solving perspective from a local or project-specific scale, to an expanded scale defined by natural sediment processes. It recognizes that the physical system and associated ecological system are modified and respond beyond the limited dimensions and time frames of individual projects. The larger spatial and longer temporal perspectives of RSM require the integration of a broad range of disciplines along with collaborative partnerships among stakeholders.

4 Potential benefits of RSM

These benefits can be realized in terms of cost savings (near-term and long range), improved management and use of sediment resources for a broad range of benefits, as well as in terms of valuable intangible benefits. These benefits can be characterized as "technical," "programmatic," and "institutional".

4.1 Technical Benefits

(1) New engineering techniques to optimize and conserve sediment -Bypassing of beach quality

sand at inlets and implementing regional rather than project scale approaches.

(2) Foundations for future studies and projects in region – The improved process models, data and information management tools will benefit both current and future studies and projects.

(3) Dredged Material Management plans can provide an important vehicle for developing and executing the regional approaches to sediment management, particularly when developed regionally, rather than for individual projects.

4.2 Programmatic Benefits

(1) Process efficiencies

A. Potential reductions in rehandling of material, improved channel efficiency and associated cost savings over the longer term.

B. Increased disposal site capacity and reduced need to acquire new sites.

(2) Environmental

A. Stabilized habitat for listed species

B. Sediment as a resource

C. Potential new sources of desirable sediment.

4.3 Institutional

(1) Stronger partnerships - Partnerships among coastal and watershed stakeholders leading to improved business processes, data sharing, greater cooperation and collaboration among parties.

(2) Better information – Improved understanding of regional sediment processes and the interrelationships of projects and management actions contribute to the improved knowledge about problems, causes and solutions. This in turn contributes to the development of more effective and efficient management approaches.

(3) Identification of institutional obstacles so they can be addressed. – Some issues may be addressable through clarification of policy, or revisions to business practices. Some issues may need to be addressed through multi-agency or other partnership efforts.

5 Examples to RSM works

RSM can be illustrated with a hierarchy of examples:

(1) The simplest involves coordination of dredging activities in the coastal zone for the purpose of establishing regional sediment budgets, reducing project costs and protection or restoring environmental resources. Efforts may involve using the suitable dredged material from an inlet nearshore to feed an eroding beach, rather than disposing of it offshore. Placement of the material near shore could make the material available to the littoral system, potentially enabling natural processes to move it onshore.

(2) Moving beyond an individual project, the "pairing of projects" has the potential to produce economies of scale in planning or construction, along with more effective projects and problem

solving due to the incorporation of system relationships. "Project pairs" can ultimately produce cost savings, and in theory this savings can involve different civil works funding accounts, where the savings is realized at the civil works program level. For example, dredging for inlet or navigation channel maintenance could be linked with a beach nourishment project, where, instead of the dredged material being disposed of off-shore and the sand for beach nourishment being obtained from an off -shore source, the dredged material could be used directly in the beach nourishment projects, assuming the material is suitable.

(3) Examples of broader application would include coordinating all civil works projects and studies related to the sediment in a region – comprehensive studies with dredged material management plans, new projects and potentially regulatory decisions.

At each of these levels benefits may be realized by the improved integration of coastal engineering projects and programs with those of other agencies. RSM has the potential to result in not only significant cost savings through coordination of construction activities, but also development of regional data and information that will enhance regional planning and management capabilities.

6 Suggestions on the framework for developing RSM strategies for Xiamen

A conceptual framework composed of alternative actions, projects, or sediment management practices appropriate for a Xiamen Region (includes the riverine systems, the port, Gulang Yu Island, and the eastern coastal zone and its beaches) for developing RSM strategies, along with management plans is outlined below. Working through this framework will be an iterative process. Information provided at each step advances the knowledge base for decisions and recommendations along the way. Stakeholder and public involvement may vary with each strategy and plan, but is integral to each part of the framework.

6.1 Specifying Sediment-related Problems and Opportunities

(1) Recognition of the Region: Identifying and defining the region by means of region based sediment system, boundaries, sectoral division within the boundaries, and management objectives and issues.

(2) Distinguishing of Sediment Concerns and Needs: In view of erosion, accretion, sediment demands, and structures.

(3) Identifying Public and Private Stakeholders Interests: Includes several of the following: channel maintenance and other works involving dredging, habitat protection or restoration, beach nourishment and renovation, beach and sediment use regulation, bank erosion reduction, sedimentation problem in channels and jetties, and others.

6.2 Listing and Estimating the Conditions

(1) Collecting the available information: Which contributes to the comprehension of historic, present, future sediment conditions, along with associated planning and management implications. It also includes overland transport and sediment transport through riverine systems (rivers, estuaries, etc.), and

mechanism of coastal transport.

(2) Identification and Formulation of Alternative RSM Plans: Including various numerical models in order to be utilized to estimate the regional sediment transport, optimize alternative plans, and asses the cumulative impacts of multiple projects within the region.

(3) Evaluation and Comparison of Alternative RSM Plans: Consideration of the following aspects (parameters) of magnitude, location, timing, duration, benefits or disadvantages. Judgment of the effects of tradeoffs, cost-effectiveness of outputs relative to different types of effects and preferences.

(4) Selection and Implementation of RSM Strategy.

7 Conclusion: proposal of the specific studies under the Xiamen RSM plan:

As we mentioned above, we defined the Xiamen Region as Jiulong River, distributaries and headlands, Xiamen Port, Gulang Yu Island, N-S direction navigation channel located at the port which, we assume, has a profound effect on the sediment flow, and the eastern coastline where residents and tourists use these beach areas for recreation, tourism and housing needs. These same beaches also provide habitat for various fauna and flora. Erosion from storms and tides often threatens coastal areas, including material loss of or damage to sandy beaches.

A complex array of variables which are involved in the determination and identification of RSM are given below.

8 Technical program implementation

A key element for the successful regional sediment management is the regional sediment budget. The sediment budget assists in identifying longshore sediment transport rates, sediment transport patterns and pathways, areas of erosion and accretion, and understanding the reasons for and magnitude of beach and bathymetry change over the region. Through the sediment budget, regional impacts resulting from proposed modifications to sediment and project management can be predicted. A preliminary or conceptual regional sediment budget was created based on the available historical information and utilizing the Sediment Budget Analysis System (SBAS) (Rosati and Kraus 1999). The conceptual budget quantified the knowns and qualified the unknowns relative to the sediment transport over the region. The sediment budget provided direction to the program by identifying regions where data collection, information, and policy are needed (primarily riverine system). For this purpose, as the first step, the process to implement RSM is illustrated in Figure 4.

8.1 Engineering tools

The following engineering tools are identified as necessary for the regional sediment management:

(1) A regional sediment budget including budgets at subregional and project levels.

(2) Numerical models to evaluate hydrodynamic conditions, sediment transport, and shoreline change at regional, subregional, and project scales.

(3) A data management tool for managing and storing historic and new data, and a tool for performing analysis of data and model results; the tools will allow sharing of information and data.

The following data are necessary to perform the regional coastal processes management:

(4) Hydrodynamic and meteorological data: waves, water levels, currents, winds, and storm data.

(5) Historic bathymetric, topographic, and shoreline data.

(6) Regional, continuous, current, and synoptic bathymetric and topographic surveys.

(7) Data acquisition and monitoring, includes field collection of the necessary data, and surveying (data relevant to waves, currents, tides, drifts, longshore currents, etc, and bathymetric, hydrographic surveys)

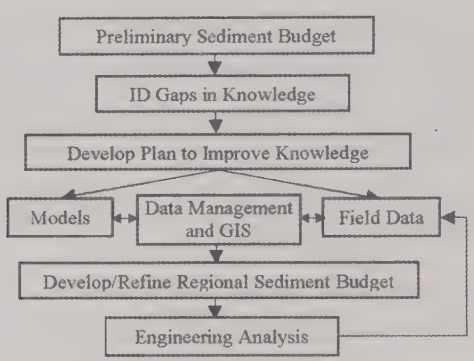

Fig.4 Process to implement RSM

8.2 Numerical model application

The modeling efforts provided an understanding of regional coastal processes including wave transformation, sediment transport, shoreline change, tidal circulation, and water-level fluctuations. The models were then focused at the subregional and project scales to refine the sediment budget and begin evaluation of proposed project modifications to improve sediment management. Related works are:

(1) Wave transformation studies,

(2) Longshore sediment transport and shoreline change

(3) Water levels and circulation / tides and tidal effects

(4) Comparisons between transport rates derived from the available physical data and those computed from the hindcast wave information should be provided.

8.3 Dredged material management

In order to classify the dredged materials for the possibilities of future use and offshore disposal, the following studies should be conducted:

(1) Bulk sediment analysis and identification of their geotechnical, sedimentelogical properties;

(2) Testing and analysis bioaccumulation and toxicity levels of the dredged materials.

Acknowledgements

This project was supported by the National Natural Science Foundation of China under the contracts Nos. 4027066, 40472156

References

[1] Carter R W G. Coastal environments [A]. An introduction to the physical, ecological and cultural systems of coastlines. Academic Press, 1991

[2] Gravens M B. Sediment Management at Perdido Pass Alabama [J]. Proceedings, Coastal Sediments, 2003, Clearwater Beach, F L.

[3] Lillycrop L S, Wozencraft J M (2003a). Technical lessons learned for Regional Sediment Management [J]. Proceedings, National Conference on Beach Preservation Technology 2003, Ponte Vedra F L, February, 2003, 12-14.

[4] Lillycrop L S, Wozencraft J M (2003b). Engineering tools for regional sediment management [J]. Proceedings, Coastal Sediments 2003, Clearwater Beach, FL, May, 2003, 18-23.

[5] Nittrouer C A. The Process of Detrital Sediment Accumulation in a Continental Shelf Environment: An Examination of the Washington Shelf [J]. Ph.D. Thesis, University of Washington, Seattle, Washington, 1978.

[6] U. S. Army Engineer Portland Distric. Draft Integrated Feasibility Report for Channel Improvements and Environmental Impact Statement: Columbia and Lower Willamette River Federal Navigation Channel [J]. U. S. Army Corps of Engineers, Portland District, Portland, Oregon, 1998.

区域沉积物管理概论

雷怀彦[1,2]，Serif BASOGLU[1]，史跃中[1]，林炳煌[1]，龚承林[1]

（1. 厦门大学海洋与环境学院，近海海洋环境工程国家重点实验室，福建 厦门 361005；2. 中国科学院地质与地球物理研究所，气体地球化学重点实验室，甘肃 兰州 730000）

摘 要：就“区域沉积物管理”（简称 RSM）概念与方法进行了系统论述，以厦门地区为例阐述了 RSM 研究的必要性和重要性，并对如何应用区域沉积管理来处理海岸冲刷、淤积与港口码头建设过程中可能遇到的问题进行了深入浅出的讨论，同时，提出了发展 RSM 的战略构想与框架。

关键词：区域沉积物管理（RSM）；资源；海岸带；疏浚

Prediction of Petroleum Prospect in the South Yellow Sea Basin Using Satellite Remote Sensing

GONG Jianming [1, 2], CHEN Jianwen [1, 2], LIANG Jie [2], ZHANG Zhixun [2], LIU Chuang [3], LU Zhenquan [4], HUANG Fulin [2]

1. *Ocean University of China, Qingdao* 266003, *Shandong, China;*
2. *Qingdao Institute of Marine Geology, China Geologic Survey, Qingdao* 266071, *Shandong, China;*
3. *Institute of Geographic Sciences and Natural Resources Research, Chinese Academy of Sciences, Beijing* 100101, *China;*
4. *Institute of Mineral and Resources, Chinese Academy of Geological Sciences, Beijing* 100037, *China*

Abstract: Using satellite remote sensing to measure the sea surface temperature of the East China Sea Shelf Basin can serve the purpose of predicting the petroleum prospect in the South Yellow Sea Basin. The satellite thermal infrared temperature anomaly area always repeats in the same position as the proved oil prospect area in the East China Sea Shelf Basin, and coincides well with both the CH_4 content curve at the water-atmosphere interface and the seafloor geochemical anomaly. The sea surface temperature anomaly areas of the South Yellow Sea Basin in the satellite remote sensing image go banded along 123°30′ in the S-N direction, and naturally follow the aeromagnetically interpreted eastern nose-type uplift that shows a S-N strike. The north and south ends of the eastern nose are considered as good oil prospect areas because temperature anomaly often occurs there.

Keywords: temperature anomaly; satellite remote sensing; oil prospect; the South Yellow Sea

Introduction

Recently the application of satellite thermal infrared remote sensing to resource exploration and environmental and hazard monitoring is gaining more and more attention in the world. From the end of 1980s to 1990s, Qiang et al. [1] and Huang et al. [2] used this method for China's petroleum prospecting and got good results [3].

Satellite-based thermal infrared remote sensing is an infrared-imaging technique to record infrared radiations in the form of images depending upon different infrared radiations and temperatures of ground objects offered by a satellite thermal infrared sensor during its application to remotely sensing the Earth's surface. The present satellites for monitoring georesources and environments usually adopt wavelengths of medium and far infrared wave bands, and to say in detail, atmospheric windows such as 35 - 18, 2.0 - 2.4, 3.5 -4.1, 4.5 - 5.5, and 8 - 14 μm are used to scan temperature distributions in the Earth's surface, water bodies and clouds. Such distributions of temperatures are very similar to actual situations although

Received on April 20, 2006

only relative intensities of thermal radiation energy of the surface features are recorded in the images.

Before an earthquake, a large area of temperature-increment anomaly usually appears in the satellite thermal infrared image, which results from gas (such as CH_4) releasing out of the Earth's surface due to the pre-earthquake compression stress of the crust and then incrementally heating under the inducing actions of the transient electric field and solar radiation to lead to temperature increment anomalies in the lower atmospheric layer or on the sea surface. Our study results indicate that the temperature increment anomalies are obviously distributed along faulting structures, especially at the junctions of different fault zones.

US satellite TERRA launched on 18 of December 1999 has its seven bands (20, 22, 23, 29, 31, 32, and 33) of MODIS capable of providing information of changes in ground surface or water surface temperatures, which gives a precision up to 0.3 k for sea surface temperature inversion and 1 k for ground surface temperature inversion [4-5], much more precise than the data from old meteorological satellites that used thermal infrared bands to reflect temperature anomalies of surface objects.

The authors try to predict oil prospect in the South Yellow Sea using the satellite remote sensing method by inference from knowns to unknowns.

1 Satellite remote sensing and oil-gas fields of the East China Sea

Supported by the National Natural Science Foundation (49271054) in the 1990s, Huang et al. [2] finished their research on the relationship between satellite thermal infrared temperature anomaly and sea-land oil accumulation, approached for the first time the possibility to search for marine hydrocarbon by means of satellite remote-sensing, and discovered that in the satellite images for the Pinghu petroleum area in the East China Sea, the temperature increment anomaly always appeared in the same position [6], in good coincidence with the CH_4 content curve at the water-atmosphere interface and with the seafloor geochemical anomaly (Figs. 1-4). Fig.1 was mapped by Li et al. [7] on the basis of the integrated study on pore water, dissoluble Fe and ΔC oil geochemical indexes of the East China Sea surface sediments, and we can see that the temperature anomaly areas in Fig.1 superpose with those showed by satellite thermal infrared images of Figs.2-4, and the Pinghu oil area lies within the anomaly. Moreover, CH_4 content in the lower atmospheric layer is somewhat different between oil and non-oil areas, and that in the former (Chunxiao-1-well in the East China Sea) is higher than in the latter (Fig.5). Such temperature and hydrocarbon composition anomalies at the water-atmosphere interface very probably result from the microseepage of hydrocarbon in submarine oil and gas pools [8-13].

2 Satellite remote-sensing and oil prospect area of the South Yellow Sea

The South Yellow Sea Basin is the only sea area where oilfields have not been discovered yet, and separated from the East China Sea Shelf Basin by the boundary line linking the Yangtze River mouth with

the Cheju Island of Korea. It is a rift basin with five tectonic units (Qianliyan uplift, Yantai depression, Laoshan uplifting zone, Qingdao depression, and Wunansha uplift) from north to south (Fig.6).

2.1 Temperature increment anomaly in the South Yellow Sea Basin

Compared with the East China Sea, the South Yellow Sea Basin has a generally weak tectonic intensity and low magnitude of earthquakes. According to statistics, there have not occurred earthquakes of over magnitude 5 in the basin since 2002, and therefore the temperature anomaly reflected in satellite images of the South Yellow Sea is usually less than 1 k. To recognize such small temperature anomalies, we have chosen a high-precision TERRA satellite to conduct the present study.

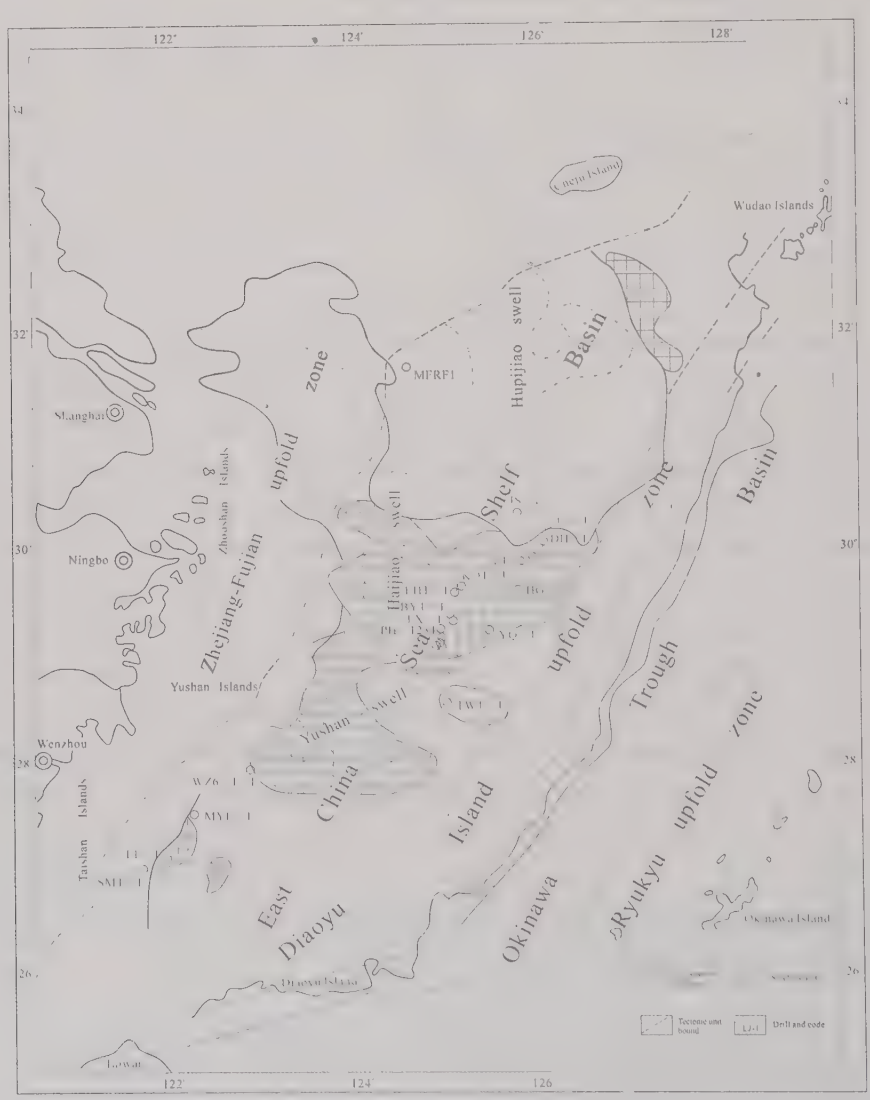

Fig.1 Oil geochemical prospect area in the East China Sea Shelf Basin (after Li et al., 1993 [7])

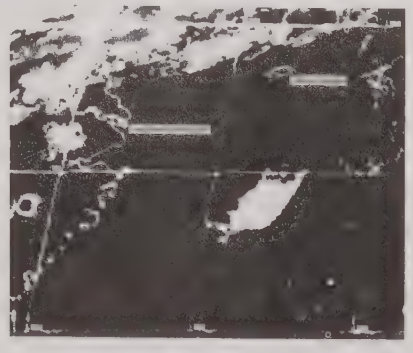

Fig.2 Pinghu Oilfield temperature anomaly showed by GMS satellite thermal infrared image taken during September of 1991

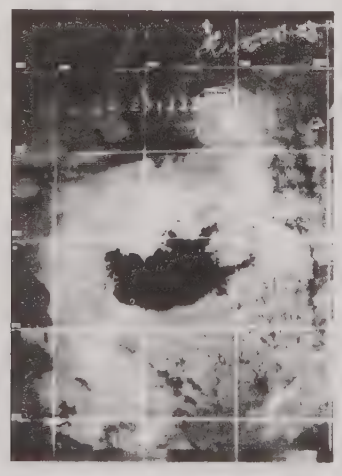

Fig.3 Pinghu Oilfield temperature anomaly showed by NOAA satellite thermal infrared image taken during September of 1992

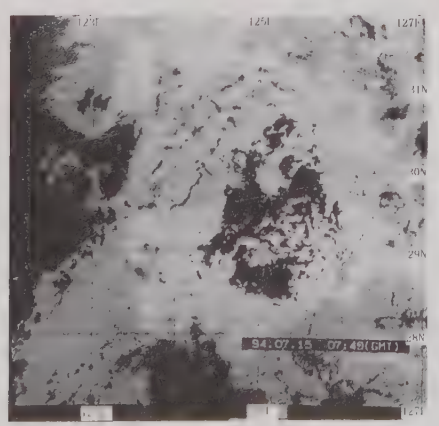

Fig.4 Pinghu Oilfield temperature anomaly showed by NOAA satellite thermal infrared image taken during July of 1994

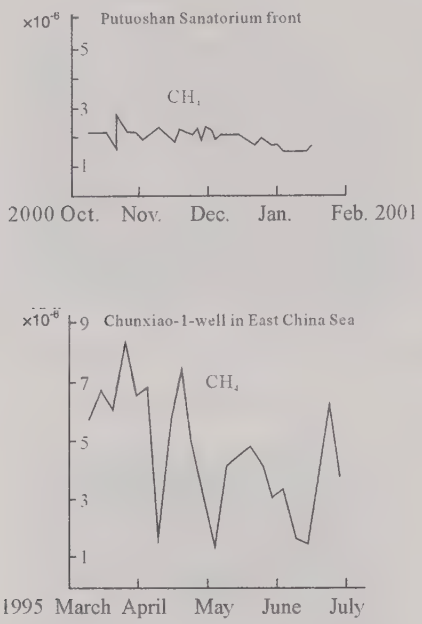

Fig.5 Comparison of CH_4 content in the lower atmospheric layer between oil and non-oil areas (after Huang et al., 1998 [2])

The basin-coverage MODIS data first went through atmospheric, radiant and geometric corrections, and were then processed with de-clouding, aim calibration and intensification. In 2002, only three days met with temperature anomalies in the South Yellow Sea, and Fig.6 gave their distributions. The green in the figure represents the anomaly found on 26 of September, which spreads in an evident concentric-ring pattern with the central temperature about 1 k higher than in the ambient sea area. This is the clearest anomaly discovered during the present study. The purple stands for the temperature anomaly on 17 of the same month, distributed from 34° to 35°N and between 123° and 124ºE and also has its central temperature 1 k higher than the surrounding. The blue is the anomaly on 17 of July with only 0.25 k higher in the middle. We can see from Fig.6 that temperature anomalies of these three days overlap each other. The central positions of the anomalies lie at 36.699ºN, 123.589ºE and 35.073ºN, 123.825ºE respectively, with the anomalies running in a circular way and trending regionally in S-N direction. The anomalies at these two positions mainly correspond with the south side of the Yantai depression and the east side of the Qingdao depression in the tectonic division map of the South Yellow Sea, while the other areas show unclear temperature anomalies (Fig.6).

Thus, it is inferred from the MODIS temperature anomalies that the oil prospect areas in the South Yellow Sea are concentrated on the south side of the Yantai depression and the east side of the Qingdao depression.

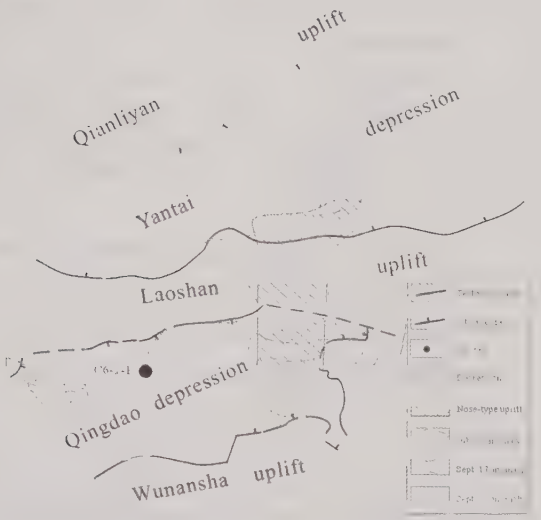

Fig.6 Comprehensive map of remote sensing temperature and aeromagnetic anomalies in the South Yellow Sea Basin

2.2 Aeromagnetic anomalies in the South Yellow Sea

Analysis results from aeromagnetic data of the South Yellow Sea have revealed that there is a nose-type tectonic uplift (near 123°30′E, 34° - 35°30′N) extending in the near S-N direction in the east of the study area (Fig.6). It is inferred from the aeromagnetic data there exists a Mesozoic sediments-infilled "depression" close to either side of the nose uplift, with the depression on the west side much larger in area than the east-side one. And these two depressions make up the west and east parts of the present Laoshan uplift respectively. The nose uplift itself consists of a series of westward-dipping nose-like swells and eastward-lifting wedge-shaped sags. These swells are considered as Paleozoic and Mesozoic products overlain directly by Neogene with Paleogene absent in between. Faults that generally bound the swells have been complicated due to later magmatic activities.

The nose uplift stands between the east and west depressions, so it can guide a way to hydrocarbon in the two depressions (especially the west-side one), if Paleozoic and Mesozoic strata are good oil source rocks in the South Yellow Sea [14].

3 Discussion and conclusions

Compared with the East China Sea, the South Yellow Sea has a low amplitude of sea surface temperature anomaly in the satellite remote-sensing image, for which there are following two reasons: firstly, the South Yellow Sea may not possess so good oil prospect in the shallow structures as the East China Sea; secondly, the shallow structural layers have weak tectonic activities and there are good

regional capping rocks in the South Yellow Sea Basin, from which we draw an inference that deep structural layers (including Paleozoic and Mesozoic) may be of favorable petroleum prospect in the basin.

It seems feasible enough to use remote sensing images to look for hydrocarbon in the South Yellow Sea Basin, because in satellite infrared images, temperature anomalies always fall into the proved Pinghu petroleum area that also shows a relatively high CH_4 content at the water-atmosphere interface and evident seafloor geochemical anomaly.

We used the high-precision TERRA satellite to do the present study because of the low sea surface temperature anomaly in the satellite remote sensing images of the South Yellow Sea Basin. According to temperature anomaly areas from MODIS data, they were found mainly located on the south side of the Yantai depression and on the east side of the Qingdao depression.

In addition, it is known from aeromagnetic data of the Yellow Sea that a S-N-running nose uplift lies in the east of the Laoshan uplift zone corresponding to the most evident temperature anomaly in the data. The Mesozoic depression on either side of the nose uplift is regarded as the major area to accommodate oil migration, and thus of good petroleum prospect by inference.

In general, shallow structural layers in the South Yellow Sea are probably poorer in oil formation than in the East China Sea, but the deep structures (including Paleozoic and Mesozoic) of the former may have relatively good oil prospect, and the most favorable ones are distributed at the south and north ends of the nose uplift, which can be chosen as reference areas for future petroleum explorations in the South Yellow Sea.

References

[1] Qiang Z J, Lin C G, Huang F L et al. A new remote sensing method for searching for oil enrichment zone—satellite thermal infrared detecting technique [J]. Chinese Science Bulletin, 1994, 39(18): 1 725-1 726.

[2] Huang F L, Zhang X H, Xia X H et al. Distributions of methane and homologen in lower atmospheric layer over eastern China and sea areas [J]. Chinese Science Bulletin, 1998, 43(16): 1 767-1 771.

[3] Xu X D, Xu X M, Ma S D et al. Study on the origin of atmospheric temperature anomaly before an earthquake [J]. Acta Seismologica Sinica, 1995, 17(1): 123-127.

[4] Liu C, Ge C H. Characteristics and application of MODIS remote sensing data in US earth observation system (EOS) [J]. Remote Sensing Information, 2000, 3: 45-48.

[5] Gong J M, Liu C, Lu Z Q et al. A new generation of satellite remote sensing to be used in the international seafloor gas hydrate explorations [J]. Marine Geology Letters, 2002, 18(2): 29-31.

[6] Guo D F. Theoretic basis and practice of remote sensing technique to be directly used for looking for oil. Environmental Remote Sensing [M], 1995, 1: 45-51.

[7] Li W X, Liu J, Huang Z L. Study on pore water, dissoluble Fe and ΔC oil chemical indexes of surface sediments in the East China Sea [J]. Shanghai Geology, 1993, 2: 1-8.

[8] Cheng T J, Wang Z S, Wu X M et al. Near Surface Indication and Geochemical Exploration of Hydrocarbon Migration [M]. Beijing: Petroleum Industry Press. 1999, 198.

[9] Wu C Z (translation). Eruptive microseepages: a basic approximate pattern for underground light hydrocarbon movement [J]. Chemical Exploration for Oil and Gas, 1996, 1: 24-29.

[10] Wang F Y. Remote sensing study for hydrocarbon microseepages in an area of eastern China [J]. Remote Sensing for Land & Resources, 1990, 4: 36-40.

[11] Wang F Y. Chemical mechanism formed by oil microseepage anomaly in remote sensing image [J]. Remote Sensing for Land & Resources, 1993, 1: 59-62.

[12] Zhu Z H, Wang W Y, Peng X L. Using remote sensing technique to directly detect hydrocarbon microseepage [J]. Chinese Science Bulletin, 1990, 35(16): 1 257-1 260.

[13] Feder A M. Remote sensing detection of microseepages in hydrocarbon exploration [M]. Proceedings of the International Symposium on Remote Sensing of Environment; Remote Sensing for Exploration Geology. Environ. Res. Inst. Mich. Ann. Arbor. M1. USA. 1985, 79-91.

[14] Li P L. Cretaceous in the South Yellow Sea: an oil exploration domain that should be paid attention to [J]. Marine Geology and Quaternary Geology, 1986, 16(4): 49-53.

卫星遥感预测南黄海盆地油气远景

龚建明[1,2]，陈建文[1,2]，梁杰[2]，张志珣[2]，刘闯[3]，卢振权[4]，黄福林[2]

(1.中国海洋大学，山东 青岛 266003；2.青岛海洋地质研究所，山东 青岛 266071；3.中科院地理科学与资源研究所，北京 100101；4.中国地质科学院矿产资源研究所，北京 100037)

摘 要：为了预测南黄海盆地油气远景，利用卫星遥感对东海陆架盆地进行海面温度测量。东海陆架盆地已知油气远景区与卫星热红外温度异常区具有原地重复性，与水气界面 CH_4 含量曲线及海底化探异常吻合程度很好。南黄海盆地卫星遥感海面温度异常区沿南北向 (123º30′) 呈带状分布，与航磁解释出的南北向分布的东部鼻状隆起吻合较好。由于温度异常区主要分布在南黄海盆地东部鼻状隆起的南北端，故推测东部鼻状隆起的南北端具有较好油气远景。

关键词：温度异常；卫星遥感；油气远景；南黄海

Preliminary Discussion on the Sea Water Quality Status in the 2008 Olympics Boat-sailing Field and Adjacent Area

SHI Xiaoyong , CHEN Lili , ZHU Chenjian , WANG Xiulin

College of Chemistry and Chemical Engineering, Ocean University of China, Qingdao 266003, *Shandong China*

Abstract: A cruise of survey in the 2008 Olympics boat-sailing field and adjacent area was carried out on August 28th, 2003. Preliminarily analysis on the eutrophication status was made on the basis of the content of dissolved inorganic nitrogen (DIN), dissolved inorganic phosphate (PO_4-P), dissolved oxygen(DO) and chemical oxygen demand (COD) as well. The results indicated that in most of the survey area, water quality was in accordance with the 1st class National Seawater Standard except the average concentration of petroleum hydrocarbon which was beyond the 2nd class National Seawater Standard. The concentrations of PO_4-P as well as DIN were mainly influenced by the runoff or drainage from lands, with a comparatively higher concentration in the coastal areas from the Fushan Bay to the Shilaoren bathing beach. The distribution of eutrophication index (EI) showed that part of the survey area was in a state of slight eutrophication. The eutrophication was mostly influenced by the land runoff or drainage and related factors. The sea water quality of the Olympic boat-sailing field was fine and just slightly polluted on the whole.

Keywords: the 2008 Olympic boat-sailing field; nutrients; eutrophication; pollution

Introduction

Qingdao will be the city that will undertake the Olympic Boat-sailing Game, as the partner city of Beijing Olympic Games in 2008. And the excellent oceanic environment is the most important factor for the Olympic Games to go on wheels. However, along with the rapid development of economy and increased exploitation of oceanic resources, the coastal area is facing more and more pressure and the sea area environment is being threatened. The environment quality of part of the sea area worsened and the trend has not been kept within limits [1-3]. The main factor contributing to the coastal area environmental pollution is the sewage discharged from land [1]. About ten thousand tons of dissolved inorganic nitrogen, over one thousand ton of dissolved inorganic phosphate and several hundred tons of petroleum hydrocarbons are discharged to the coastal area every year, and the quantity is increasing every year [2]. At present, the investigations for the coastal area environmental quality status are mainly focused on the Jiaozhou Bay, only few on the 2008 Olympics Boat-sailing field. In this paper, the eutrophication status is discussed on the basis of the investigation for the environmental factors carried out in the 2008 Olympics Boat-sailing field. It will provide a foundation of correlative decision for the study of the distribution, source and control countermeasure of the main contamination and for the excellent sea

Received on July 11, 2007

water quality in the 2008 Olympics Boat-sailing field.

1 Sampling and analysis

The cruise of survey in the 2008 Olympics boat-sailing field and adjacent area was carried out on August 28th, 2003. There were 23 sampling stations (Fig.1) which were deployed in three layers, including the surface, middle and bottom layers. Depth of these stations varied from 8 m to 44 m. Niskin bottles (20 dm^3) were used to taken samples from three layers for analyzing dissolved inorganic nutrient (DIN and PO_4-P), chemical oxygen demand (COD), dissolved oxygen (DO) and pH. Nutrient samples were filtered immediately with Whatman GF/F membrane filters (Φ25 mm, constant weight) and kept in polythene plastic bottles, reserved in ice bucket until laboratory analysis. Analysis of nutrient samples used the Technicon™AA-II autoanalyzer (German, Brown-Luby Co.) according to the methods recommended in "The Specifications for Marine Monitoring" [4] (the precision of the measurement is 99.38 % for DIN and 98.02 % for PO_4-P). COD, DO and pH were measured using alkaline permanganate method, Winkler method and pH meter pH method, respectively [6]. Petroleum hydrocarbon samples were only collected in surface layer using an oil free glass sampler, acidified and extracted immediately, reserved in ice bucket until analysis with the UV spectrophotometric method [4]. The precision of the measurement is 98.3 % and the detection limit is 0.05 mg/L, respectively. The seawater quality was evaluated according to the "Sea Water Quality Standard of the People's Republic of China"（GB 3097-1997）in this paper.

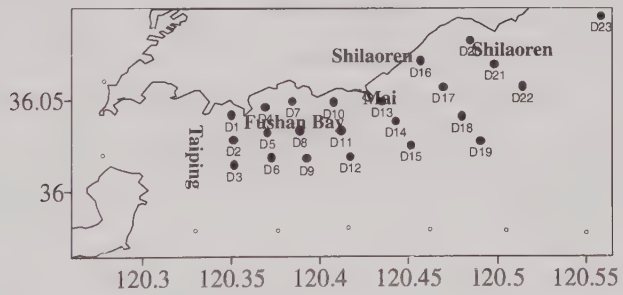

Fig.1 The 2008 Olympics Boat-sailing Field and Sampling Stations

2 Results and discussion

2.1 Horizontal distribution

2.1.1 PO_4-P and DIN

PO_4-P: In the survey area, the concentration of PO_4-P ranged from 0.29 to 0.67 μmol/L and the average was 0.36 ± 0.05 μmol/L (Tab.1), with a small vertical variation. In most of the survey area, the water quality reached the 1st Class National Seawater Standard, except one in the bottom layer (station

D21) near Shilaoren area. The pollution caused by PO_4-P was mitigated obviously compared with the survey in September 2001[5]. The distribution of PO_4-P showed that it was higher near shore and lower in outer sea on the whole (Fig.2), higher in the Taiping Bay and adjacent area, and the Shilaoren Bathing Beach adjacent area as well, lower around Maidao Island, indicating that the distribution of PO_4-P was mainly influenced by the terrestrial runoff or sewage discharge.

DIN: The concentration of DIN in the survey area ranged from 3.72 to 13.15 μmol/L, with an average of 8.91 ± 2.39 μmol/L (Tab.1). Though the DIN concentration has a little increase compared with the survey of September 2001 [5], it is in accordance with the 1st Class National Seawater Standard. The distribution pattern presents that the DIN concentration is higher near shore and lower in the outer sea on the whole (Fig.2). The concentration of DIN nearby the Shilaoren Bathing Beach was higher, which was mainly influenced by the land runoff or drainage.

2.1.2 DO and pH

Dissolved Oxygen (DO) in the survey area ranged from 6.12 to 7.41 mg/L, with an average of 6.78 ± 0.34 mg/L, which was lowered from surface to bottom layer. pH ranged from 7.95 to 8.30, with an average number of 8.09 ± 0.08, with little change in the vertical direction(Tab.1). The concentrations of DO and pH were in accordance with the 1st Class National Seawater Standard as a whole.

2.1.3 COD and petroleum hydrocarbon

COD: COD concentration in the survey area ranged from 0.74 to 1.73 mg/L, with an average of 1.06 ± 0.18 mg/L, which has little change in the vertical direction (Tab.1). The concentration of COD was in accordance with the 1st Class National Seawater Standard as a whole. The higher COD area was nearby Maidao Island and the lower area (only in surface layer) was nearby Shilaoren which seems influenced by the land drainage or runoff (Fig.2). Furthermore, there also has a higher COD concentration area in the southwest part of the survey area, indicating that the COD may also be influenced by the exchange with the outer sea area to a certain extent.

Petroleum hydrocarbon: The concentration of petroleum hydrocarbon in the survey area ranged from 0.02 to 2.30 mg/L, with an average of 0.41 ± 0.55 mg/L. The average petroleum hydrocarbon concentration was beyond the 3rd Class National Seawater Standard (Tab.1), about 78.26 % of the stations were beyond the 2nd Class National Seawater Standard, 34.78 % of the stations beyond the 3rd Class National Seawater Standard and 21.74 % of the stations beyond the 4th Class of National Seawater Standard, respectively. The pollution status of petroleum hydrocarbon was worse compared with that in August, 2001. There were high concentration areas near Maidao Island, Shilaoren Bathing Beach and Shilaoren adjacent area (Fig.2), which may be caused by the frequent movement of minitype boats in summer, the fastigium of tourism.

In most of the survey area, the water quality was in accordance with the 1st Class National Seawater Standard, except petroleum hydrocarbon, showing that the survey area belonged to the clean sea area as

a whole. The average concentration of petroleum hydrocarbon was beyond the 3rd Class National Seawater Standard, which may be caused by the pollution of minitype boats. The concentrations of PO_4-P and DIN in the survey area were mainly influenced by the terrestrial runoff and were higher inshore from Fushan Bay to Shilaoren area.

Tab.1 Value and variation range of environmental parameters

C/μmol·L^{-1}	Surface layer		Middle layer		Bottom layer		Whole area
	/Mean ±S.D.	Range	/Mean± S.D.	Range	/Mean± S.D.	Range	/Mean ±S.D.
PO_4-P	0.36 ±0.03	0.31-0.42	0.36 ±0.03	0.29-0.44	0.37 ±0.07	0.30-0.67	0.36 ±0.05
DIN	8.61 ±2.82	3.72-13.15	9.23 ±2.17	4.87-12.94	8.97 ±2.15	5.81-13.13	8.91 ±2.39
DO/mg·L^{-1}	7.05 ±0.21	6.61-7.41	6.76 ±0.32	6.21-7.23	6.52 ±0.24	6.12-6.99	6.78 ±0.34
pH	8.13 ±0.10	7.95-8.30	8.08 ±0.06	7.98-8.18	8.06 ±0.06	7.97-8.17	8.09 ±0.08
COD/mg·L^{-1}	1.03 ±0.13	0.77-1.29	1.13 ±0.24	0.74-1.73	1.04 ±0.15	0.85-1.33	1.06 ±0.18
Petrol/mg·L^{-1}	0.41 ±0.55	0.02-2.30	/	/	/	/	0.41 ±0.55
EI	0.93 ±0.33	0.38-1.36	1.12 ±0.47	0.60-2.30	1.02 ±0.46	0.56-2.36	1.02 ±0.42

Note: "/"means the concentration of petroleum hydrocarbon from middle layer and bottom layer wasn't surveyed, so there was no data.

2.2 Eutrophicatin status in the survey area

Based on the analysis of environmental parameters in the 2008 Olympics boat-sailing field and adjacent area, DIN, PO_4-P, DO and COD were used to discuss the eutrophication status of the survey area.

Among the methods which were used to evaluate the internal eutrophication status [6-11], the formula (1) was used to calculate the eutrophication index to assess the eutrophication status in the survey area [8].

$$EI = \mathrm{COD} \times \mathrm{DIN} \times \mathrm{DIP} / 1500 \quad (1)$$

Where, *EI* is the eutrophication index, COD is the chemical oxygen demand (mg/L); DIN is the issolved inorganic nitrogen concentration (μg/L); and DIP is the dissolved inorganic phosphate concentration (μg/L) [7]. $EI \geq 1$ means the seawater is in a state of eutrophication, the higher the *EI* value is, the worse the eutrophication status is.

In the survey area, the *EI* value ranged from 0.38 to 2.36, with an average of 1.02 ± 0.42. The *EI* value in 43.48 % of all survey stations was less than 1, indicating that the survey area was in slight eutrophication status. The distribution pattern presents that the *EI* value was higher nearshore and lower in the outer sea area on the whole. The higher *EI* area was in the west part of survey area, and the nearshore area from Fushan Bay to Shilaoren Bathing Beach as well (Fig.2).

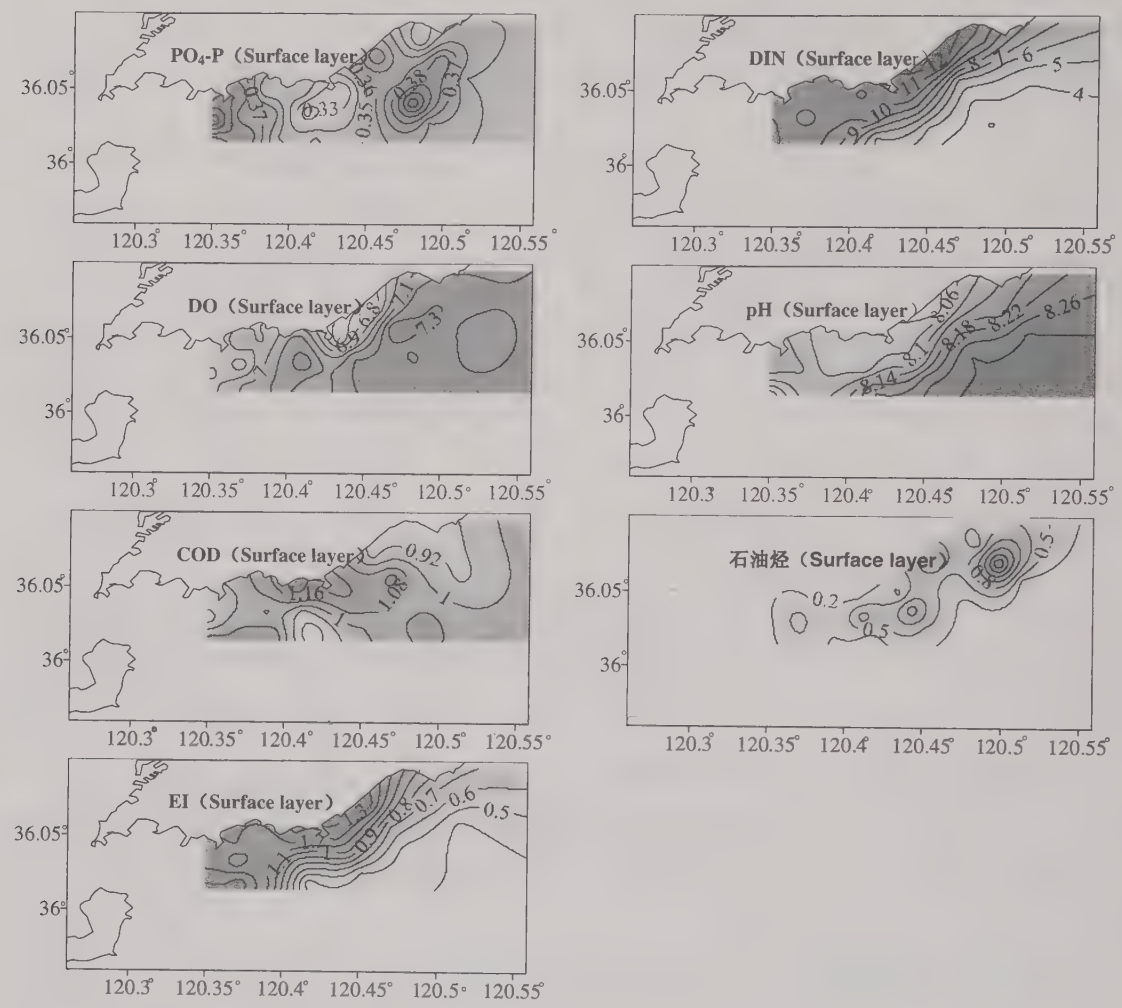

Fig.2 Horizontal distributions of some parameters

In the survey area, the *EI* distribution was similar to that of DIN, indicating that DIN contributed more to eutrophication than PO_4-P. As a whole, the eutrophication status in the 2008 Olympics boat-sailing field and adjacent area was mainly influenced by the terrestrial runoff.

3 Conclusions

According to the field survey which was carried out in the 2008 Olympics boat-sailing field and adjacent area on August 28, 2003, the seawater environmental parameters as well as the eutrophication index (*EI*) were discussed preliminarily.

a) The PO_4-P concentration in the survey area ranged from 0.31 to 0.67 μmol/L, with an average of

0.36 ± 0.06 μmol/L, and the DIN concentration ranged from 3.72 to 13.15 μmol/L, with an average of 8.91 ± 2.39 μmol/L, respectively. The COD and petroleum hydrocarbon concentrations ranged from 0.74 to 1.73 mg/L and 0.02 to 2.30 mg/L, respectively, and the average value was 1.06 ± 0.18 mg/L and 0.41± 0.55 mg/L, respectively. The water quality in most of the survey area was in accordance with the 1st Class National Seawater Standard, except petroleum hydrocarbon. The petroleum hydrocarbon was the dominant pollutant, the average concentration of which was beyond the 3rd Class National Seawater Standard.

b) PO_4-P and DIN concentrations in the survey area were mainly influenced by the land drainage or runoff as a whole, meanwhile the petroleum hydrocarbon was possibly influenced by the pollution of minitype boats.

c) In the survey area, the eutrophication index *EI* ranged from 0.38 to 2.36 with an average of 1.02 ± 0.42. The distribution of *EI* shows higher near shore and lower in the outer sea area on the whole. *EI* values in 43.48 % of the stations were less than 1, indicating the trend that part of the survey area was in a state of slight eutrophication.

To sum up, the sea water quality of the Olympics boat-sailing field was fine as a whole. The petroleum hydrocarbon was the dominant pollutant and the concentration was relatively high compared with the 1st and 2nd Class National Seawater Standard. Now it is necessary to transform the minitype boats to decrease the petroleum hydrocarbon pollution, and reduce the discharge capacity from land to ensure each environmental parameter was in accordance with the 1st Class of National Seawater Standard and guarantee the excellent sea water quality in the 2008 Olympic Boat-sailing field.

Acknowledgements

The paper was supported by the National Key Technologies R&D Program (2002BA904B06), Project continuously funded by the Shandong Natural Science Foundation (L2000E01), "Green Olympics" specialized program of Qingdao Municipal Science and Technology Commission (HAK1203).

References

[1] Qingdao Oceanic and Fishery Administration. Public Report Marine Environment of Qingdao in 2001. Qingdao Oceanic and Fishery Administration, Qingdao, 2002

[2] Qingdao environmental protection bureau. Public Report of Environment State of Qingdao in 2001, Qingdao environmental protection bureau, Qingdao, 2002

[3] State Oceanic Administration People's Republic of China. Public Report of China Marine Environment in 2002, State Oceanic Administration People's Republic of China, Beijing, 2003

[4] "Marine monitoring criterion" Editorial Board. Marine Monitoring Criterion. China Ocean press, Beijing, 1991, 254-257

[5] Li R X, Wang B D, Wang Z L, et al. The Status of chemical and biological factor and mesocosm experiment of eutrophication to cause bloom in the area for the Olympic sailing games in Qingdao [J]. Acta Ecologica Sinica, 2004, 24 (4): 837-842

[6] Lin R G. Review of the assessing methods for coastal eutrophication [J]. Marine Environmental Science，1996, 15 (2) : 28-31

[7] Lin C Q. Assessment and inquiry on the eutrophication in the near shore of Dalian [J]. Marine Environmental Science, 1994, 13 (4) : 63-67

[8] Sun Y, Chen J F, Zhang Y C. Analysis on chemical parameters of eutrophication in Jiaozhou Bay [J]. Marine Environmental Science,1993, 12 (3-4) : 25-31

[9] Zou J Z, Dong L P, Qin B P. Elementary study on eutrophication and red tide in Bohai [J]. Marine Environmental Science, 1983, 2 (2) : 41-5

[10] Tian J Y, Dong J Y. Investigation of organic pollution and red tide organism at the Yellow River estuary seawaters [J]. Marine Environmental Science, 1983, 2 (1) : 46-53

[11] State Oceanic Administration, People's Republic of China. Marine culture monitoring technology criterion, State Oceanic Administration People's Republic of China, Beijing, 2002, 4

2008 年奥运会帆船赛场海域环境质量状况

石晓勇，陈莉莉，祝陈坚，王修林

（中国海洋大学化学化工学院，山东 青岛 266003）

摘 要：于 2003 年 8 月 28 日对奥运帆船赛场海域海水水质要素进行了现场调查，并以无机态氮（DIN）、无机态磷（PO_4-P）、化学耗氧量（COD）、溶解氧（DO）为化学指标参数，探讨了该海域的富营养化状况。结果表明，奥运会帆船赛场海域除石油烃外，大部分海域符合国家一类海水水质标准，石油烃平均含量超过国家二类水质标准。该海域调查海区 PO_4-P、DIN 主要受陆源排放影响，特别是浮山湾至石老人沿岸海域含量较高。部分区域已经开始呈现轻微富营养化状态，富营养化状况主要受陆源排放等因素的影响。整体上奥运会帆船赛场海域水质良好，污染较轻。

关键词：奥运帆船赛场；营养盐；富营养化；污染

海 洋 通 报（英文版）

HAIYANG TONGBAO

2007 年 10 月　第 9 卷　第 2 期

目　次

海洋磁力测量仪器系统检验方法研究 …… 边 刚 等 (11)

BDRM 理论在双轴海洋声道中的应用 …… 张 林 等 (17)

碘化钾碱性高锰酸钾法测量海水化学需氧量不确定度的研究 …… 张世强 等 (24)

南中国海北部大亚湾水温和赤潮的变化 ……余 景 等 (33)

亏损生物对大亚湾养殖珍珠贝的滤食、呼吸和排泄的影响 …… 苏振霞 等 (42)

南海北部秋季微型浮游动物摄食和种类组成的初步研究 …… 苏 强 等 (53)

中国点叶藻科（褐藻门）新记录种 …… 栾淑君 等 (60)

南岛鹿回头珊瑚礁与全新世高海平面 …… 黄德银 等 (70)

区域沉积物管理概论 …… 雷怀彦 等 (81)

卫星遥感预测南黄海盆地油气远景 …… 龚建明 等 (89)

2008 年奥运会帆船赛场海域环境质量状况 …… 石晓勇 等 (96)

Marine Science Bulletin

Marine Science Bulletin publishes papers on marine science and technology including physical oceanography, chemical oceanography, marine biology, marine geology, environmental oceanography, estuarine & coastal sciences, marine technology, digital ocean, coastal zone management, ocean engineering, marine economics, etc., and aims to promote international academic exchange.

Editor-in-Chief: LIN Shaohua (林绍花)

Associate Editor-in-Chief: HE Guangshun (何广顺) YANG Ying (杨 鹰)

Executive Editor: LIN Baofa (林宝法) HE Xuewu (何学武) ZHANG Deshan (张德山)
ZHANG Xiaoxian (张潇娴) QIU Wenjing (邱文静) WANG Zhankun (王占坤)
CHENG Xiuchun (程秀春)

Marine Science Bulletin **(Vol. 9 No. 2 Oct. 2007)**

Responsible Institution:
State Oceanic Administration of China
Edited and Published Semi-annually by:
National Marine Data and Information Service
Address: 93 Liuwei Road, Hedong District, Tianjin 300171, China
E-mail: msb@mail.nmdis.gov.cn

ISSN1000-9620
CN12-1271/N